DEVELOPMENT OF MICROFLUIDIC PLATFORM FOR CONTINUOUS EXTRACTION OF DIAGNOSTICS PLASMA PROTEINS FROM WHOLE BLOOD DURING CARDIAC SURGERY

By

KIANA ARAN

A Dissertation submitted to the

Graduate School-New Brunswick

Rutgers, The State University of New Jersey

and

The Graduate School of Biomedical Sciences

University of Medicine and Dentistry of New Jersey

In partial fulfillment of the requirements

For the degree of

Doctor of Philosophy

Graduate Program in Biomedical Engineering

Written under the direction of

Professor Jeffrey D. Zahn

And approved by

_____

_____

_____

_____

January, 2012

ABSTRACT OF THE DISSERTATION

DEVELOPMENT OF MICROFLUIDIC PLATFORM FOR CONTINUOUS EXTRACTION OF DIAGNOSTICS PLASMA PROTEINS FROM WHOLE BLOOD DURING CARDIAC SURGERY

By Kiana Aran

Dissertation Director:
Professor Jeffrey D. Zahn

This work, describes the design, fabrication and testing of a microfluidic platform for the continuous extraction of blood plasma from a circulating whole blood sample in a clinically relevant environment to assist in continuous monitoring of a patient's inflammatory response during cardiac surgeries involving extracorporeal circulation (ECC) procedures such as cardiopulmonary bypass (CPB) and extracorporeal life support (ECLS) procedures.

The microfiltration system consists of a two-compartment mass exchanger with two aligned sets of PDMS microchannels, separated by a porous polycarbonate membrane. Using this microdevice, blood plasma can be continuously separated from blood cells in a real-time manner with no evidence of bio-fouling or cell lysis. The technology is designed to continuously extract plasma containing diagnostic proteins such as complements and cytokines using a significantly smaller blood volume as compared to traditional blood collection techniques. The microfiltration device was evaluated using a

simulated CPB circulation loop primed with donor human blood and in-vivo piglet model of ECLS in a manner identical to clinical surgical setup. The microfiltration device was able to continuously extract small volume of cell-free plasma (2.5 ml) from unmodified circulating blood over extended period of time (over 5 hours) in order to study the immune activation during CPB and ECLS procedures. The simple and robust design and operation of the microdevice will allow surgeons and clinicians autonomous usage in a clinical environment to better understand the mechanisms of injury resulting from cardiac surgery, and allow early interventions in patients with excessive postoperative complications to improve surgical outcomes.

Ultimately, monolithic integration of this microfiltration device with a continuous microimmunoassay would create an integrated microanalysis system for tracking inflammation biomarkers concentrations in patients for point-of-care diagnostics, reducing blood analysis times, costs and volume of blood samples required for repeated assays.

Additionally, the microfiltration technology was tested to continuously extract pathogens *E.coli*) from blood for treating sepsis. Using this device approximately 22% of the E.coli was removed from the blood in the reservoir over a period of 80 minutes. These results demonstrate the ability of the microfiltration system to continuously remove bacteria from blood.

ACKNOWLEDGEMENTS

First and foremost I want to thank my advisor Professor Jeffrey Zahn. I appreciate all his contributions of time, ideas, and funding to make my Ph.D. experience productive and stimulating. He was always supportive when he knew I needed to juggle priorities. I am forever grateful for that. Thank you

I would also like to gratefully acknowledge the enthusiastic supervision and numerous stimulating discussions of my committee member, Professor Akif Ündar. His vision "If the course of just one child's life is improved as a result of this research, then we have surely reached our goal", was a big inspiration.

I am very grateful to the remaining members of my dissertation committee, Professor Laura Fabris and Professor John K-J. Li. Their academic support and personal cheering are greatly appreciated. Thank you.

I would also like to thank Dr. Joseph Clark, Dr. Elizabeth Carney, Dr. Feng Qiu and Dr. Qi Sun in Penn State Hershey Children's Hospital for their help, input, valuable discussions and accessibility during our clinical experiments.

My colleagues in BIOMEMS Lab. also deserve my sincerest thanks, their friendship and assistance has meant more to me than I could ever express. I could not complete my work without invaluable friendly assistance of Lawrence Sasso, Mercedes Morales, Alex Fok, Neal Kamdar, Jack Zheng and Jean Lo.

I must acknowledge my staunch supporters Amir Jamshidi and Nasrin Alvari for their love and support during these years.

I would like to thank my family for all their love and encouragement. My father Ghazi Aran, who always pushed me to move forward and my mother Fozi Malek for her unconditional love. I owe them everything and wish I could show them just how much I love and appreciate them.

Lastly, I am forever indebted to my husband Ali for his understanding, endless patience and encouragement and my son, Danial who has given me the strength and courage to continue when it was most required.

DEDICATION

To my husband and my son, Ali and Danial

for all their love and support.

TABLE OF CONTENTS

LIST OF TABLES

LIST OF ILLUSTATIONS

Chapter 1 : Introduction

1.1 Research Motivation

Patients who undergo cardiac surgeries often suffer from systemic inflammatory responses, particularly when mechanical circulatory support devices such as cardiopulmonary bypass (CPB) or extracorporeal life support (ECLS) are used. Despite considerable advances in surgical protocols, clinical patient management and pre and post-operative care, systemic inflammation still remains a problem which can dramatically affect patient recovery, length of hospitalization and long term quality life.

Extracorporeal circulation (ECC) techniques, including CPB and ECLS, have been widely used during open heart surgery and respiratory and circulatory support. The use of CPB and ECLS have revolutionized how cardiac surgeries are performed by allowing complicated valve replacement and cardiac repairs, congenital defects in pediatric patients, coronary artery bypass grafts (CABG) and even heart transplants.

1.1.1 Cardiopulmonary bypass (CPB)

A cardiopulmonary bypass (CPB) procedure is commonly used during open-heart repairs in pediatric and adult patients. The father of surgical cardiopulmonary bypass (CPB) for humans was John H. Gibbon, Jr, MD. The idea of CPB arose when Dr. Gibbon witnessed the collapse of a patient with a massive pulmonary embolism after a general surgical operation performed in Massachusetts General Hospital in 1930. This dramatic clinical experience determined Dr. Gibbon lifetime research in developing a machine that could

take over the function of the heart and lungs. 23 years later and after the first successful application of CPB, generations of cardiac surgeons have been able to operate on millions of human hearts to correct complicated congenital heart defects, cardiac valve disorders in the young and old, atherosclerotic coronary artery obstructions, and large aneurysms of the thoracic aorta.[1] The idea of CPB procedure is to provide total support of heart and lung function for a matter of hours to facilitate cardiac operations, where motionless heart is required. The procedure starts by inserting a venous cannula into the right atrium in order to withdraw unoxygenated venous blood into the venous reservoir. The blood is then pumped into the membrane oxygenator where it gets oxygenated. Arterial filter then removes the air bubbles from the oxygenated blood. The oxygenated blood is then returned via an aortic cannula to all other organs bypassing the heart and lungs (Figure 1-1).

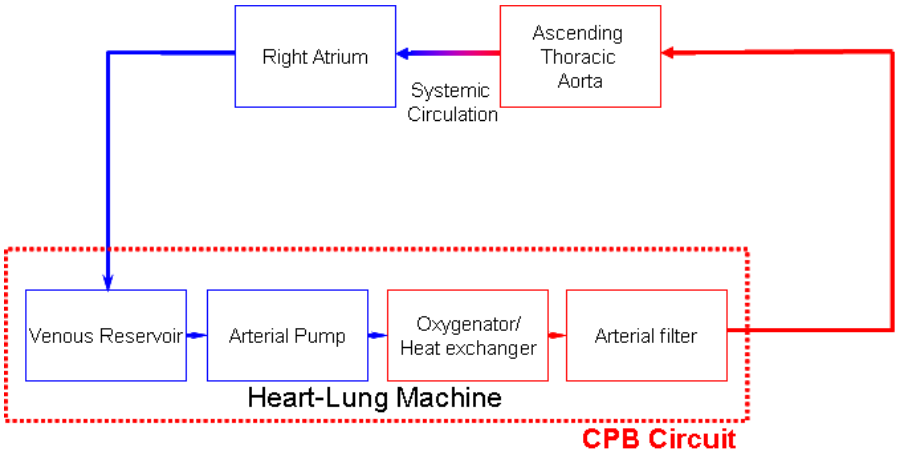

Figure 1-1: Schematic of the Cardiopulmonary Bypass Circuit

During the past several decades, the mortality rates after open-heart surgeries with or without CPB declined dramatically, but the morbidity on vital organs are still common in particular high-risk patients. [2-5].

1.1.2 Extracorporeal Life Support (ECLS) Procedure

Extracorporeal life support (ECLS) is a modified form of cardiopulmonary bypass used to provide tissue oxygen delivery for a prolonged period of time (days to weeks) in patients with respiratory and/or cardiac failure. During ECLS procedure, first blood is drained from the venous circulation into the ECLS circuit where oxygen is added and carbon dioxide is removed, oxygenated warmed blood then is pumped back to either arterial or venous circulation. From a general point of view, there are two methods of support for ECLS: veno-arterial circulation for both oxygenation and hemodynamic assistance and veno-venous extracorporeal oxygenation, for respiratory function substitution. Venoarterial extracorporeal support provides total cardiopulmonary support, where blood is withdrawn from venous circulation, exchanging O_2 and CO_2, and then returning to patient's arterial circulation. Venovenous extracorporeal support provides pulmonary support by withdrawing deoxygenated blood from the venous system, exchanging gases and returning the blood to the venous system.[6]

By early 1990s, ECLS became a standard of care for neonates and is becoming more widely used for pediatric and adult with cardio-respiratory failure. The indications for ECLS have been significantly expanded due to the improved technology and favorable outcomes. The significant improvements of ventilation and circulatory strategies, now allows more critical patients to be candidates for ECLS. Today ECLS is used in congenital heart surgery for several indications including failure to separate from cardiopulmonary bypass (CPB), postoperative low cardiac output, pulmonary hypertension, bridge to transplantation and for routine support following staged repair of hypoplastic left heart syndrome. [7-10] The Extracorporeal Life Support Organization

(ELSO) International Summary of the ECLS Registry reports that as of July 2010, the number of pediatric and adult patients receiving ECLS support for both respiratory and cardiac indications increased steadily throughout the 1990s These series demonstrated cumulative respiratory and cardiac runtime of 38,540 hours with average survival rate of 52.6% in neonatal and pediatrics and a cumulative respiratory cardiac runtime of 3,594 hours with average survival rate of 45.5% in adults.

1.1.3 Post-Operative Complications Associated with CPB and ECLS Procedure

Patients receiving ECC procedures remain at high risk for post-operative complications such as vital organ dysfunctions that can lead to multi-organ failure and even death. The damaging effects of CPB procedure are most attributed to prolonged interaction of blood with synthetic surfaces of the extracorporeal circuit along with other factors, such as shear stress generated by blood pumps, tissue ischemia/reperfusion injury, types of oxygenators, hemodilution, donor blood products, non-pulsatile perfusion, administration of heparin and protamine, surgical trauma and hypothermia and an inflammatory response which increases with increasing length of CPB and may continue long after the discontinuation of CPB.[11-14]. Patients undergoing ECLS also suffer from morbidity and mortality as a result of ECLS pathophysiological and mechanical failure (such as oxygenator failure, pump or heat exchanger malfunction, air in circuit or cannula problem).[15, 16] This can be due to increased duration of ECLS which was found to correlate with decreased survival. [9] ECLS complications were found to be significant

predictors of poor outcome. Ischemic brain injury, intracranial hemorrhage and renal dysfunction were noted to be an important risk factor associated with ECLS. [17]

Several studies have clearly shown that cardiac surgery induces systemic inflammatory responses syndrome (SIRS), particularly when ECC is used. The intensity of the systemic inflammatory response appears to be directly correlated with the severity of ECC-related complications but its mechanism is poorly understood. [18] Previous studies have clearly shown that CPB and ECLS cause alteration in the levels of biomarkers related to inflammation, tissue damage and other tissue pathologies. [12, 19-21] Investigators have also documented that there are significant correlations between the SIRS and several biomarkers including complement and cytokines. [22-27]

The damaging effects of CPB and ECLS worsen in neonatal and pediatric patients because of low blood volume and immature immune systems. [28] The apparent increasing use of this technology, especially in newborn populations, is raising concerns about long-term clinical outcomes of the procedure. An estimated of 0.8% of neonates are born with a congenital heart defect of varying complexity and approximately half of them require open heart surgery during the first year of life. The average duration of neonatal respiratory ECLS has also increased from 144 hours in 1990 to 209 hours. However, the survival rate has steadily decreased from about 80% to 67%. [15, 16, 29] Additionally, many of the surviving children encounter complications induced by ECC, including neurological problems, ischemic brain injury, intracranial hemorrhage and renal dysfunction. [30-32] For example the adverse neurological outcomes of pediatric cardiac surgeries have been attributed to systemic inflammatory response but the extent to which the systemic inflammatory response is related to postoperative cognitive decline

is not clear. Also a prospective study from 2001 reported a high incidence of cognitive decline 5 years after coronary artery bypass grafts (CABG) surgery which requires ECC techniques.[33]

Minimizing SIRS would significantly assist in protection of vital organs including the brain, kidneys and the heart itself and is also important for improving functional outcomes of patients by reducing peri-operative complications. In one study continuous ultrafiltration was employed to improve end organ perfusion and function. [34] This suggest that methods to limit the inflammatory mediators while on ECC, may be of potential benefit for future research in an effort to improve organ perfusion during ECC and prevent development of end organ dysfunction that may lead to serious morbidity and high mortality.

Currently, there is no effective method to prevent the systemic inflammatory response syndrome in patients undergoing ECC procedures. However, study of the effect of pro-inflammatory and the anti-inflammatory cytokines levels change in time is a way to an earlier diagnosis and therefore prevention of post-operative complications associated with ECC. The ability to correct the underlying pathophysiological events which is a determinant factor in the survival of patients is not possible without continuous and timely measurement of inflammatory biomarkers associated with post operative complications.

The type of biomarkers to be monitored to detect the post-operative injury is very important. However, selecting a biomarker also depends on the ability to detect it in plasma, availability of standardized commercial assays and prior studies indicating the

significance of a particular biomarker to a specific injury. More recent studies have shown that monitoring multiple biomarkers can yield more information about the pathobiology of the injury. [27]

1.2 Monitoring Inflammatory Response to Mechanical Cardiopulmonary Support Systems

A variety of hematological tests are commonly used for the rapid and accurate diagnosis and prognosis of medical conditions which promote immunological activation such as infectious diseases, autoimmune disorders, wound healing and trauma, as white blood cells continuously respond to pathological changes within the body.[35] Diagnostic blood analysis devices, typically require cell-free plasma, as the presence of cells such as RBCs can block the active detection site and interfere with many detection systems for biochemical components of the blood.[36] Preliminary diagnostics of disease usually relies on measurement of blood components concentration in separated plasma such as urea, glucose, electrolytes, proteins and antigens. Blood samples are usually acquired using venipuncture utilizing blood volume of 3-5 ml.

1.2.1 Current Technology

Current technology uses conventional blood collection techniques such as vacutainer tubes and conventional assays that measure protein concentration, such as the enzyme linked immunosorbent assay (ELISA) and immunofluorocytometry to provide measurements of the effects of cardiopulmonary support systems on activation of complements and cytokines hours or days post support with very low sampling intervals of 1 hour or more over a total monitoring period of 24 to 48 hours. Figure 1-2 indicates

cytokine Il-6 concentration versus time before and after a CPB procedure. During the entire CPB procedure until protamine is administered, there is a significant increase in the IL-6 concentration but no data points tracking this rise. The next data point is after protamine is given to reverse the effects of anticoagulation.[37] Even the most recent studies on inflammatory responses during ECC procedures, suffer from lack of temporal information between each data. Figure 1-3 shows average values of the results from detecting the changes in several biomarkers in pediatric patients (ages ranged from 3 months to 4 years old) undergoing various cardiac procedures requiring CPB. As it can be seen in the Figure 1-3 and Table 1-1 the levels of IL-6 and IL-8 increased significantly during CPB and remained higher than their pre-CPB levels even 24 hours post-CPB. The levels of TNF-α and IL-1β did not increase significantly and instead the level of TNF-α was decreased during CPB. [27] The reported information about the rise of inflammatory biomarkers during actual surgical procedure in not only limited, but also is not consistent between different studies.

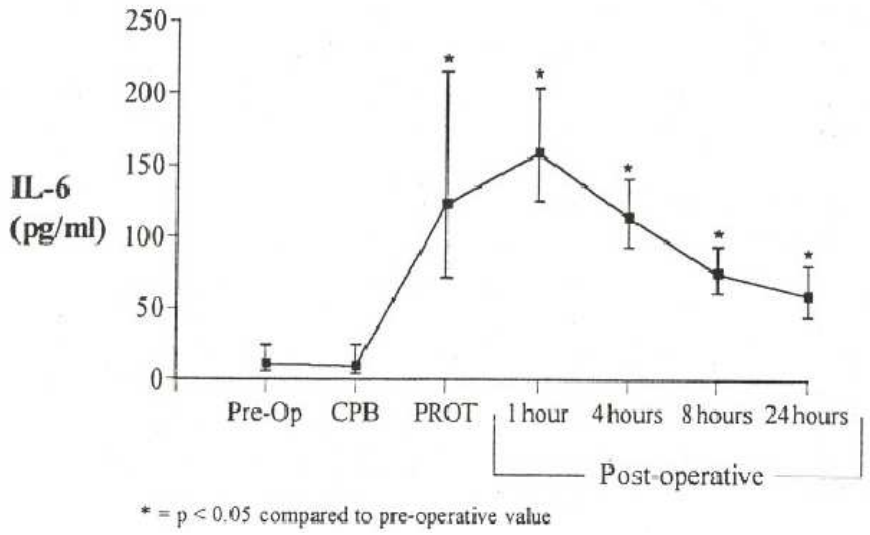

Figure 1-2: Changes in interleukin 6 (IL-6) levels in 16 patients undergoing modified Fontan procedure. (CPB=Cardiopulmonary bypass, Pre-Op=preoperative, PROT=protamine).[37]

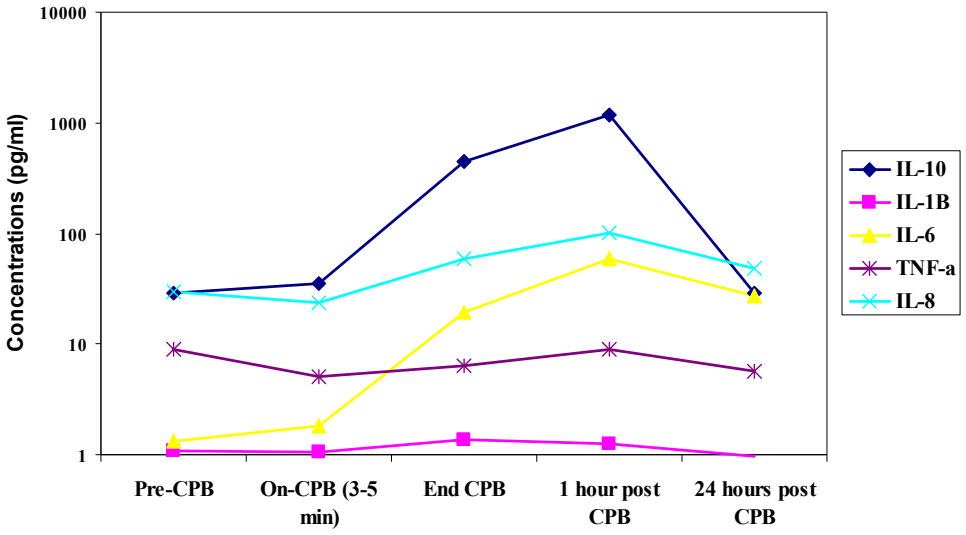

Figure 1-3: Schematic display of average values of biomarkers in pediatrics patients (ages ranged from 3 months to 4 years old) undergoing various cardiac procedures requiring CPB.[27]

Table 1-1: Values of biomarkers in pediatrics patients in pg/ml (ages ranged from 3 months to 4 years old) undergoing various cardiac procedures requiring CPB.[27]

	IL-10	IL-1β	IL-6	IL-8	TNF-α
Pre-CPB	28.58	1.1	1.34	30.18	8.92
On-CPB (3-5 min)	35.71	1.05	1.84	23.96	5.15
End CPB	448	1.38	19.56	59.72	6.36
1 hour post CPB	1168	1.27	59.84	100.99	8.92
24 hours post CPB	28.88	0.97	27.09	48.6	5.74

There are significant advantages of continuous blood analysis to measure the systemic inflammation during CPB and ECLS as compared to conventional techniques. Real-time monitoring of inflammation will help clinicians and researchers identify significant changes in systemic inflammation in real-time and therefore enables the surgical team to perform clinical adjustment if needed. Additionally, real-time measurement will help researchers better understand the effect of clinical pharmacological agents including anesthetic drugs, different modes of perfusion and oxygenation, blood transfusion and temperature on systemic inflammation. One example of a significant benefit which could be provided by real-time monitoring of inflammation biomarkers is that in most children's hospitals in the US and abroad blood ultrafilitration (UF) or modified ultrafiltration is used at the end of the surgery to hemoconcentrate the circulating blood which has the added benefit of removing proinflammatory cytokines.[38] However, since cytokines concentration is not measured during ultrafiltration, the ultrafiltration is ended only based on blood hematocrit level. Real time monitoring of inflammatory proteins

would enable the surgical team to end ultrafiltration based on cytokine concentrations instead of just by blood hematocrit level and assist in managing post operative inflammation.

Continuous blood analysis for real-time monitoring of inflammation requires the continuous extraction of blood protein from whole blood. Conventional assays such as vacutainer tubes for blood collection requires several ml of blood which is much greater than the amount required for assays such as enzyme linked immunosorbent assay (ELISA) and immunofluorocytometry which require about 50 to 100 μl of blood plasma per sample. These techniques are not compatible with the use of serial samples to study the time course of inflammatory processes because the amount of blood than can be withdrawn from patient is limited. Additionally, successive blood analysis is impossible to implement in neonates or infants due to their small total blood volume (total blood volume of a 3 kg neonate is only 240 ml). However, the study of inflammatory responses is extremely beneficial in neonates and infants who are more susceptible to the systemic inflammatory response syndrome due to higher metabolic demands, immature organ systems with altered homeostasis.

The proposed study is designed to develop an approach to continuously separate plasma inflammatory biomarkers such as cytokine and complement using a miniaturized technology that requires a very small amount of blood sample in order to evaluate the effect of circuit components and surgical protocols on activation of immune response.

1.2.2 Miniaturized Technology for Continuous Plasma Separation

More recently, significant research efforts have been made in microfluidic and miniaturized lab-on-a-chip blood analysis devices which can offer rapid analyses with minimal sample and reagent requirements. [39] To date, many methods for particle and blood cell separations in microfluidic systems have been demonstrated. Some of these techniques have been applied to fractionate specific cell types or molecules from blood while other technologies are focused on efficient cell free plasma separation from blood samples for clinical analysis. [40] Active separation modalities have certain disadvantages such as high cost, complex fabrication and restricted portability which make them undesirable for clinical applications. Purely hydrodynamic separations are more attractive in clinical application because they do not require an external field. Hydrodynamic microfluidic approaches to blood fractionation have been based on structuring of flow profiles based on microchannel design and geometry and/or operating flow conditions. These approaches are based on inertial force particle focusing, deterministic lateral displacement devices, hydrophoretic filtration, separation using the Zweifach-Fung effect, physical separation using microstructures and membrane filtration. [36, 39, 41-51]

Many different hydrodynamic approaches to blood cell fractionation and plasma separation from blood have been demonstrated. For example, separation of blood cell components, such as platelets and RBCs from diluted whole blood (2% blood in PBS) was accomplished using inertial flow fields in curved microchannels. This device consists

of inlets, a filter and 62 asymmetric separation turns, and 5 outlets to collect the filtrate. (Figure 1-4)[52]

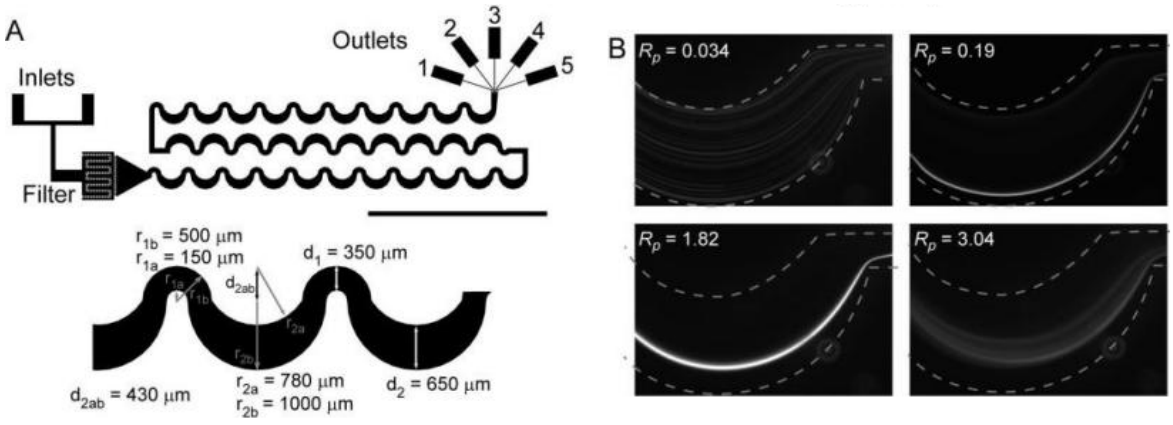

Figure 1-4: (A) The device design using inertial flow to separate plasma from blood. (B) Images of 10-μm beads within the device are shown for increasing flow rates.[52]

Lateral migration of red blood cells which results in cell free plasma layers has also been used to separate plasma from whole blood. In one report using lateral migration, the channel geometry was modified in order to expand the dimension of the cell free region at high flow rates (Figure 1-5). However, the human blood was extremely diluted (1:20) in order to achieve extraction efficiency of about 10%.[46]

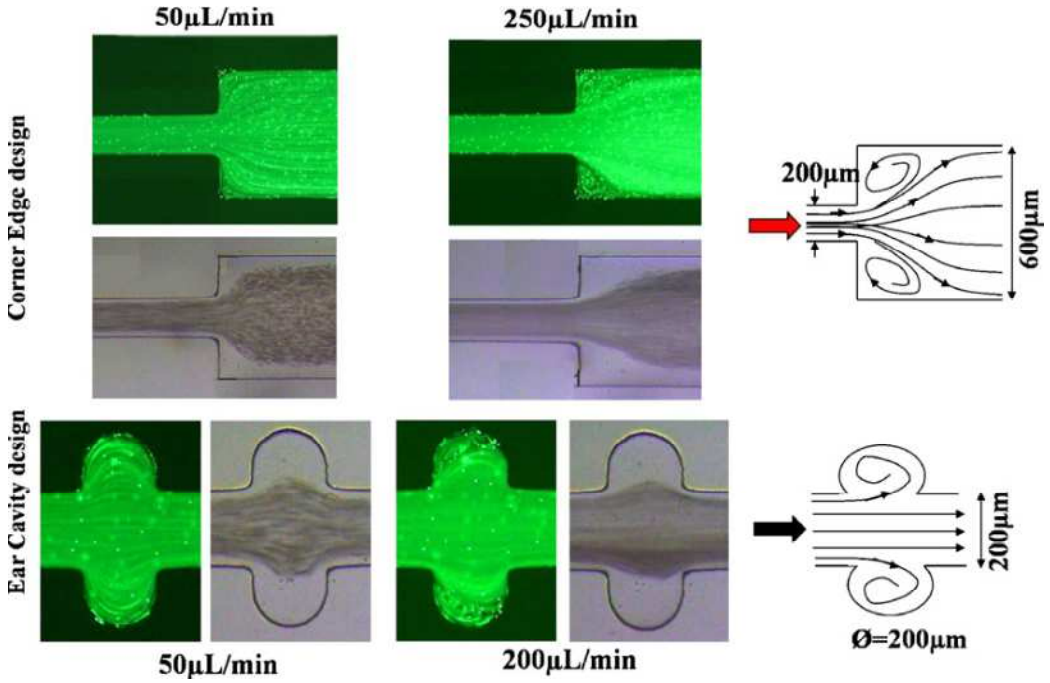

Figure 1-5: Shows the cell-free layer using lateral migration and different channel geometry. The sample is a mixture of 1/20 diluted blood and 0.5µm fluorescent beads.[46]

The Zweifach-Fung bifurcation law was also used to continuously separate plasma from whole blood, by controlling the flow rate ratio between a main blood channels and bifurcating plasma channels. This device has one whole blood inlet, a plasma outlet and a concentrated whole blood outlet. The channels were specially designed so that cell centroids would always be beyond a bifurcating streamline separating the plasma channel and main channel flows so that plasma could be continuously 'skimmed' away from the device without cell contamination (Figure 1-6). [48] Using this microdevice, which required accurate flow control through channel design dimensions, a plasma volume of

25% was collected but the volume percent of plasma collected decreased as blood hematocrit decreased.

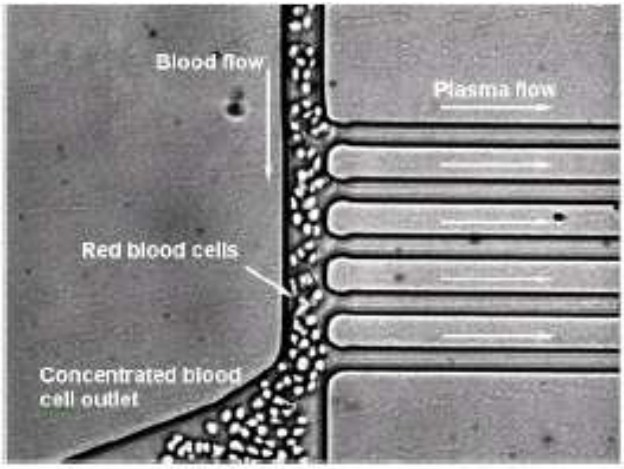

Figure 1-6: Images of the microfluidic blood plasma separation device based on Zweifach-Fung bifurcation law. [48]

In one report, a better plasma yield (40%) was reported using Zweifach–Fung bifurcation law at very high flow rates (10 ml/hr). However, purification efficiency of the plasma was low and the blood was extremely diluted (Hematocrit ~ 3%).[53] Also in another device the Zweifach–Fung, Fahraeus and the pinched flow fractionation effect were combined to separate human plasma from red blood cells using a range of temperatures and flow rates. This device was reported to operate at high flow rates of up to 200 ml/min. However, the mean percentage of plasma collected in this device was about 3.5%.[54]

Another hydrodynamic separation approach termed hydrophoresis has been used to separate blood cells from plasma, by creating structured rotational flows with slanted structures and particle filters (Figure 1-7). In this device blood plasma was separated from diluted (1:2 in PBS) rat blood using a microfluidic device with 12 μm-height slanted obstacles at 0.5 μL min-1. Blood cells were focused to the right-side of the channel and approximately 30% of plasma was separated.[41]

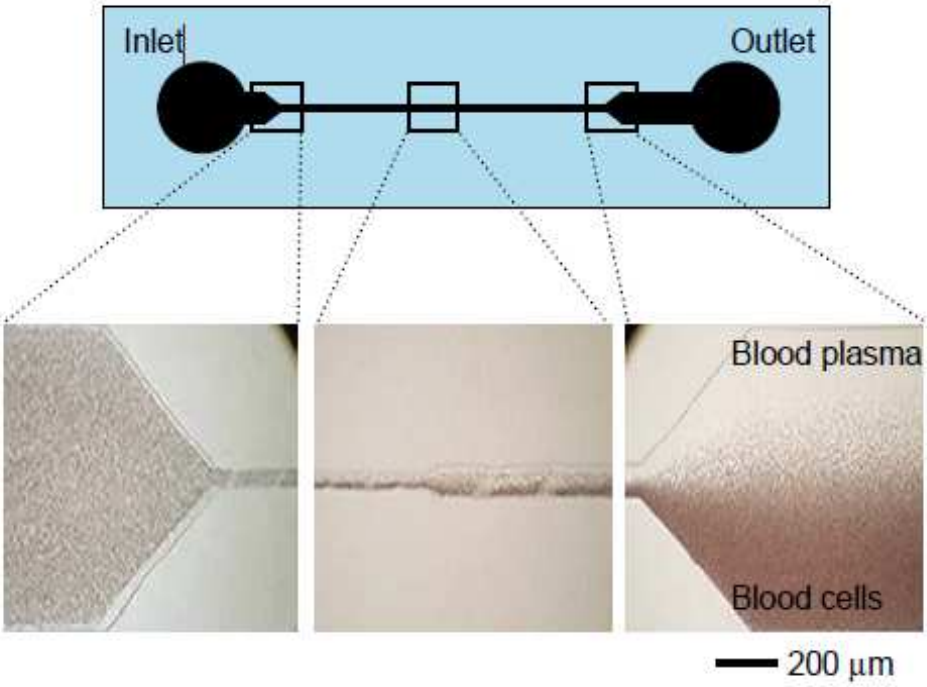

Figure 1-7: Schematics and a picture of the microfluidic channel using the hydrophoresis principle.[41]

Other specially designed microstructures within microfluidic devices have been used to directly filter plasma from blood. For example, in-situ polymerization was used to fabricate a microporous membrane within the microfluidic channel in order to separate

plasma from diluted (1:20) rabbit whole blood placed in a hypotonic solution using dead-end filtration (Figure 1-8). In this device a small volume of the pre-polymer is drawn into the channel by capillary pressure the channel is then tilted to move the pre-polymer into a desired location where it is photo-polymerized. (Figure 1-8 a). Filter channels are designed in the system and they are filled with the pre-polymer mixture. (Figure 1-8 b). Using this microdevice, separation of two samples of 3 μm and 45 μm fluorescent bead is shown in Figure 1-8 c. Additionally blood cells were separated from highly diluted rabbit whole blood but only 20 μl of plasma volume could be collected before the device was completely clogged due to accumulation of blood cells. (Figure 1-8 d). [45]

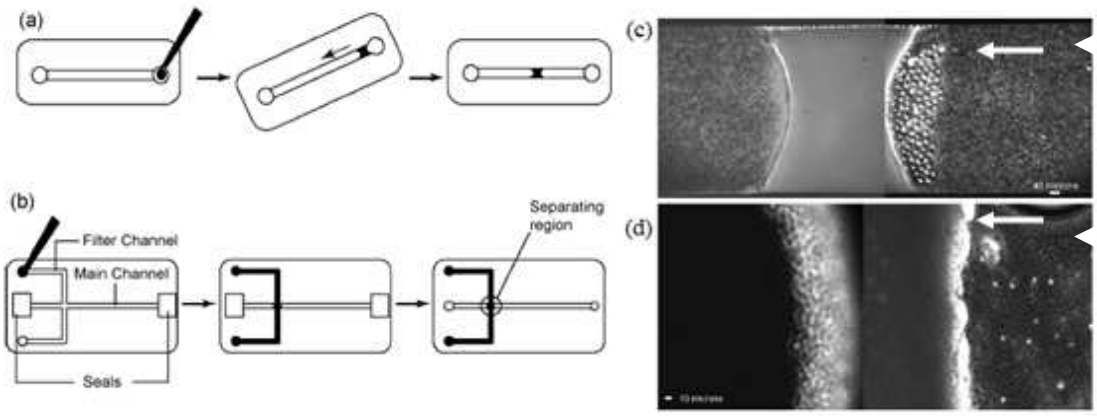

Figure 1-8: A membrane-based microfluidic device was fabricated using in-situ polymerization to fabricate a microporous membrane within the microfluidic channel in order to separate plasma from diluted blood. [45]

Alternatively, cross-flow filtration can be implemented to continuously clear particles from the filter surface, especially when dealing with complex fluids such as blood. In one report, a transverse-flow planar microfilter was designed to separate plasma from whole

bovine blood based on capillary action (Figure 1-9). In this device the filter was fabricated as a series of rectangular channels,‘‘pores’’, placed on both sides of the filtration channel. However, only a very small amount of plasma (maximum of 45 nl) was extracted after filtration and the quality of plasma was not tested since the plasma was not extracted from the device but significant hemolysis was observed as red coloration of the plasma. [36]

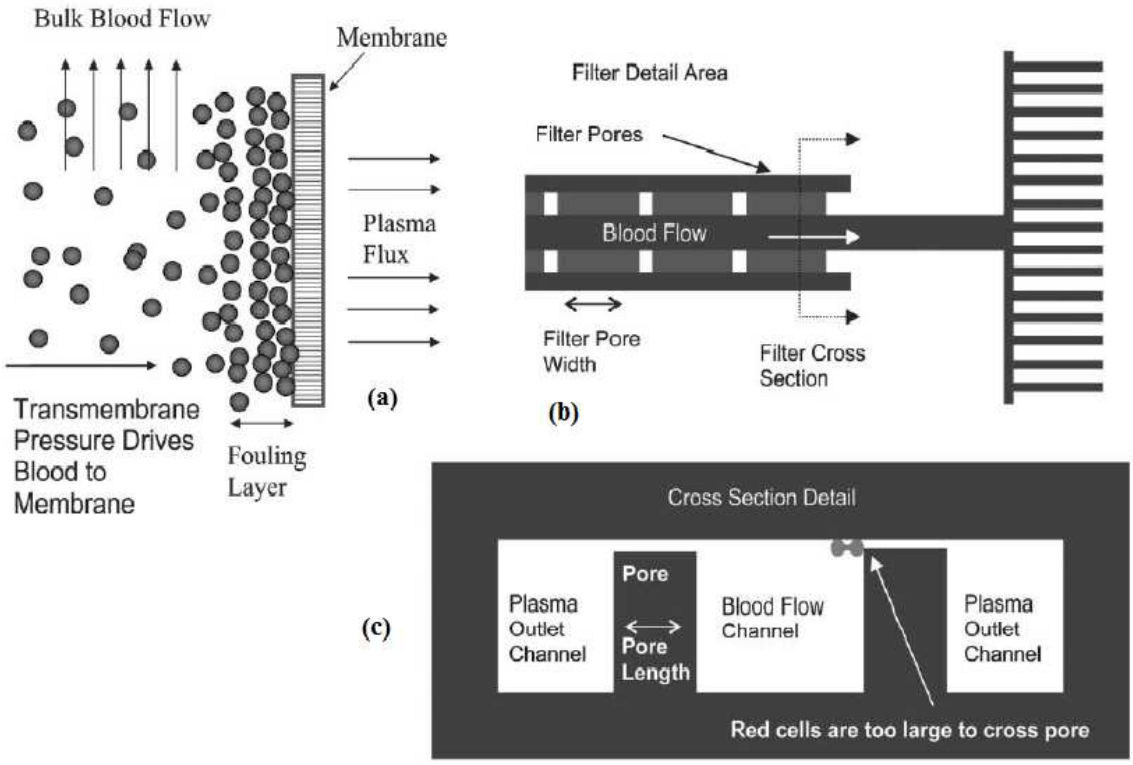

Figure 1-9: (a): Illustration of a Cross flow filtration using a flow parallel to a membrane. (b) Schematic of the microfilter (c) Microfilter cross section [36]

Porous polymer membranes have been also used as the semipermeable barrier in cross-flow filtration devices. These filters are commercially available in different pore size and

are very well suited for microfluidic blood applications as their pore size can be precisely selected at dimensions commensurate with blood cell exclusion. In one study, a microfilter with different types of commercially available porous polymer membranes was developed to separate plasma from whole blood. [47] However, while using this device, the filtrate showed evidence of hemolysis when the blood hematocrit was increased above 20% and fluid leakage around the filter was noted.

As described above, most of the reported plasma separation microdevices suffer from low separation efficiency, low throughputs, and leakage at high pressure, fouling and clogging which causes inconsistent output flow rates over time.

1.2.2.1 The Importance of Blood Model in Evaluation of Blood-Handling Microfluidic Devices

An important drawback of existing blood separations microfluidic devices is that they tend to involve blood dilution, either prior to entering or within the microfluidic device and more importantly almost none of the reported blood analysis microdevices have been tested in a clinical setting using undiluted whole blood.

A key factor to adequately and reliably predict a device's clinical performance, especially blood analysis devices is laboratory evaluation using a proper blood model. Factors such as blood species, RBC dimension, blood viscosity, blood hematocrit and blood temperature should be considered when evaluating a blood analysis system. Additionally, it is important to validate and predict blood damage attributed with engineering flow

parameters such as shear forces, cell exposure time and adverse biologic responses such as hemolysis and platelet activation.

Blood is a non-Newtonian fluid and its viscosity changes with shear rate. The non-Newtonian features of human blood comes from suspended cells in blood because studies have shown that plasma is a Newtonian fluid.[55] Red blood cells (RBCs) are the most important suspended particles in whole blood and the rheological properties of whole blood correlate highly with the concentrations of RBCs or blood hematocrit. Hematocrit is the volume percentage of red blood cells in whole blood and is the most important determinant of whole blood viscosity. The relation between the apparent viscosity and shear rate at different blood hematocrit level in whole blood (•), defibrinated blood (*x*), and washed cells in a Ringer solution (◦) is shown in Figure 1-10. As it can be seen in this figure at Hct=0 fluids behave Newtonian and small cell aggregation can affect the viscosity. As the hematocrit increases (Hct= 45%) at small shear rate cell aggregation can greatly affect the blood viscosity but it has less effects as shear rates increases. At very high hematocrit levels (Hct=90%) cell aggregations does not affect the blood viscosity. The figure also indicates that the human whole blood at all hematocrit levels has a higher viscosity compared to human defibrinated blood which does not have fibrinogen for cell aggregation. Also the viscosity of defibrinated human whole blood is higher than washed cell in ringer solution. Washed cell in Ringer solution is obtained by removing plasma and substituting it with a medium with near physiological conditions and this lowers the blood viscosity dramatically. These are important finding when using blood models for device evaluation as compared to real blood rheology. [56]

Blood viscosity also changes at different temperature which must be taken into account when evaluating the device performance. Figure 1-11 shows the relation between human blood and shear rate at different temperature.[56]

Performance of microfluidic devices using whole blood, defibrinated blood or washed cells in a ringer solution can vary because the viscosity varies between these three models which affect the blood flow resistance and therefore microdevice performance. The ideal blood model to evaluate the device is human whole blood with normal physiological hematocrit level.

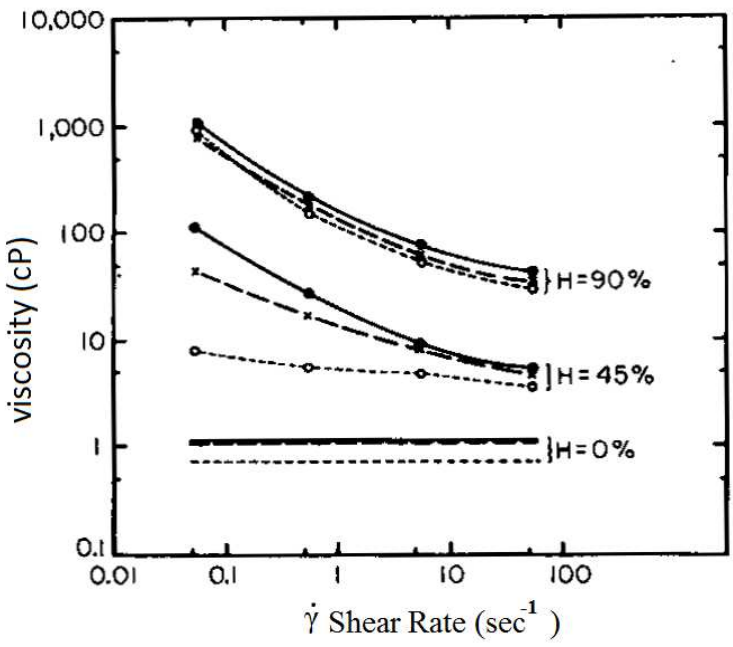

Figure 1-10: The relation between the apparent viscosity and blood hematocrit in whole blood (•), defibrinated blood (*x*), and washed cells in a Ringer solution (◦). From Fung[56]

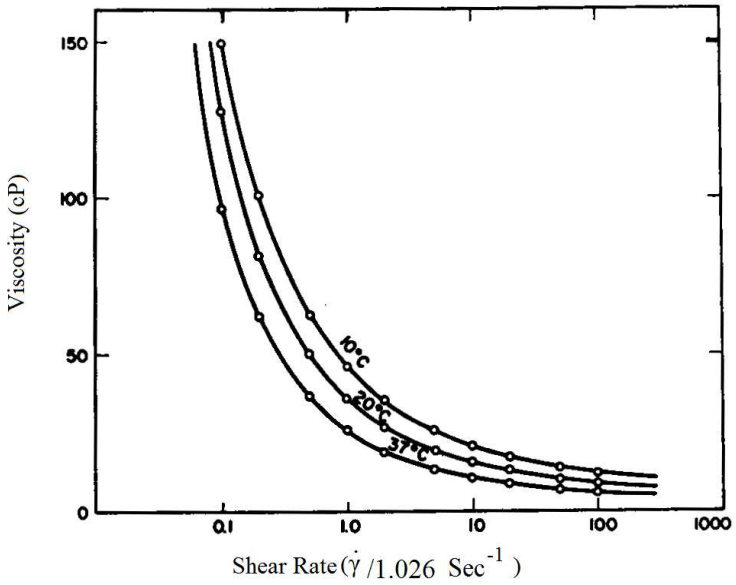

Figure 1-11: Relation between human blood and shear rate at different temperature, From Fung[56]

1.3 Research Objectives

The above discussion substantiates the need for the development of a disposable low-cost continuous plasma separation microdevice to improve upon existing microdevices. Membrane based filtration was used in this project because the mass flux between microfluidic channels can be precisely controlled by incorporating membranes with various pore sizes in between the channels. One approach toward membrane integration with microfluidic channels has been to construct a laminated device consisting of different layers of aligned microchannels separated by a porous polymer membrane. This approach was used to develop high throughput membrane-based cross-flow microfiltration microdevice to extract 100% cell-free plasma from unmodified whole blood, which can operate at high pressures with no evidence of membrane leakage. In

Chapter 2, the detailed description of the microfiltration device fabrication and transport mechanism is discussed.

In **Chapter 3**, various experimental set-ups were constructed to test the filtration efficiency of the microfiltration device using sheep's blood.

In **Chapter 4**, as a first step towards the incorporation of a microfiltration device in clinical settings, the microfiltration device was integrated with a simulated CPB circuit and was evaluated using freshly drawn human blood.

In **Chapter 5**, to further investigate the microfiltration device performance within a clinical environment, it was evaluated during in-vivo animal model of ECLS to continuously separate plasma protein from unmodified piglet whole blood.

In **Chapter 6**, the ability of a microfiltration device to separate bacteria from whole blood for sepsis treatment was tested.

Finally, conclusions and future work are discussed in **Chapter 7**

Chapter 2 : A Membrane-Based Microfiltration Device for Plasma separation from Whole Blood

2.1 Introduction

Among several available separation techniques, membrane-based filtration has been considered as one of the most promising techniques and also has been used in a wide range of field applications. [42, 43] Porous polymer membranes have been used as the semipermeable barrier in cross-flow filtration devices. These filters are commercially available in different pore size and are very well suited for microfluidic blood applications as their pore size can be precisely selected at dimensions commensurate with blood cell exclusion. These membranes are available in a wide range of materials and exhibit very high pore density and excellent filtration efficiency. Membrane-based filtration devices are usually easy to fabricate and very simple to handle. One approach toward membrane integration with microfluidic channels has been to construct a laminated device consisting of different layers of aligned microchannels separated by a porous polymer membrane. This approach was used to develop a high throughput membrane-based cross-flow microfiltration microdevice to extract 100% cell-free plasma from unmodified whole blood. The membrane-based microfiltration device developed in this work relies on a novel method of irreversible membrane integration with the microfluidic device which can operate at high pressure with no evidence of membrane leakage and with no sign of cell lysis or clogging for extended periods of time to improve upon existing microdevices.

2.2 Microfiltration Design and Basic Principles of Operation

The microfluidic microdevice which was designed based on cross-flow filtration, consisted of two PDMS layers of microchannels, separated by porous polycarbonate membrane (PCTE) (Nucleopore Polycarbonate Track-Etch Membrane, Whatman, Florham Park, NJ). The schematic of the two compartment microfiltration device is shown in Figure 2-1 and the schematics of alignment of the channels are shown in Figure 2-2.

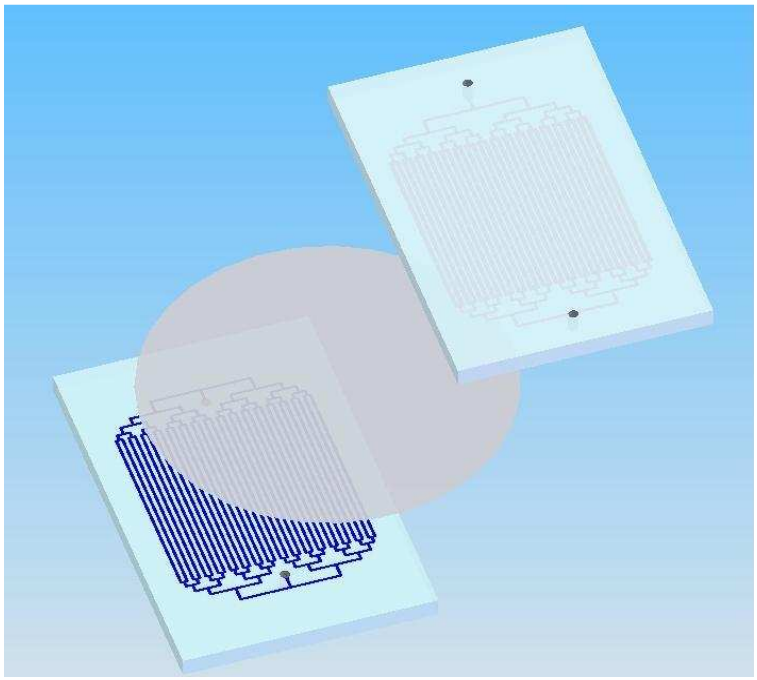

Figure 2-1: Schematic of the two compartment microfiltration device.

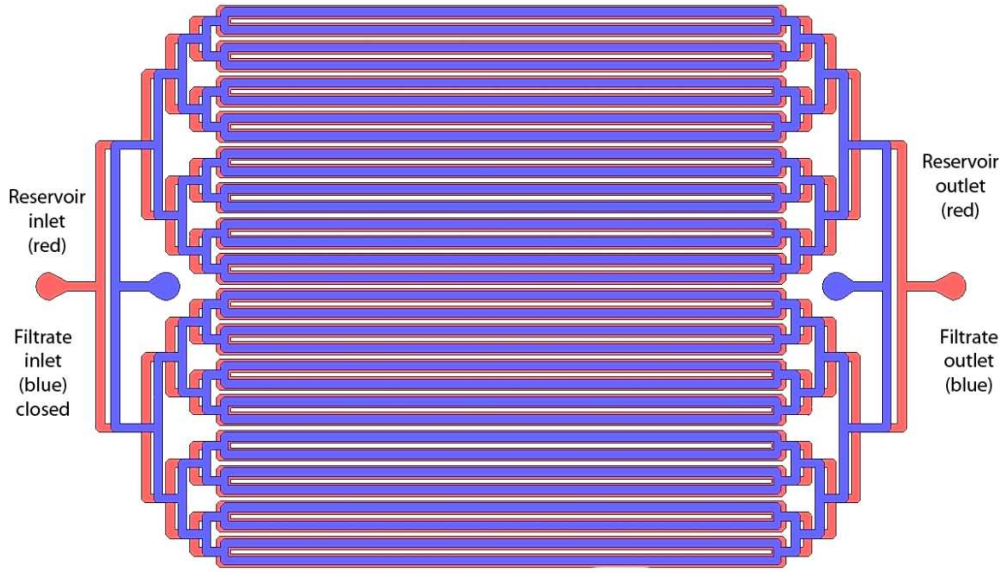

Figure 2-2: Schematics of alignment of the microfiltration channels (note: image was created by former lab member, Alex Fok)

Blood flows through the channels on one side of the device (reservoir channels) and filtrate plasma flows through the membrane and into the channels on other side of the membrane (filtrate channels). The schematic of cellular and molecular transport is shown in Figure 2-3. The membrane acts as a barrier between the large cells such as RBCs and small cells such as plasma proteins and is only permeable to cells and molecules smaller than its pore size.

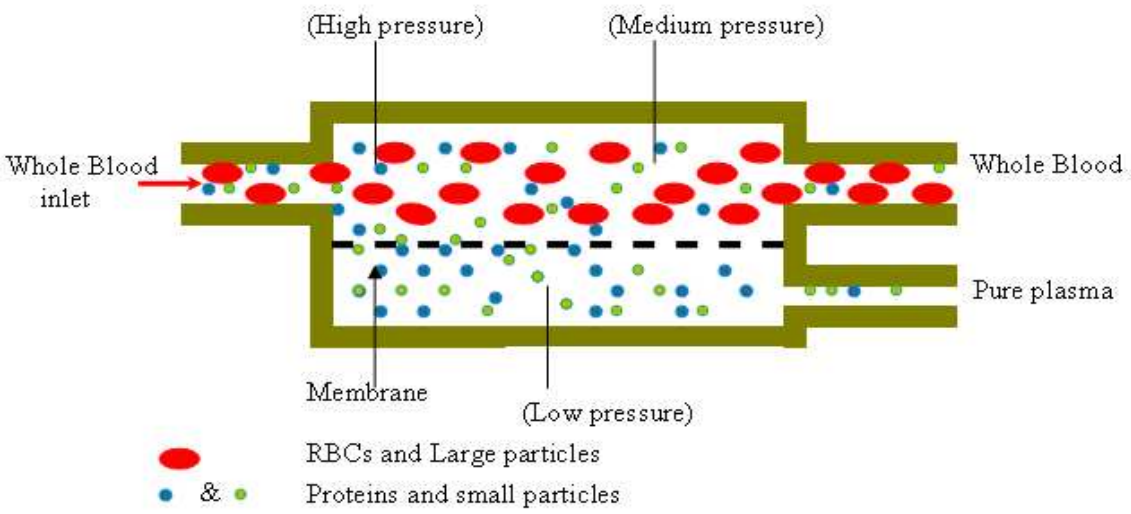

Figure 2-3: Schematics of the transport mechanism in membrane-based microfiltration device

After a blood sample is introduced into the reservoir channel, the pure plasma is filtered across the membrane based on the membrane pore size, the pressure in the reservoir channel and the relative flow resistances between the membrane and the reservoir and filtrate channel.A schematic illustration of a resistive electrical circuit corresponding to the hydraulic circuit of the microfiltration device is shown in Figure 2-4. In this model the notation and symbols are adopted similarly to that of electrical circuits.

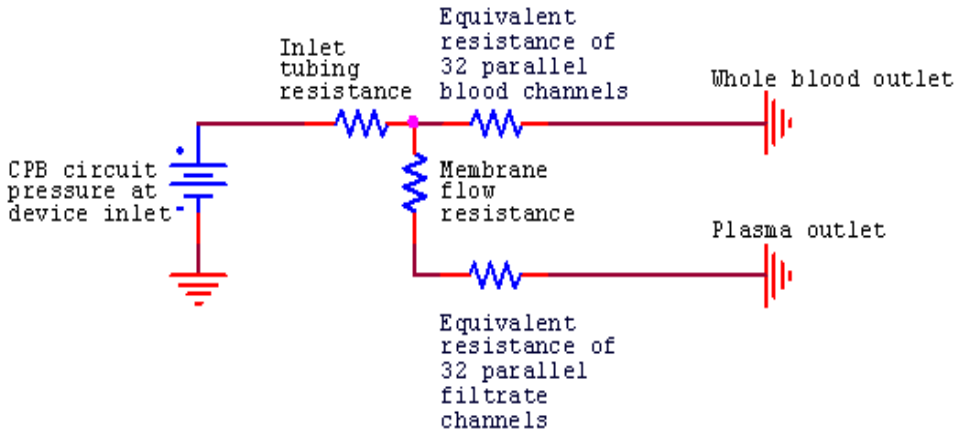

Figure 2-4: A diagram of a resistive circuit corresponding to the microchannel network of the microfiltration device

The voltage source at the input represents the circuit pressure at the blood inlet of the microdevice. R_{Rsrv} and R_{Filt} are resistances which represent the equivalent fluid flow resistance of the reservoir and filtrate microchannels respectively. R_m represents the membrane pore fluid flow resistance. The reservoir (blood) and filtrate (plasma) outlet are at atmospheric pressure, thus they are considered to be at ground potential.

The hydraulic resistance for the rectangular cross section channel (R_{Rsrv} and R_{Filt}) can be calculated using equation 2.1. [57]

$$R_{Rsrv} = \frac{12\mu L}{W H^3 N}\left[1 - \frac{H}{W}\left(\frac{192}{\pi^5}\sum_{n=1,3,5,\ldots}^{\infty}\frac{1}{n^5}\tanh\left(\frac{n\pi W}{2H}\right)\right)\right]^{-1} \tag{2.1}$$

In this equation, N is the number of channels, L is the length of each channel, μ is the dynamic viscosity of blood for the reservoir and the viscosity of plasma for filtrate solution, W is the width of a single channel, and H is the height of the channel

The mass transport across the membrane is due to pressure difference across the membrane. The flow resistance in a pressure-driven flow in cylindrical tubes (such as membrane pores) can be calculated assuming that the filtered plasma is incompressible and Newtonian and the pressure difference changes only across the membrane and neglecting the pressure drop along the microchannel. Hence, the Navier-Stokes equation (2.2) and the Continuity equation (2.3) for viscous incompressible fluid can be used to calculate the membrane pore resistance and the inlet tubing. [58]

$$\frac{\partial \boldsymbol{u}}{\partial t} + \boldsymbol{u} \cdot \nabla \boldsymbol{u} = -\frac{\nabla p}{\rho} + \nu \nabla^2 \boldsymbol{u} \tag{2.2}$$

In this equation is ν is the kinematic viscosity, u is the velocity of the fluid parcel, P is the pressure, and ρ is the fluid density.

$$\nabla \cdot \boldsymbol{u} = 0 \tag{2.3}$$

The membrane pore resistance can be calculated using equation 2.4

$$R_{Pore} = \frac{8\mu T}{\left[\pi \left(D/2\right)^4\right] N} \tag{2.4}$$

In this equation μ is the dynamic viscosity of blood plasma at 35 °C, T is the thickness of the membrane, D is the pore diameter and N is the number of pores exposed to blood. The number of pores is a function of the pore density and the available diffusion area and can be calculated using equation 2.5.

$$N_{Pore} = \rho_{Pore} A = \rho_{Pore} (N_{Chan} W_{Filtrate} L) \quad (2.5)$$

In this equation ρ_{Pore} is the pore density which varies depending on the manufacturer's specifications (see Table 2-3) and A is the total filtration channel's area.

However, the results obtained from the resistive electrical circuit model may not be applicable for an actual microfiltration microdevice because the separation efficiency greatly depends on the molecule size and shape, protein biofouling with long-term blood infusion and complications due to membrane pores being clogged at high flowrate.

2.3 Fabrication

The microfiltration device consists of two layers of microchannels, separated by a porous polycarbonate membrane. Blood flows on one side of the membrane (reservoir channels) and plasma flows through the membrane and to the other side of the membrane (filtrate channels). The microfluidic microdevice was fabricated in polydimethylsiloxane (PDMS) (Sylgard 184, Dow Corning, Midland, MI) using soft lithography.[59, 60] .The chrome mask was used in contact photolithography with negatively patterned SU-8 photoresist (MicroChem, Boston, MA) on a silicon wafer and then PDMS was molded against the master. The mask of the fluidic channels is shown in Figure 2-5.

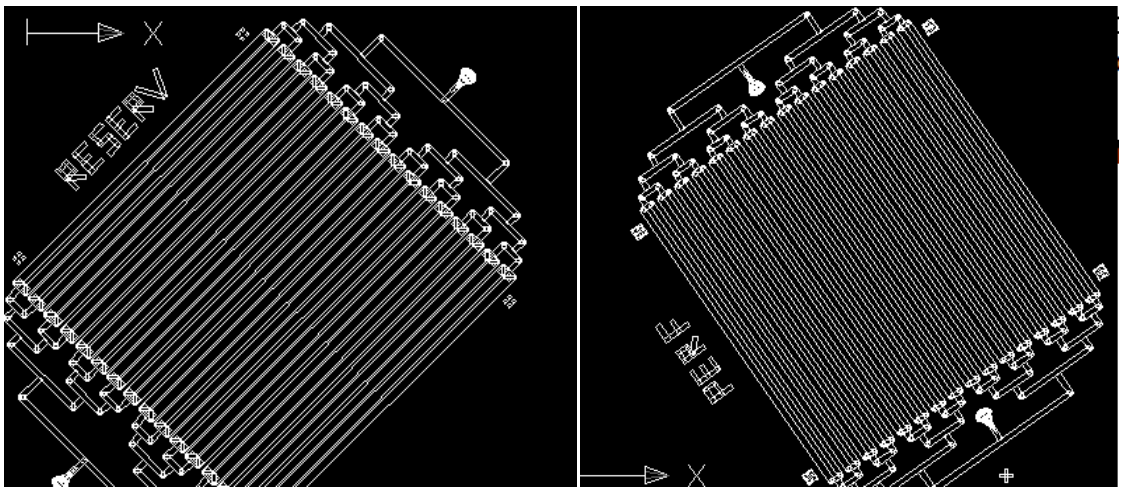

Figure 2-5: (Left) Mask for SU8 reservoir microfluidic channels. (Right) Mask for filtrate microfluidic channels

In order to fabricate the filtrate channels, SU-8 2025 was used (soft lithography process flow is shown in Table 2-1. SU-8 2150 was used to fabricate the reservoir channels (soft lithography process flow is shown in . The reservoir channel was designed to be 600 μm wide and filtrate channel was designed to be 400 μm wide and both channels were 25 mm long. Having a wide reservoir channel will reduce the risk of high shear stress which can irreversibly damage and lyse the red blood cells. To maximize the filtration area 32 parallel channels were designed in each layer. The microfluidic channel in the reservoir side was determined to be 135 μm thick, and the microfluidic channel in the filtrate side was determined to be 40 μm thick after the standard SU-8 soft lithography procedures.

Table 2-1: Photolithography procedure for 40 micron thick Filtrate Channel using SU-8 2025

Process Flow	Description	Time
Substrate Cleaning Procedure	• Soaking the silicon substrate in acetone solution • Soaking the silicon substrate in isopropyl alcohol (IPA) • Soaking the silicon substrate in deionized (DI) water • Rinse under DI water • Blow dry with filtered nitrogen or filtered air and place in the oven at 200 ºC	10 min 10 min 10 min 2 min 30 min
Spinning Photoresist	• Dispense 1 ml of photoresist for each inch of substrate diameter. • Spin at 500 rpm with acceleration of 100 rpm/second • Spin at 2875 rpm with acceleration of 300 rpm/second	5-10 sec 30 sec
Soft Bake	• Place on a hot plate of 65ºC • Place on a hot plate of 95ºC	2 min 5 min
Exposure	• Under the UV lamp exposure energy of 300 mJ/cm^2	------
Post Exposure Bake	• Place on a hot plate of 65ºC • Place on a hot plate of 95ºC	1 min 3 min
Develop	• Soak in SU-8 developer	5 min
Rinse and Dry	• Rinse in IPA and dry	-------

Table 2-2: Photolithography procedure for 130 micron thick Reservoir Channel using SU-8 2150

Process Flow	Description	Time
Substrate Cleaning Procedure	• Soaking the silicon substrate in acetone solution • Soaking the silicon substrate in isopropyl alcohol (IPA) • Soaking the silicon substrate in deionized (DI) water • Rinse under DI water • Blow dry with filtered nitrogen or filtered air and place in the oven at 200 ºC	10 min 10 min 10 min 2 min 30 min
Spinning Photoresist	• Dispense 1 ml of photoresist for each inch of substrate diameter. • Spin at 500 rpm with acceleration of 100 rpm/second • Spin at 3000 rpm with acceleration of 300 rpm/second	5-10 sec 30 sec
Soft Bake	• Place on a hot plate of 45ºC • Place on a hot plate of 65ºC • Place on a hot plate of 85ºC • Place on a hot plate of 95ºC • Place on a hot plate of 85ºC • Place on a hot plate of 75ºC • Place on a hot plate of 55ºC	5 min 5 min 10 min 30 min 5 min 5 min 2 min
Exposure	• Under the UV lamp exposure energy of 280 mJ/cm^2	------
Post Exposure Bake	• Place on a hot plate of 55ºC • Place on a hot plate of 65ºC • Place on a hot plate of 85ºC • Place on a hot plate of 95ºC • Place on a hot plate of 85ºC • Place on a hot plate of 65ºC	2 min 4 min 3 min 10 min 3 min 3 min
Develop	• Soak in SU-8 developer	15 min
Rinse and Dry	• Rinse in IPA and dry	-------

2.4 Membrane Material

In order to develop an efficient blood separation technology, a polycarbonate material was selected. Polycarbonate membranes (PCTE) are made from a thin, microporous polycarbonate film material which is well-suited for blood assays. PCTE membranes are commercially available with varying pore sizes and density as shown in Table 2-3. Figure 2-6 and Figure 2-7 show SEM images of 200 nm and 400 nm pore-size PCTE membranes.

Table 2-3: PCTE membrane performance characteristics (www.sterlitech.com)

Pore Size (a) (um)	Pore Density (b) (pores/cm^2)	Nominal Weight (mg/cm^2)	Nominal Thickness (c) (um)
20	4×10^4	1.1	3
14	5×10^4	0.6	6
12	1×10^5	0.9	8
10	1×10^5	1.1	10
8	1×10^5	0.8	7
5	4×10^5	1.1	10
3	2×10^6	0.9	9
2	2×10^6	1.1	10
1	2×10^7	1.1	11
0.8	3×10^7	0.9	9
0.6	3×10^7	1.0	9
0.4	1×10^8	1.0	10
0.2	3×10^8	1.1	10
0.1	4×10^8	0.7	6
0.08	4×10^8	0.7	6
0.05	6×10^8	0.7	6
0.03	6×10^8	0.7	6
0.01	6×10^8	0.7	6

a. Tolerance + 0%m -20%
b. Tolerance +/-15%
c. Tolerance +/-10%

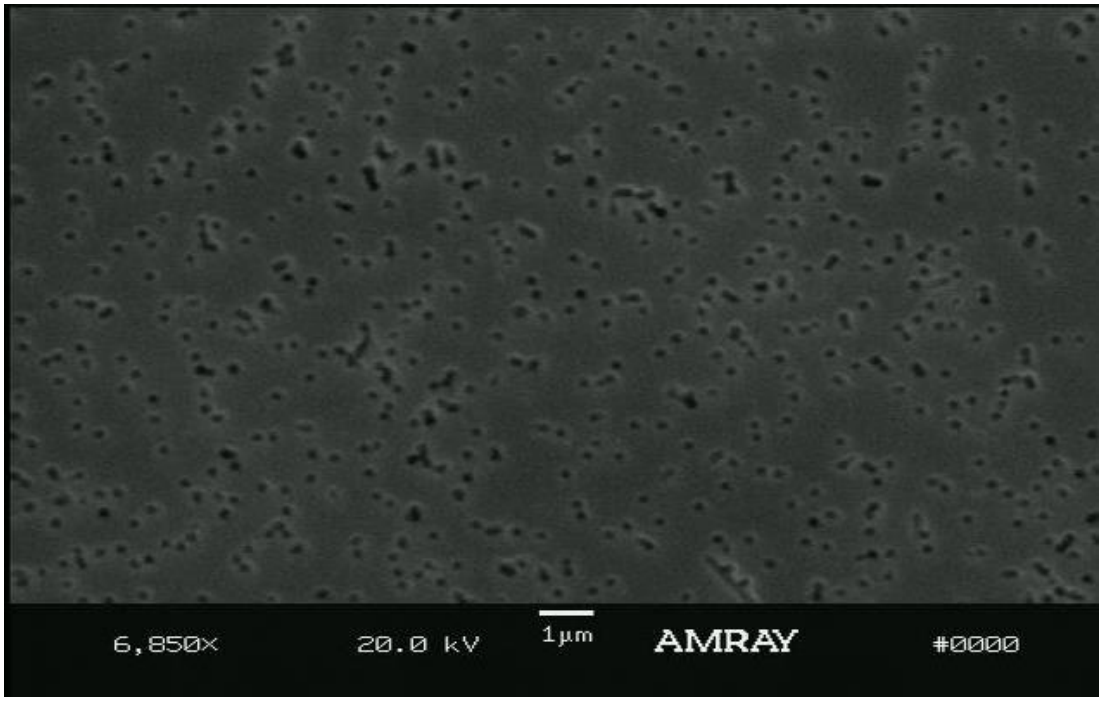

Figure 2-6: SEM image of a 200 nm pore size PCTE membrane

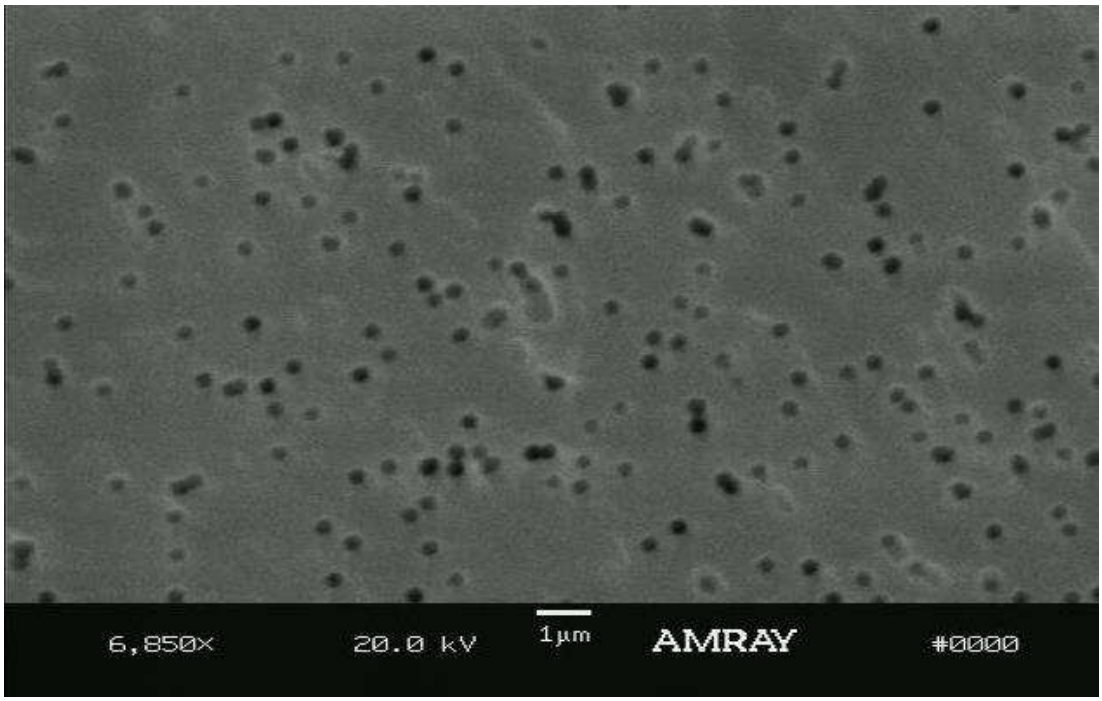

Figure 2-7: SEM image of a 400 nm pore size PCTE membrane

The biocompatibility of the material is a key factor for the material used for blood handling devices. Exposure of blood to non-physiological surface of the membrane can leads to immediate protein adsorption of plasma proteins at the membrane surface. The initial adsorption of albumin and/or fibrinogen results in adsorption and adhesion of other blood proteins and platelets which ultimately result in polymerization of fibrin onto the surface and reducing the filtration efficiency and ultimately membrane clogging. [61] Polycarbonate membranes are reported by the manufacturer to be low in protein binding However, the advantage of using biocompatible material to reduce protein adsorption can be extended by coating the surface of the membrane with anticoagulant.[62]. Anticoagulation can be used to modulate thrombus formation by chemically arresting the coagulation pathway to extend membrane lifetime.

2.5 Methods of integrating membranes into devices

A critical design consideration in fabricating a membrane based filtration microdevice is how to best achieve reliable bonding between different membrane materials with molded PDMS or glass microfluidic layers.[63] Bonding of membrane and device materials is further complicated in devices consisting of multiple channel layers or complex channel designs. Various approaches to bonding PDMS to polymer membranes have been reported, such as direct thermal bonding or bonding following plasma oxidization. In thermal bonding the layers are gently pressed together and cured at a temperature higher than the membrane material's glass transition temperature. Thermal bonding can create permanently laminated structures, but also tends to cause wrinkling of the membrane due to the different thermal expansion coefficients of the individual layers. It can also cause distortion of the membrane's pores or complete pore collapse, changing the membrane

transport properties. Oxygen plasma activation of both the membrane and PDMS surfaces followed by direct bonding can create laminated structures. However, plasma activation only creates a weak bond between the membrane and the PDMS microdevice for a wide range of membrane materials including polycarbonate (PCTE), polyethersulfone (PES), and polyethylene terephthalate (PETE). Another popular bonding method involves the use of epoxy or PDMS prepolymer as an intermediate ‘‘glue’’ layer between the PDMS and the membrane to improve the bonding strength.[63-66] This approach presents problems such as partially clogging the membrane's pores and thus reducing the flux across the membrane, as well as the trapping of air bubbles along the membrane boundaries and PDMS channels.[63, 66] In one of the reported techniques, the use of PDMS prepolymer liquid as a bonding glue was implemented by adjusting the thickness of the glue layer to avoid gap formation along the edges of the membrane when it is sandwiched between two PDMS layers.[64] In this method the thickness of the PDMS glue was adjusted by mixing uncured PDMS to various concentrations in toluene. Thin film deposition was another bonding approach investigated in which the membrane is coated with a thin SiO_2 layer by sputtering for direct plasma bonding of the membrane to PDMS structures.[67] This method is not only more expensive but also relies upon the amount of SiO_2 sputtered on the membrane surface, and this may cause inconsistent bonding results and changes in membrane transport properties. A final approach for incorporating membranes into microfluidic devices is to encapsulate a piece of membrane within a cavity in a bonded PDMS–PDMS device.[68] In this type of incorporation, the membrane is not physically bonded with the structure, but is instead constrained at the edges by the PDMS bond. In this case it is possible for fluid to leak around the edges of

the membrane at high pressures, and the membrane may become distorted if the PDMS is stretched.

Recently, a new method has been proposed for bonding between polymethylmethacrylate (PMMA) and PDMS plates, as well as between two PMMA plates [69]. This method is based on the chemical surface modification of the substrates and does not require pressure or high temperatures to initiate the bond. In this method, an organic polymeric substrate is coated with a silane solution of 3-aminopropyltriethoxysilane (APTES), followed by plasma activation of the surfaces to be bonded, resulting in an irreversible bonding of the two substrates. APTES has been used in various applications as a coupling agent or adhesion promoter and pretreatment for coatings. In another study, APTES was used to modify the surfaces of silicon or glass substrates in order to bond these substrates to chemically activated fluorinated ethylene propylene (FEP).[70]

2.6 Developing a Novel Method for Membrane Integration using APTES Modification

In this study, the use of APTES was extended as a method for integration of nanoporous polycarbonate (PCTE), polyethersulfone (PES) and polyester terephthalate (PETE) membranes to PDMS and glass microfluidic channels with an irreversible bond. The three membrane types tested have been selected because they have been specifically developed for low protein binding, and have been widely used in microfluidic systems. Therefore, developing a reliable bonding method can be extremely beneficial to facilitate integration of these types of membranes to microfluidic devices.

2.6.1 Experimental Methods

2.6.1.1 Bonding of Porous Polymer Membrane to PDMS and Glass Substrates

The bonding procedure for direct bonding of a membrane to a PDMS or glass substrate is shown schematically in Figure 2-8. A commercial solution of APTES (Sigma-Aldrich, St. Louis, USA) was diluted in water to 5% by volume and placed on a ceramic-top hotplate set to 80°C. PCTE, PES, or PETE (SterlitechInc Kent, USA) membranes were activated in an oxygen plasma chamber for 1 min (600 mTorr, 100 W) and then immersed in the APTES solution for 20 min. The solution was covered during the heating process to prevent water evaporation. After 20 min., the membrane was removed from the APTES solution with tweezers and was placed on a cleanroom wipe to dry. Then, the surfaces of the membrane and a fully cured PDMS microdevice were activated in an oxygen plasma chamber (600 mTorr, 100 W) for 20 seconds (Figure 2-8a). The membrane and the treated microdevice were immediately brought into contact (Figure 2-8b). When the membrane comes in contact with the PDMS device, an immediate irreversible bond is formed. In order to bond the membrane to multiple PDMS layers in a sandwich structure, after bonding the membrane to PDMS as described above, the bonded laminate and a second PDMS layer were similarly activated in an oxygen plasma, brought into contact and subsequently pressed together (Figure 2-8c).

The membrane/PDMS laminate could also be bonded to the second plasma-treated PDMS layer without plasma activation of the bonded laminate. For PCTE and PETE membranes, the bonding was instantaneous and no pressure was applied to initiate the bond. However, for PES membranes, pressure was applied by means of a weight placed

on top of the layered structure for 24 hours in order to achieve a strong and reliable bond between the PES membrane and PDMS layer.

For glass microdevices the same procedure was carried out substituting glass for the PDMS layers, and a similar irreversible bond was obtained. A longer bonding time (at least 48 hours) was required in order to achieve irreversible bonding between PES membranes and glass microdevices.

Also, the surface of the glass or PDMS could be functionalized using a corona discharge instead of an oxygen plasma. However, a corona discharge should not be used to activate the membrane surface since the discharge often damages the membranes creating small tears where the discharge contacts the membrane. It has also been found that while the bonding between oxygen plasma-treated PDMS and a membrane is immediate for PCTE and PETE membranes, it takes about a minute for these membranes to bond to corona-treated PDMS. However, no external pressure is needed to initiate the bonding in either case. The APTES functionalized membranes can be peeled off from corona-treated PDMS and realigned within the first minute. This may be useful for accurate alignment between different layers of multi-layer devices.

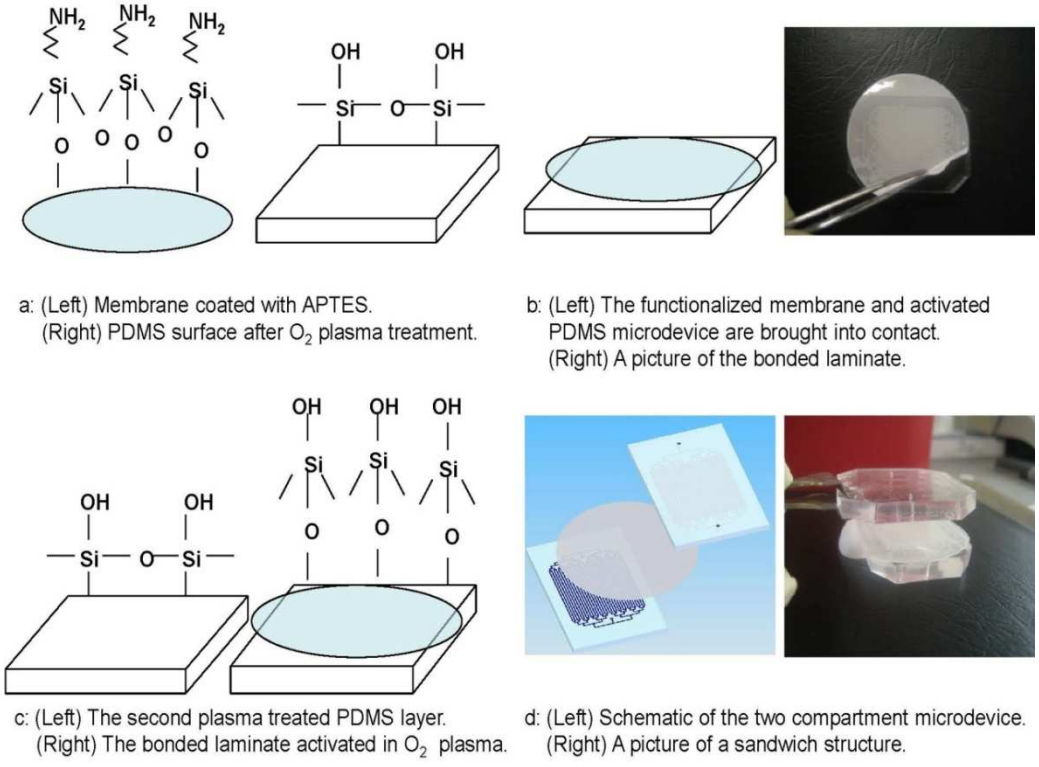

Figure 2-8: Schematic of the bonding process between a porous membrane and a PDMS substrate.

2.6.1.2 Bond Strength Testing

To measure the maximum pressure that the integrated microdevice was able to withhold without the membrane delaminating from the PDMS layers, water was infused into the inlet of the reservoir channels at a flow rate of 120 µl/min via a syringe pump, and the outlet of the reservoir was blocked and connected to a pressure sensor with a maximum pressure reading of 227.8 kPa (Honeywell Sensing and Control, ASDX030G24R). The inlet and outlet of the filtrate channels were blocked to allow pressure to build within the device. The pressure within the device was recorded to determine the burst pressure of

the device. In this study, two other commonly used bonding methods were evaluated on identical test devices to compare each technique. In one method, the PCTE membrane was bonded to the PDMS layers by using the previously reported PDMS prepolymer glue technique[3]. In another method a low viscosity two-part epoxy (EPO-TEK 301, Epotek, Billerica, MA) was used to bond the PCTE membrane to PDMS. The results obtained from these two techniques were compared with that of using APTES surface modification for bonding. Each device was tested in three conditions to simulate common device storage conditions: 1) evaluating the devices right after infusing water into dry devices; 2) after filling the device with water for 72 hours; 3) after submerging the devices in water for 72 hours.

2.6.2 Experimental Results

The use of APTES for microchannel-membrane bonding allowed the fabrication of complex channel designs with integrated porous membranes and multilayer PDMS or glass multichannel structures. Irreversible bonding between the microchannel and membrane layers without deformation of the channel structures or membrane was achieved. The bonding was leakage free along the channels and membrane edges. The bonding strength was preliminarily evaluated after bonding PDMS or glass to both PCTE and PETE membranes by attempting to manually peel the membrane from a glass or PDMS microfluidic device. The membrane could not be peeled from the microchannel surface without breaking the membrane into small pieces, or ripping a piece of PDMS from the structure indicating the strength of the bond was greater than the fracture strength of the materials. The results from testing the APTES bonding strength under applied pressure via a pressure sensor showed that the membrane bond was able to

withhold more than 227.8 kPa, which was the maximum limit of the pressure sensor, without any sign of delamination (Figure 2-9).

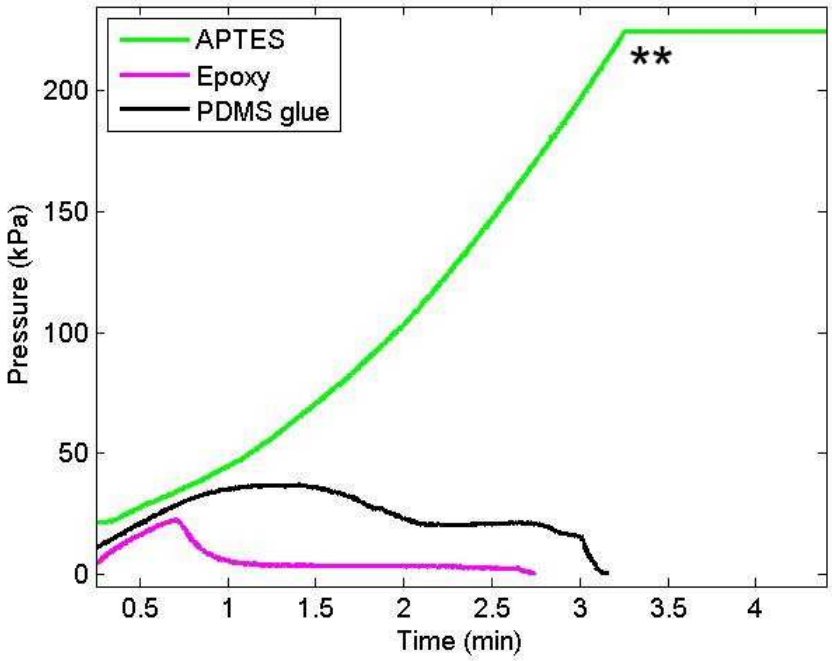

Figure 2-9: Representative plots showing burst pressure for dry devices using three different bonding techniques. The APTES coated membrane was able to withhold much higher pressure (more than 227.8 kPa) compared to PDMS or epoxy bonded membranes.

**** Maximum limit of the pressure sensor.**

The pressure in this test was only relieved by the inlet tubing becoming physically dislodged from the device. To compare the bonding strength of this technique over those using PDMS pre-polymer or two-part epoxy glue, identical test devices were used under applied pressure. The results shown in Table 2-4 demonstrate that for the same experimental conditions there is a significant increase in bonding strength using the

APTES surface modification technique. To further test the bonding strength in the presence of water, two additional tests were carried out. In one test, the channels of the microdevices were filled with water and stored at room temperature for 72 hours. In another test the microdevices were filled and completely immersed in water for 72 hours.

Table 2-4: Comparison of bonding methods in different storage conditions

Test Method	Dry Device	Channels filled with water (72 hours)	Device submerged in water (72 hours)
APTES surface modification	> 227.8 kPa	> 227.8 kPa	132.2 kPa
PDMS glue	26.58 kPa	12.5 kPa	0 kPa, membrane delaminated
Epoxy glue	22.31 kPa	13.25 kPa	0 kPa, membrane delaminated

The bonding strength for APTES coated membranes remained very strong (over 227.8 kPa) in devices stored at room temperature for 72 hours with the device channels filled with water, but decreased dramatically in glued membranes. Complete immersion of the devices in water for an extended period of time weakened the membrane bonding strength for all three tested bonding methods. The maximum pressure the APTES bonded membrane withheld after complete immersion in water was 132.2 kPa, compared to the glued devices which completely delaminated when water infusion began and thus supported no pressure. While the APTES bonded membrane started to delaminate from

the channel walls at a pressure of 132.2 kPa, it did not separate from the PDMS at the edges of the microdevice. After about 10 minutes the PDMS began to bulge which eventually caused the membrane to rupture. The APTES bonding strength was further evaluated in a device stored at room temperature for 30 days with the device channels filled with water, and was able to withstand over 187 kPa, which still indicates a robust bond between the APTES coated membrane and PDMS layers.

2.7 Evaluation of APTES Coated Porous PCTE Membrane after Blood Exposure

The polycarbonate membranes used in this study were reported by the manufacturer to be hydrophilic and low in protein adsorption. However, since the membranes surface were modified via APTES in order to create the laminated structures, it was critical to identify any unfavorable biological interactions or excessive protein adsorption due to APTES treatment, which could potentially alter the membrane filtration properties. The influence of APTES conjugation on biofilm formation in polycarbonate material was studied using Quartz Crystal Microbalance with Dissipation monitoring (QCM-D). Additionally the effect of APTES coating on physical properties of the membrane pores and biofilm formation on the PCTE membrane surface was evaluated by measuring the filtrate flowrate over time and evaluating the membrane morphology using Scanning Electron Microscopy (SEM).

2.7.1 Quartz Crystal Microbalance with Dissipation monitoring (QCM-D).

In order to study protein adsorption occurring at the membrane surface, a Quartz Crystal Microbalance with Dissipation monitoring (QCM-D) (Q-Sense, Goteborg, Sweden) and

gold coated quartz crystals with fundamental resonant frequency of 5 MHz and a diameter of 14 mm were used. QCM-D is a well suited technology for dynamic monitoring of the absorbed protein mass onto material surfaces.[71, 72]

2.7.1.1 Experimental setup

The crystals were cleaned prior to experiments by soaking them in tetrahydrofuran (THF) for 15 min followed by exposure at 80 °C to a 5:1:1 by volume mixture of distilled water, ammonium hydroxide and hydrogen peroxide for 15 min. The quartz crystals were then thoroughly rinsed with deionized water and gently blown dry under a flow of nitrogen gas and placed in a UV chamber for 10 minutes. The gold side of each crystal was then coated with 50 nm of 1% w/v polycarbonate polymer solution in chloroform (Fisher Scientific) and left in a vacuum chamber for 24 hours. Two polycarbonate coated crystals were mounted in two separate QCM-D flow chambers with the coated surface exposed to the solution and a stable baseline response of the quartz crystals in water at 80 °C was established. In preparation for adsorption of APTES modified surface, 5% APTES solution (prewarmed to 80 °C prior to use) was perfused through one flow chamber, at a high flow rate of 0.117 ml/min (in order to maintain the 80 °C temperature for polymer-APTES interaction) for 20 min while water was still perfused through the other flow chamber. This procedure of treating the polycarbonate coated crystals with APTES was similar to the procedure carried out to treat the polycarbonate membranes in the fabrication of the microdevices. The system was then left to cool down and stabilized at 35 °C (normothermia). In order to compare the adsorption of protein into both APTES treated and non-coated crystals, first phosphate buffered saline (PBS) was perfused through both chambers for 20 minutes and then sheep's blood plasma was perfused

through the system at a flow rate of 80 µl/min for 20 minutes. Desorption was performed immediately after the adsorption reached steady state by replacing the plasma solution with PBS solution and the final frequency change at each time point was measured in the presence of PBS after it reached the steady state. This procedure was repeated 4 times to study protein adsorption over time. The kinetics of plasma protein adsorption and desorption were followed by changes in resonant frequency and dissipation.

In order to obtain the thickness of the adsorbed protein layer, raw frequency and dissipation data obtained from QCM-D were experimentally fit to a Voigt model described by Voinova et al, using the supplied software.[73] According to this model the relationship between the frequency and dissipation shifts (Δf and ΔD) can be fit to the following the equations:

$$\Delta f \approx \frac{1}{\pi \rho_0 h_0}\left\{\frac{\eta_3}{\delta_3}+h_1\rho_1\omega-2h_1\left(\frac{\eta_3}{\delta_3}\right)^2\frac{\eta_1\omega^2}{\mu_1^{\,2}+\omega^2\eta_1^{\,2}}\right\} \tag{2.7}$$

$$\Delta D \approx \frac{1}{\pi f \rho_0 h_0}\left\{\frac{\eta_3}{\delta_3}+2h_1\left(\frac{\eta_3}{\delta_3}\right)^2\frac{\eta_1\omega}{\mu_1^{\,2}+\omega^2\eta_1^{\,2}}\right\} \tag{2.8}$$

In these equations the viscoelastic properties of the protein layers are represented as four parameters: layer density (ρ_1), viscosity (η_1), shear elasticity (μ_1), and thickness (δ_1). ($\rho 0$, $h0$) are crystal density and thickness, (ρ_3, η_3, δ_3) are liquid density, viscosity and thickness and ω is the angular frequency of oscillation. The fixed parameters used in

the experimental fitting were (i) layer density ρ_1=1200 kg/m^3 (density of the layer should lie approximately between that of protein layer (1400 kg/m^3) and trapped water (1000 kg/m^3), (ii) fluid viscosity η_3= 0.001 Pa-s, and (iii) fluid density ρ_3= 1000 kg/m^3. The fitted parameters were (i) layer viscosity between η_1 =0.0005–0.01 Pa-s, (ii) layer shear modulus between μ_1 =10^4–10^9 Pa, and (iii) layer thickness between δ_1 =0–5*10^{-7} m. The mass of protein adsorbed can then be calculated using the calculated layer density and thickness. [74]

.

2.7.1.2 Results

The typical adsorption of plasma proteins onto the polycarbonate-coated crystal surface was monitored, with and without APTES modification, in real time, by simultaneously measuring of Δf s and ΔDs using QCM-D. Figure 2-10 shows a schematic diagram of the protein adsorbed to the polycarbonate polymer on a quartz crystal surface.

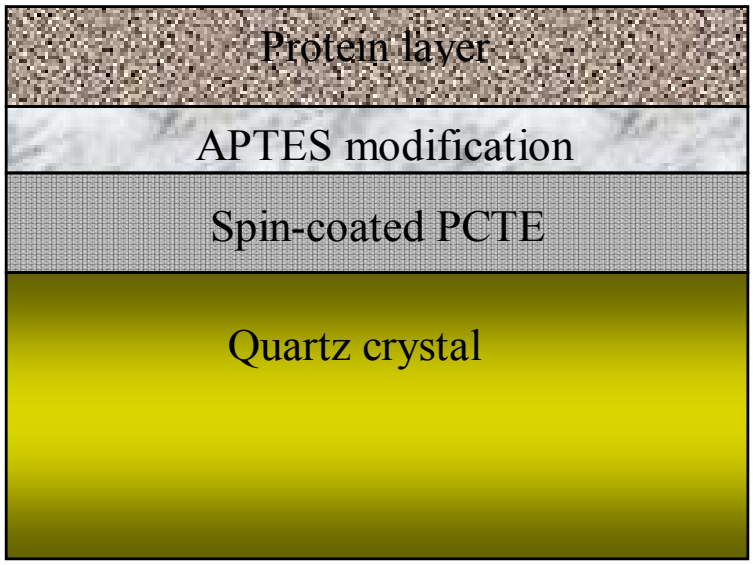

Figure 2-10: A schematic diagram of the protein polymer adsorption on a quartz crystal surface.

Figure 2-11 and Figure 2-12 show representative Δf_5 and ΔD_5 for both APTES modified and unmodified polycarbonate as functions of time when QCM-D is alternately exposed to plasma and PBS solutions. The arrows indicate the injection time of plasma, and the labels time 1 though time 4 indicate several periods of rinsing steps using PBS. Protein adsorption causes a rapid initial frequency decrease (mass increase) accompanied by a dissipation factor increase at the same rate, until the protein adsorption saturated when a slower frequency change was observed. After exchanging the plasma solution with PBS to remove the non-adherent proteins, the frequency increased again. The actual mass adsorbed to the surface was measured when the system response stabilized during PBS exposure.

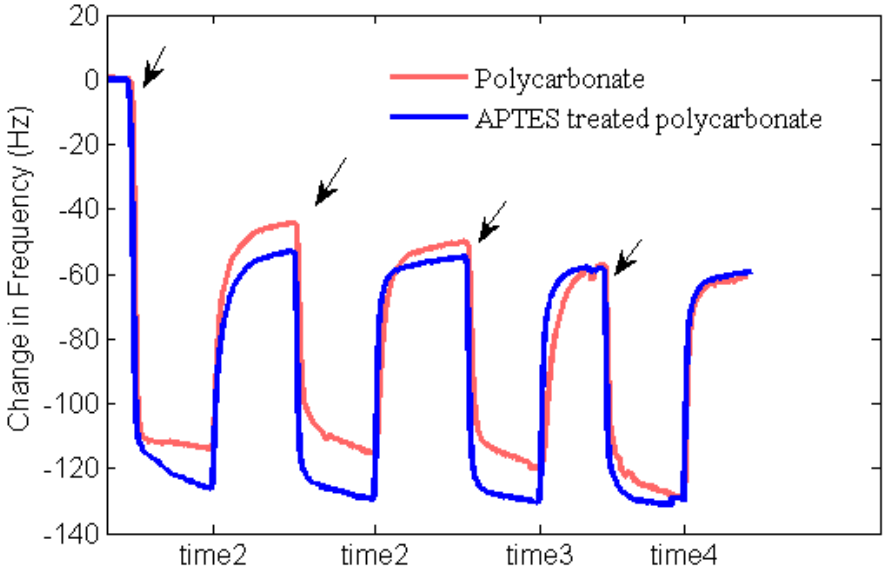

Figure 2-11: Frequency shift (Δ*f*) induced by the adsorption of plasma proteins as a function of time.

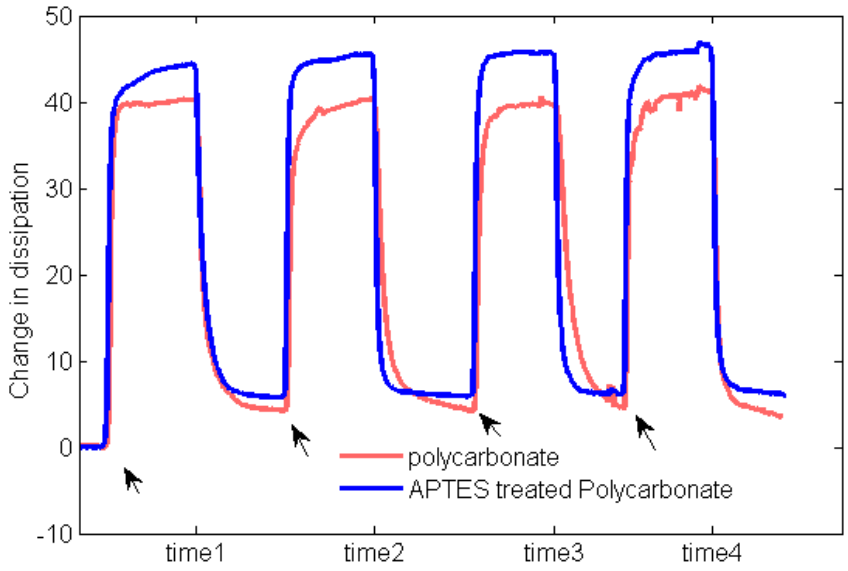

Figure 2-12: Dissipation shift (Δ*D*) induced by the adsorption of plasma proteins as a function of time.

Figure 2-13 shows the calculated mass adsorbed to the surface of APTES treated and untreated polycarbonate polymer on the quartz crystal obtained from the QCM-D data. The mass of protein initially adsorbed on untreated polycarbonate material was about 0.97 ng/m^2, whilst the mass adsorbed on APTES treated polycarbonate material was approximately 20% higher. However, the small standard deviation for both the APTES treated (σ=0.04) and non-treated (σ=0.09) crystal surfaces, indicated small degree of variation in the mass of the protein layer adsorbed over time. It is also important to note that the mass estimated by Voigt model from QCM-D includes the mass of both protein and any water that is trapped within the protein layer so that pure mass of protein is not easily quantified. In the actual devices, the extent of protein adsorption and cell adhesion also depends on the flow conditions where at higher blood flow rates the fluid shear helps prevent protein buildup.

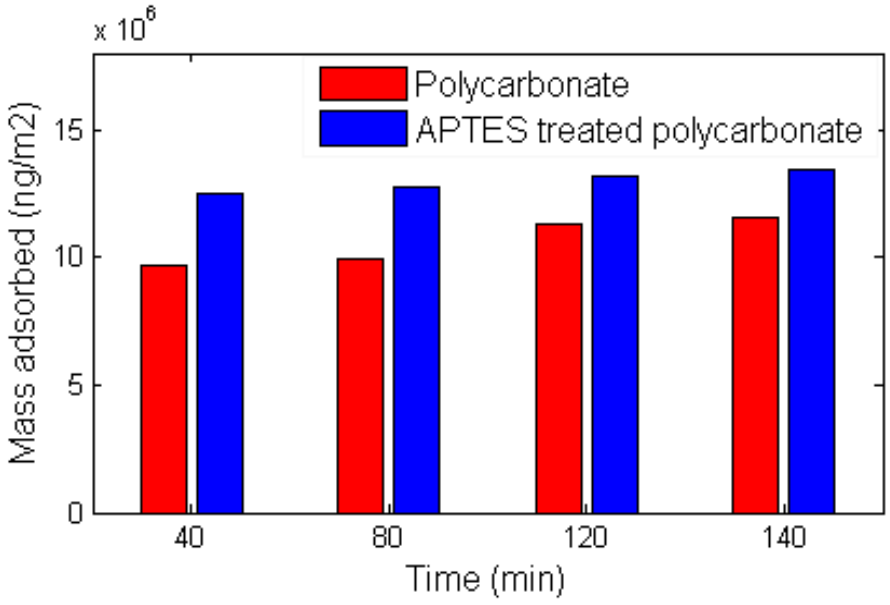

Figure 2-13: Mass adsorbed to the surface of APTES treated and non-treated polycarbonate polymer

2.7.2 Evaluating the Membrane Morphology using Scanning Electron Microscopy (SEM).

The influence of APTES conjugation on the physical properties of the membrane pores and biofilm formation on the membrane surface was explored within the microfiltration device and after exposure to blood.

2.7.2.1 Experimental setup

The microfiltration device channels were first primed using Lactated Ringers' solution (*Baxter Healthcare, Deerfield, IL)* not only to purge air bubbles from the main flow, but also to remove non conjugated APTES from the membrane surface which can cause aggregation of proteins onto the membrane surface. After priming, heparinized sheep's blood plasma (Hemostat Labs, Dixon, CA) was infused through the reservoir channels for 1 hour at a flowrate of 80 µl/min. After each experiment, nonadherent proteins were removed by washing by infusing Ringers' solution through the channels of the device. Finally the device was cut using a razor blade and a small piece of membrane was removed and fixed in 2% glutaraldehyde, dehydrated and evaluated using Scanning Electron Microscopy (SEM).

2.7.2.2 Experimental Results

The SEM images of the APTES coated membrane in a flowing system showed minimal protein adsorption to the membrane surface. The results indicated no significant gross change in pore morphology of the membranes due to the APTES conjugation or formation of biofouling layer. Figure 2-14 shows a SEM photograph of untreated

membrane and before exposure to blood and Figure 2-15 shows a SEM photograph of APTES treated membrane after exposure to blood plasma in within the microfiltration system.

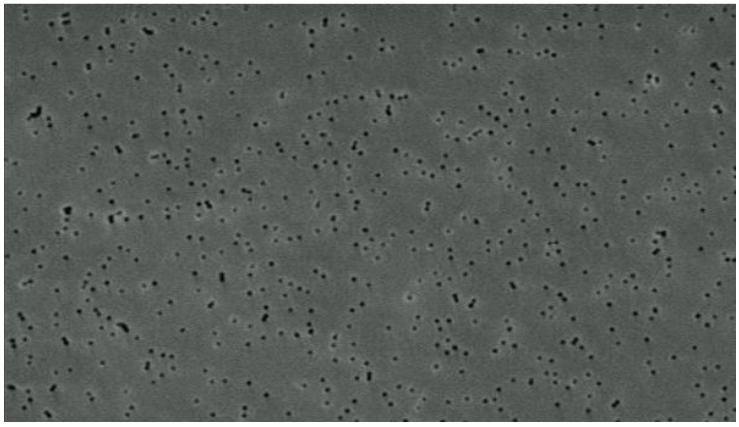

Figure 2-14: SEM image of porous PCTE membrane before exposure to blood

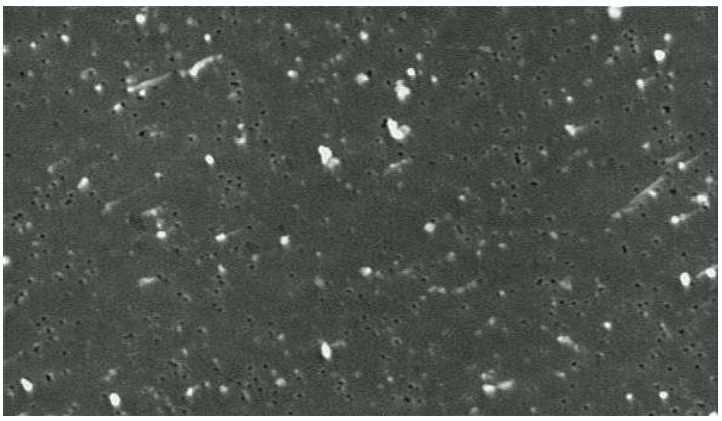

Figure 2-15: SEM image of APTES treated PCTE membrane after exposure to blood plasma

This method, based on surface modification of porous polymer membranes using APTES, exhibited a significant increase in bonding strength over other bonding techniques such as PDMS glue or biocompatible adhesives for similar test devices. The strong integration of porous polymer membranes to microdevices presented in this work

did not alter the membrane function and pore morphology which can greatly expand the reliable use of these types of membrane in more complex microstructures.

Chapter 3 Microfiltration Device Evaluation during Bench-Top Experiments

3.1 Introduction

In order to improve upon device design, the microfiltration device was evaluated in a series of bench top experiment to assess the effect of blood hematocrit on microdevice filtration efficiency. A significant problem often encountered with membrane-based filtration devices for blood separation is protein biofouling on the membrane surface, activation and adherent of platelet to the membrane surface and the high deformability of red blood cells which may lyse and/or clog the membrane pores and reduce the filtrate flux across the membrane. Additionally, high quality filtration of blood cells can be achieved using a membrane with relatively small pores, which requires high pressure for driving the plasma though the filter. High pressure can be problematic at high cell concentration as large cells are pushed into the membrane pores. In order to optimize device performance, the effects of membrane pore-size on plasma separation was also studied.

The level of blood anticoagulation also affects protein and cellular absorption to the membrane. Heparin is widely used in clinical environments as an anticoagulation to prevent blood clots from forming. The amount of heparin administered can vary depending upon clinical guidelines from light administration to patients in an emergency department or hospital room, medium levels to patients on extracorporeal life support or high doses during cardiac surgeries requiring CPB. The quantity of heparin administered

is also adjusted according to coagulation test results to make sure the level of anticoagulation is in the required therapeutic range. Additionally, heparin is commonly used to coat blood contacting devices to create a non-thrombogenic surface and for maintaining blood fluidity during blood handling procedures. As an approach to maintain the filtrate flow rate over time, especially at high hematocrit levels, some microdevices were pre-infused with heparin as an anticoagulant.

Finally, sheep's blood was chosen because of its low cost and its availability from reliable suppliers. However, sheep's blood rheology varies from that of human[75] The device efficiency can vary with blood from different species, because the changes in blood rheological behavior may result in the change of adhesion of cells and proteins to the membrane surface. For example, the size of the sheep RBCs (average diameter of 4.8 μm) varies from that of human (average diameter of 6-8 μm). This can alter the device performance to a degree.

3.2 Experimental Methods

To explore the effect of membrane flow resistance and blood hematocrit (Hct) level using the microfiltration device, experiments were performed by infusing lightly heparinized sheep blood of varying hematocrit through the reservoir of the device. Whole sheep's blood (42% Hct, heparinized to 300 IU/L heparin to prevent blood coagulation during shipping) was obtained from a scientific vendor (Hemostat Labs, Dixon, CA), and was used for experiments within two weeks of harvest. The blood was hemodiluted to 34%, 30% and 20% hematocrit by addition of Lactated Ringers solution (Baxter Healthcare Corp, Deerfield, Il) with the hematocrit verified using a Coulter cell and particle counter

(Beckman Coulter Inc., Hialeah, FL, USA). The filtration capacity of the device was then investigated using a microfiltration device with a 200 nm PCTE membrane and infusing blood through the reservoir channels at a constant flow rate of 80 µl/min over a 2 hour experimental period. The filtration capacity of the device was then investigated using a microfiltration device with a 200 nm PCTE membrane and infusing blood through the reservoir channels at a constant flow rate of 80 µl/min over a 2 hour experimental period. At this flow rate, the average shear stress in the reservoir was estimated assuming a constant viscosity and using equation 3.1. In this equation μ is the dynamic viscosity of the blood (3.5×10^{-3} $Pa{\cdot}s$), u is the average velocity of the blood along the reservoir channel and y is the channel height (135 µm).

$$\tau(y) = \mu \frac{\partial u}{\partial y} \tag{3.1}$$

Average velocity in an open flow channel, was calculated to be (1.65×10^{-2} m/s) using equation 3.2 where Q is the blood inlet flowrate (80 µl/min) and A is the channel cross sectional area.

$$u_{ave} = \frac{Q}{A} \tag{3.2}$$

Therefore, the average shear stress in the reservoir was estimated to be 4.27 dynes/cm^2 which is more than 200 times smaller than the critical shear stress required for shear induced RBC hemolysis. [76]

Discrete blood samples were collected as fractions from both the reservoir and filtrate outlets every 20 min and the collected filtrate volumes were measured at each time point to identify any reduction in filtrate flow rate due to membrane clogging.

To explore the effect of membrane pore-size using the microfiltration device, experiments were performed by infusing whole sheep's blood (Hemostat Labs, Dixon, CA), (42% Hct, heparinized to 300 IU/L) into the microdevice. The filtration capacity of the device was then investigated using microfiltration devices with either 200 nm or 100nm PCTE membrane and infusing blood through the reservoir channels at a constant flow rate of 80 μl/min over a 2 hour experimental period. Discrete blood samples were collected as fractions from both the reservoir and filtrate outlets every 20 min and the collected filtrate volumes were measured at each time point to identify any reduction in filtrate flow rate due to membrane clogging.

Additionally, as an approach to maintain the filtrate flow rate over time, especially at high hematocrit levels, some microdevices were pre-infused with heparin as an anticoagulant before infusing blood. The filtration capacity of the device was investigated using microfiltration device with 200 nm PCTE membrane and infusing 1000 IU/ml of heparin anticoagulant (2 mg of sodium heparin in 1 ml of Lactated Ringer's solution) for at least 30 min prior to infusing blood to microdevice, in order to reduce the amount of platelet adhesion to the surface of the membrane. Then sheep's blood (Hct= 39% as received) was infused through the reservoir channels of the heparin coated and non-coated microdevice at a constant flow rate of 80 μl/min over a 2 hour experimental period. Discrete blood samples were collected as fractions from both the reservoir and filtrate outlets every 20 min and the collected filtrate volumes were measured at each

time point to identify any reduction in filtrate flow rate due to membrane clogging. The filtration flow rates over time between pre-coated and non-coated microdevices were then compared.

Following each blood experiment, the microfiltration devices were cut using a razor blade, and a small piece of membrane was removed. The membranes were then fixed in 2% glutaraldehyde, dehydrated, and inspected using scanning electron microscopy (AMRAY-1830I, AMRAY, Bedford, MA) to examine the membrane surface for indications of cellular or protein absorption after being exposed to blood.

3.3 Experimental Results

Ensuring reliable operation of the device over a wide range of blood hematocrit levels and anticoagulation levels is an important factor in extending the performance of the device. The filtration efficiency of the device was evaluated using sheep's whole blood. However, the device efficiency can vary with blood from different species, because the changes in blood rheological behavior may result in the change of adhesion of cells and proteins to the membrane surface. Additionally high concentration of cellular components (high hematocrit) increases the pressure across the device, which can result in clogging of the membrane pores by blood cells. To assess the effect of blood hematocrit on the filtration capacity of the device, the volumetric flow rates at the filtrate outlet were measured over time at various hematocrit levels with whole sheep's blood infused into the inlet of the reservoir channels. The absolute reservoir and filtrate flow rates varied between experiments due to changes in blood rheology which can vary between different blood batches as well as differences in membrane pore density which

can vary greatly between membrane batches (indicated as between 1×10^5 to 6×10^8 pores/cm^2 by the manufacturer). However, a consistent trend seen over several (n=5) experiments is that the permeate flux flow rate directed to the plasma outlet decreased over time using whole blood at high hematocrit levels (~42%). However, tests with blood at various lower Hct. in the range of 20% to 34% showed that the plasma separation was efficient and did not decrease significantly over the duration of the experiments. Also, at higher hematocrit levels the filtrate flow rate was initially larger due to higher reservoir pressure induced by higher viscosity of the blood. However, the flow across the membrane decreased quickly due to the accumulation of red blood cells or adhesion of platelets at the membrane surface. Representative experimental results, obtained using one batch of blood over a set of experiments is shown in Figure 3-1. The results indicate that initial filtration flow rate is higher for high level of hematocrit (42%) but it decreases rapidly due to accumulations of RBCs or platelet at the surface of the membrane.

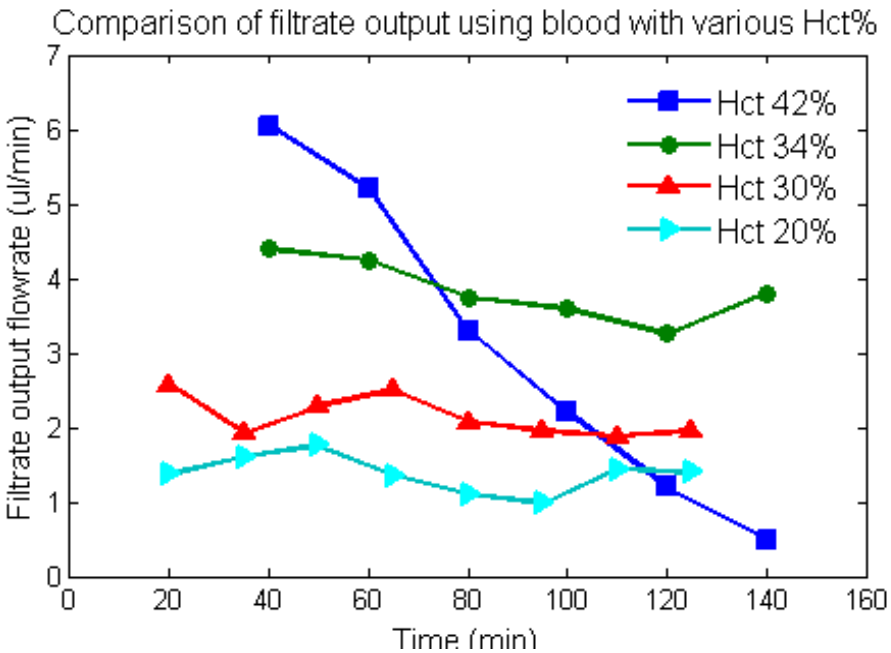

Figure 3-1: A comparison of the experimental results of the total plasma separation flow rate with respect to blood inlet hematocrit level.

SEM images of the membranes are useful to assess the degree of protein or cellular absorption which can produce biofouling of the membrane causing a decline in the filtration flux across the membrane over time. Figure 6 shows SEM images of a 200 nm membrane prior to blood exposure (Figure 3-2) and after exposure to lightly heparinized (~300 IU/L) sheep's blood (Hct~30%)(Figure 3-3). The SEM image of the membrane following exposure to sheep's blood revealed that at high hematocrit levels, protein and platelet adhesion was significant, most likely due to the lower amounts of anticoagulant used in the sheep's blood.

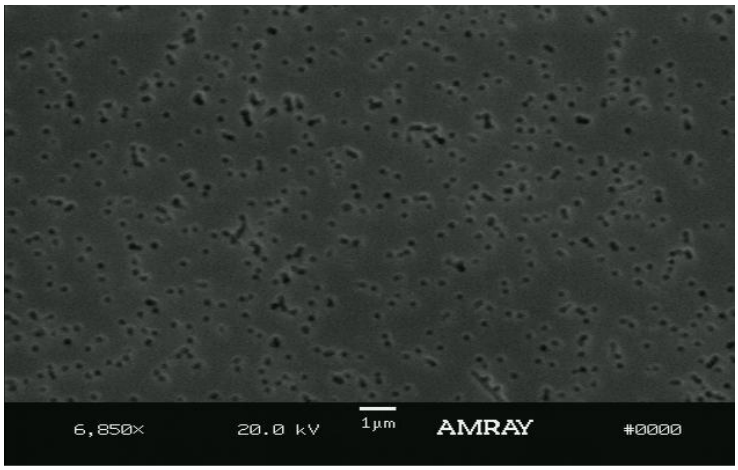

Figure 3-2: Representative SEM images of porous PCTE membrane before being exposed to blood.

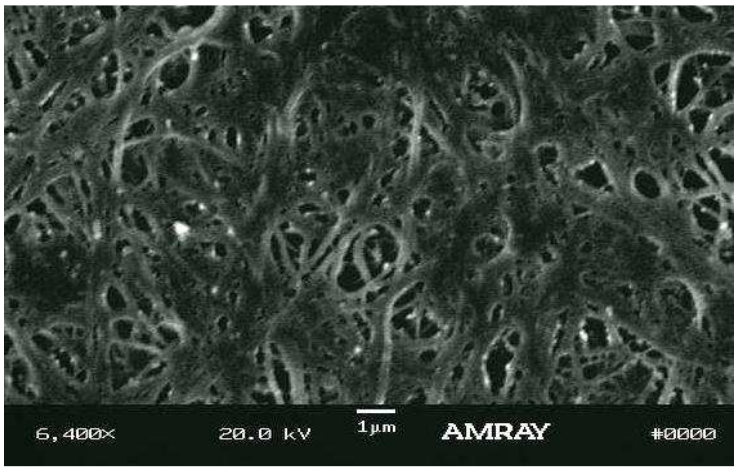

Figure 3-3: Representative SEM images of PCTE membrane after being exposed to sheep blood (Hct~30%) shows significant amount of platelet adhesion to membrane surface.

Comparison of the performance of microfiltration devices with 200 nm and 100 nm membranes (both suitable for plasma separation purposes) indicated that at a high hematocrit level, the initial filtrate flow rate is higher using 200 nm because it is less

resistive to the flow. However, the filtrate flow rate decreases faster over time as it is easier for large cells to enter and clog the pores (Figure 3-4).

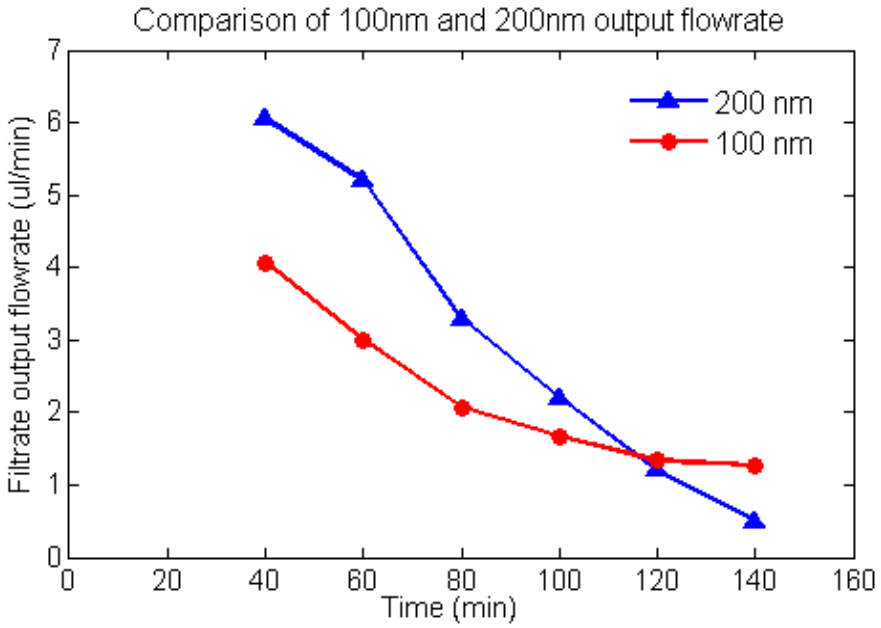

Figure 3-4: A comparison of the plasma separation flow rate for 100nm and 200nm pore size membrane.

To improve the device performance at high hematocrit levels using a 200 nm membrane pore size, the surface of the microdevice was pre-coated with an anticoagulant (heparin) in order to decrease the amount of cell adhesion on the membrane surface. When using sheep blood at high Hct levels (39% as received), the filtrate flow rate did not change significantly over time for the heparin coated microdevice but decreased rapidly and significantly using the non-coated device (Figure 3-5).

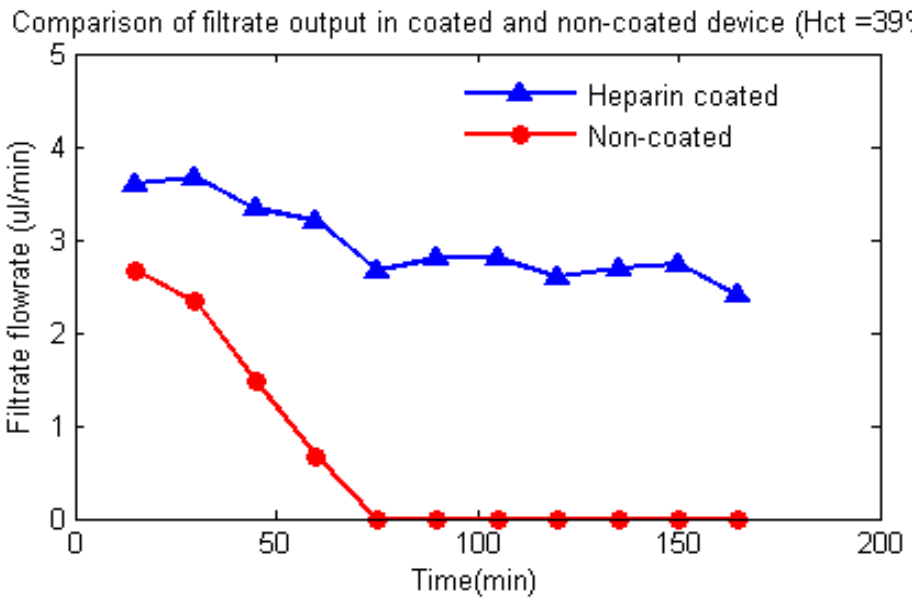

Figure 3-5: A comparison of the experimental results of the total plasma separation for anticoagulant coated and non-coated microdevice for blood Hct= 39%.

Comparison between the SEM images of a non-coated membrane (Figure 3-6) and a heparin pre-coated membrane (Figure 3-7) after exposure to lightly heparinized (~300 IU/L) sheep's blood (Hct=39%) indicated a significant decrease in cellular adhesion to the membrane surface of the pre-coated membrane. The results from SEM images, along with the results from filtration efficiency over time for anticoagulant pre-coated microdevice, demonstrate this approach is useful for maintaining the filtration efficiency over time without the need to add heparin systemically to the blood sample. The results also indicated that pre-coating the microfiltration device with a sufficient amount of anticoagulant can expand its applications to all blood Hct concentrations at any level of anticoagulation.

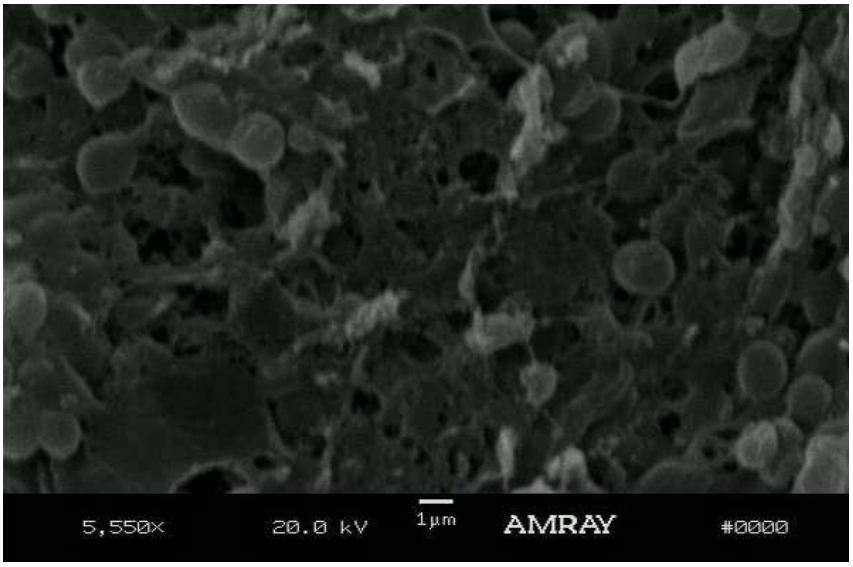

Figure 3-6: Representative SEM images of porous PCTE membrane after exposure to sheep's blood (Hct=39%)in a non-coated microdevice.

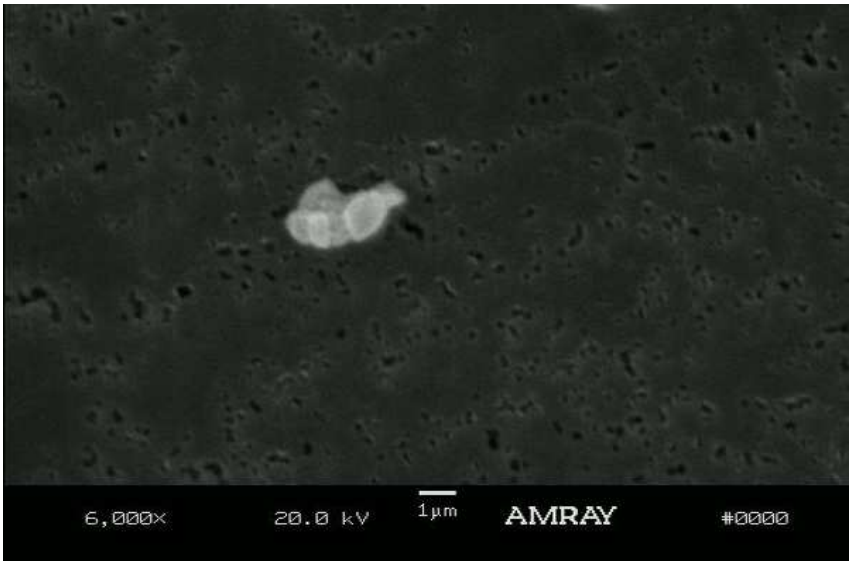

Figure 3-7: Representative SEM images of porous PCTE membrane after exposure to sheep's blood in a non-coated microdevice.

Chapter 4 : Plasma separation during simulated cardiopulmonary bypass procedure

4.1 The Importance of Simulated CPB

A simulated cardiopulmonary bypass (CPB) procedure is commonly used to evaluate pressure-flow relationships and emboli production along circuit components (e.g., pumps, oxygenators, cannulae, length and diameter of the tubing etc.). [77-80] In particular, simulated circuits allow the study of the response of blood and immune activation to extracorporeal perfusion through the circuit in the absence of other major stimulating factors such as surgical trauma or cardiotomy suction.[81] Additionally, simulated circuits allow data to be collected with relative ease compared to the use of animal models or drawing blood from surgical patients undergoing CPB procedures for analysis [48]. Nevertheless, the results from experiments on blood circulating within simulated CPB circuits can be used by physicians/researchers to improve the CPB procedure because it allows them to better understand the effect of blood interactions with different kinds of artificial surfaces (types of oxygenators, blood pumps, arterial cannulae, and different tubing coating materials) of the extracorporeal circuit which are very helpful in modifying clinical perfusion protocols to limit this inflammatory response in patients, especially in neonates and infants because of the very high circuit flow rates used (150-200 ml/kg/min vs. 50-80 ml/kg/min) compared to adults.

When using a simulated circuit it is important to note significant differences between the simulated circuit and actual surgeries which limits the ability to make direct comparisons

between the two platforms. First, any blood used in the simulated circuit is the only blood product used, whereas in a patient donor blood products are mixed with the patient's own blood and changes in electrolyte levels may be compensated for by a patient's homeostatic mechanisms or through clinical intervention.

4.2 Simulated Cardiopulmonary Bypass Circuit Components

A simulated extracorporeal circulatory circuit was assembled in order to reproduce circulation used for pediatric patients undergoing CPB. The system consisted of a HL-20 heart-lung machine with a Roller blood pump (Jostra HL-20, Houston, TX), a hollow fiber membrane oxygenator with an integrated heat exchanger module (Capiox Raby RX 05RW, Terumo Corporation, Tokyo, Japan) , a 32μm Capiox pediatric arterial filter (CX* AF02; Terumo Corporation, Tokyo, Japan) and a pediatric venous reservoir with an integrated cardiotomy filter (Capiox cardiotomy reservoir CX*CR10NX). Additionally, a second venous reservoir acted as a pseudo-patient blood reservoir. Circuit pressure was maintained via a Hoffman clamp placed on the venous line to simulate patient circulation resistance and maintain blood pressure. The blood pressure could be increased or decreased by tightening or loosening the clamp while maintaining circulation flow rate. The gas flow was maintained at 0.25 L/min with a mixture of oxygen (95%) and carbon dioxide (5%). A schematics of a Penn State Hershey simulated CPB circuit including the roller pump, oxygenator, arterial filter and venous reservoir is shown in Figure 4-1. The circuit is fed to a blood reservoir which represents the pseudo-patient with the systemic circulation resistance modeled by the tightening of a Hoffman clamp.

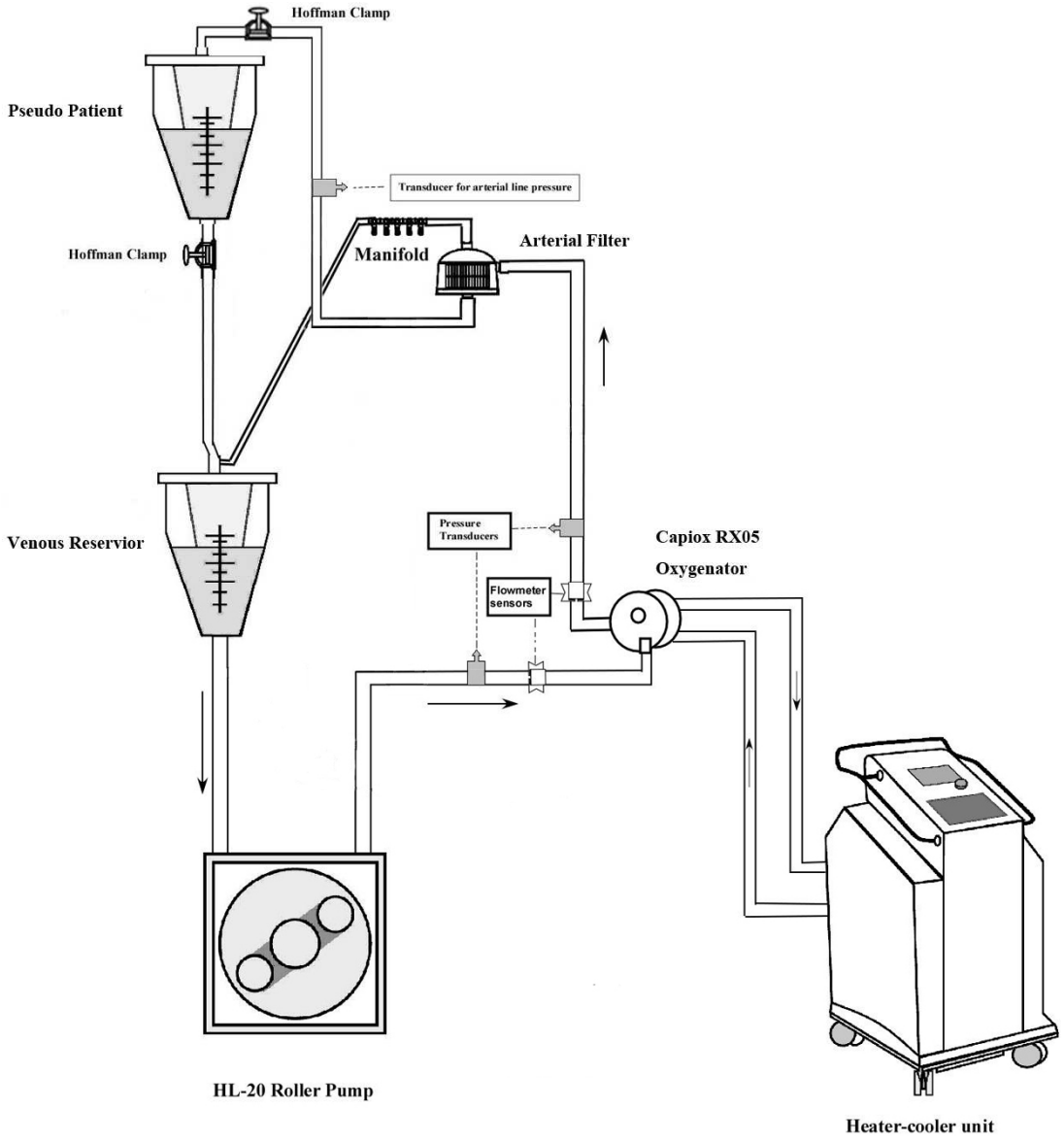

Figure 4-1: A schematic of the extracorpeal circuit. (Note: this schematics was provided by Dr. Akif Ündar)

4.3 The Effect of Human Blood Model Used During Simulated (CPB) on Activation of Immune Responses

The goal of this study was to assess whether the use of different aged human blood, used during the simulated Penn State Hershey Pediatric cardiopulmonary bypass (CPB) model (which will be used to evaluate microfiltration device performance) affects immune activation. In order to study and compare the cytokine release involved in the humeral immune response during simulated CPB, both freshly drawn whole blood used less than 1 hour after donation (n=2) and reconstituted whole blood (1 week old) (n=3) were circulated in a simulated CPB circuit under identical perfusion conditions. Discrete samples were collected in both experiments and analyzed for the proinflammatory cytokines concentrations of TNFα, IL-6, and IL-8 using immunofluorocytometry as an indicator of immune activation. The results indicated that the cytokine concentrations of freshly drawn blood increased significantly compared to the reconstituted blood over the CPB circulation time. The fresh blood activation was 2 to 3 orders of magnitude larger than the week old blood for all cytokines analyzed. These results suggest that the use of freshly drawn blood is required to evaluate immune responses to the extracorporeal circulation. The effect of different aged blood, used during the simulated Penn State Hershey Pediatric cardiopulmonary bypass (CPB) model on immune activation was studied by continuous blood sampling during CPB procedure.

4.3.1 Experimental Methods

In each experiment the simulated CPB circulation loop was primed with 500 ml of either freshly drawn human blood, drawn from healthy adult volunteers and brought into the lab

within 30 min of collection, or reconstituted whole blood samples drawn 1 week prior diluted with lactated Ringers solution. Approvals for collection and use of human blood were obtained from the Institutional Review Board (IRB) at the Penn State Hershey College of Medicine. The collected blood was hemodiluted to a hematocrit level of approximately 27 to 30% Hct by addition of lactated Ringers solution (Baxter Healthcare Corp, Deerfield, Ill). The Hct of the blood was continuously monitored with LWS-M24 Micro-Hematocrit centrifuge (LW Scientific, Inc., GA, USA) in order to maintain Hct within the range of 27% to 30% Hct throughout the experiments. The diluted blood was then circulated in a nonpulsatile perfusion at a rate of 500 ml/min at an arterial circuit pressure of 100 mmHg. Circulation parameters such as pressures and flowrates were chosen to be identical with those used during pediatric cardiac surgeries. The blood temperature was maintained at normothermic circulation (35°C) using a MAQUET Heater-Cooler (Jostra Heater-Cooler Unit HCU 30, Houston, TX) for the duration of the experiments. After priming the simulated extracorpereal circuit blood gas levels were monitored via an i-STAT 1 handheld blood analysis system (Abbott Laboratories, Princeton, NJ) to ensure blood chemistry, especially blood gases, were within acceptable physiological limits. Table 4-1 summarizes the blood chemistry analysis for old blood and fresh blood experiments after priming the circuit. When blood is stored alterations can occur in its constituents, in terms of both blood gas equilibrium, pH and electrolyte levels. In particular an increase in potassium levels due to hemolysis is common, which explains the higher potassium levels seen in the old blood samples compared to fresh blood.

4-2 summarizes the blood chemistry analysis for old blood 2 hours after priming, which indicates that the blood gases reached their physiological levels after the experiments were initiated. However, the higher potassium level is maintained due to the absence of a patient specific homeostatic compensation. After complete mixing of the blood and prime fluid was accomplished, a sample was drawn and was designated as a baseline.

Table 4-1: Blood gas analysis for each experiment after complete mixing of blood and prime solution

	old blood	**old blood**	**old blood**	**fresh blood**	**fresh blood**
pH	7.157	7.175	7.218	7.427	7.576
PCO_2 (mmHg)	75	87.4	94.2	62.9	23.9
PO_2 (mmHg)	629	617	522	337	174
BEecf (mmol/L)	-2	4	11	17	0
HCO_3 (mmol/L)	26.6	32.3	38.4	41.1	22.2
TCO_2 (mmol/L)	29	35	41	43	23
SO_2 (%)	100	100	100	100	100
Na (mmol/L)	118	126	124	163	163
K (mmol/L)	> 9.0	> 9.0	> 9.0	< 2.0	2.5
Ca (mmol/L)	< 0.25	0.73	1.16	< 0.25	> 2.5
Hct (CPB%PCU)	27.5	30	27	27	28

4-2: Blood gas analysis for old blood experiments, 2 hours after priming

	old blood	**old blood**	**old blood**
pH	7.335	7.326	7.345
PCO_2 (mmHg)	68.5	66.3	65.6
PO_2 (mmHg)	194	200	188
BEecf (mmol/L)	11	9	10
HCO_3 (mmol/L)	36.6	34.6	35.8
TCO_2 (mmol/L)	39	37	38
SO_2 (%)	100	100	100
Na (mmol/L)	122	132	133
K (mmol/L)	> 9.0	> 9.0	> 9.0
Ca (mmol/L)	< 0.25	0.85	1.04
Hct (CPB%PCU)	27.5	30	27

Over the course of each experiment, discrete 1 ml blood samples were drawn from the circuit every 20 minutes for fresh blood and every 15 minutes for reconstituted blood directly from the CPB membrane oxygenator arterial port. The blood samples were then centrifuged; the plasma was removed and snap frozen at -80°C until analyzed. The concentration of inflammatory cytokines (IL-6, IL-8 and TNF-α) were measured using an

human inflammatory cytokine cytometric bead assay (CBA) kit (BD Biosciences, San Jose, CA, USA) according to the manufacturer's instructions. The CBA immunoassay allows the detection and quantification of multiple analytes from small sample volumes with a broad detection range. Standard curves for each cytokine were generated by creating a series of incubated bead following the manufacturer's instructions. The plasma samples were used as collected without any dilution. Briefly, the cytometric assay beads were mixed, washed, and resuspended in a serum enhancement buffer. Following bead preparation, 50 µl of the calibration and collected blood samples were mixed with 50 ml of bead solution and incubated for .5 hours. Following incubation, the beads were diluted in 1 ml of wash solution, centrifuged and then all but 100 µl of wash solution was gently removed from each tube. 50 µl of Human inflammatory phycoerythrin (PE) labeling agent was then added to each tube and mixed with the beads which were resuspended by gentle agitation. The labeling agent was incubated for 1.5 hours followed by another bead washing procedure and centrifugation and finally resuspending the beads in 300 µl for analysis. The bead fluorescence intensities were evaluated using BD FACS Calibur flow cytometer and compared to the calibration intensities for quantifying cytokine concentrations. The PE labeling agent allows a multiplexed assay to be performed by isolating beads for analysis via their FSC and SSC signal and each cytokine is delineated by the bead FL3 intensity where each cytokine produces a different FL3 intensity showing individual bead populations for each cytokine of interest. The cytokine quantification is done based on the bead FL2 intensity where the bead intensity using this channel is proportional to the cytokine concentration.

4.3.2 Experimental Results

The effect of simulated CPB procedure primed with freshly drawn human blood and reconstituted 1 week old blood on the proinflammatory cytokines TNFα, IL-6 and IL-8 are shown in Figure 4-2, Figure 4-3 and Figure 4-4. At the end of the circulation time the concentration of TNFα (Figure 4-2), IL-6 (Figure 4-3) and IL-8 (Figure 4-4) concentrations in both groups using freshly drawn blood were significantly elevated compared to baseline cytokines concentrations. However, when reconstituted week old blood was used in the circulatory circuit, the concentrations of these cytokines, did not increase as significantly (or at all in some samples) compared to that of freshly drawn blood. The cytokine concentration for fresh blood was at least 2 to 3 orders of magnitude larger than the week old blood for all cytokines analyzed and showed much larger concentration increase over the circulation period compared to the week old blood.

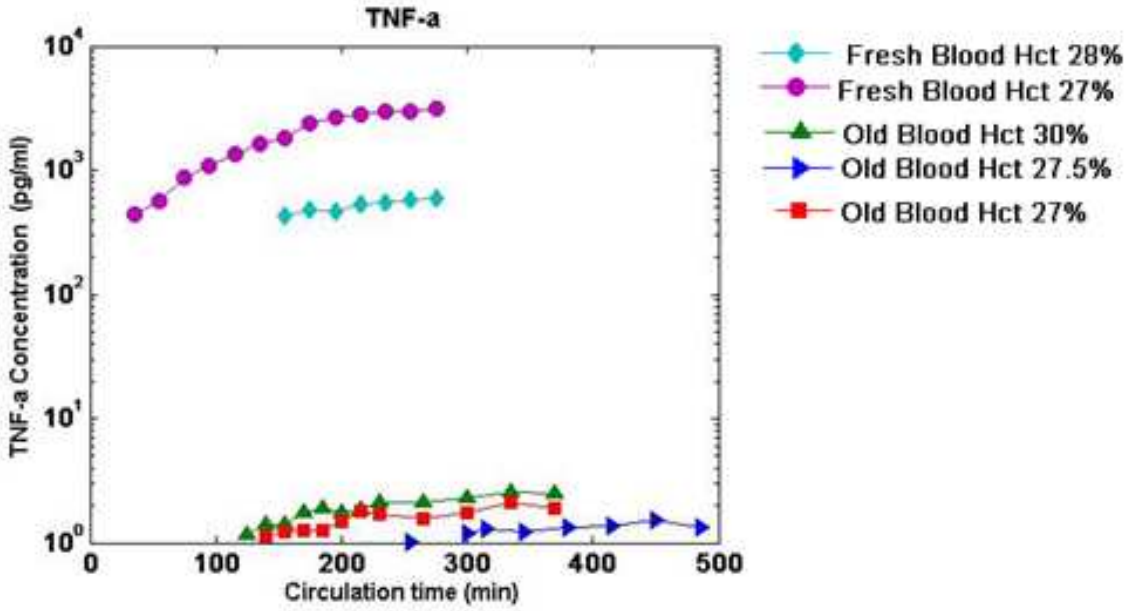

Figure 4-2: Comparison of cytokine concentration (TNF-α) when using fresh blood and reconstituted blood.

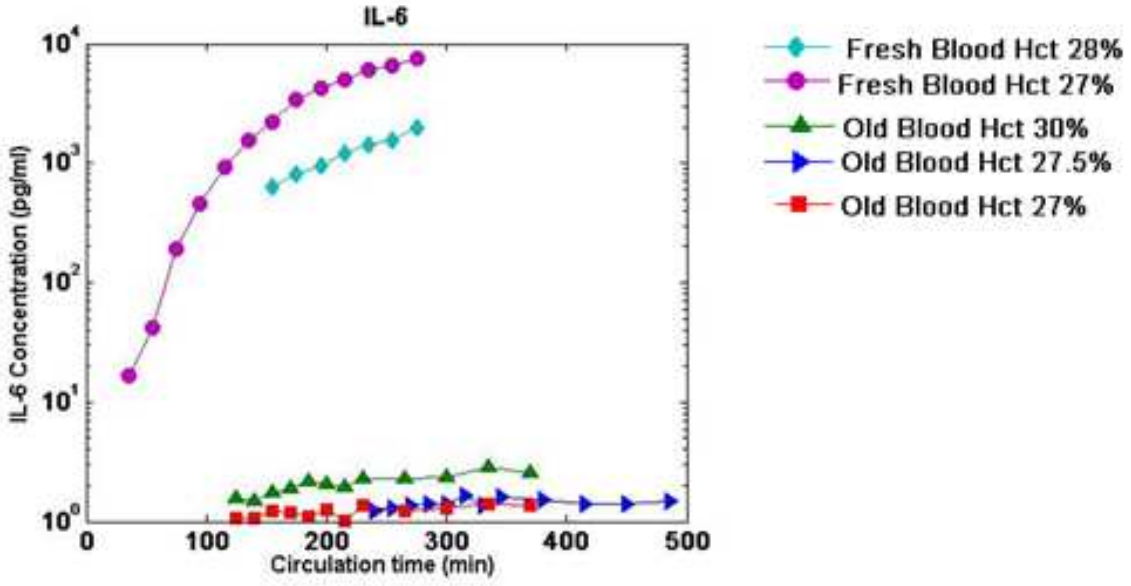

Figure 4-3: Comparison of cytokine concentration (IL-6) when using fresh blood and reconstituted blood.

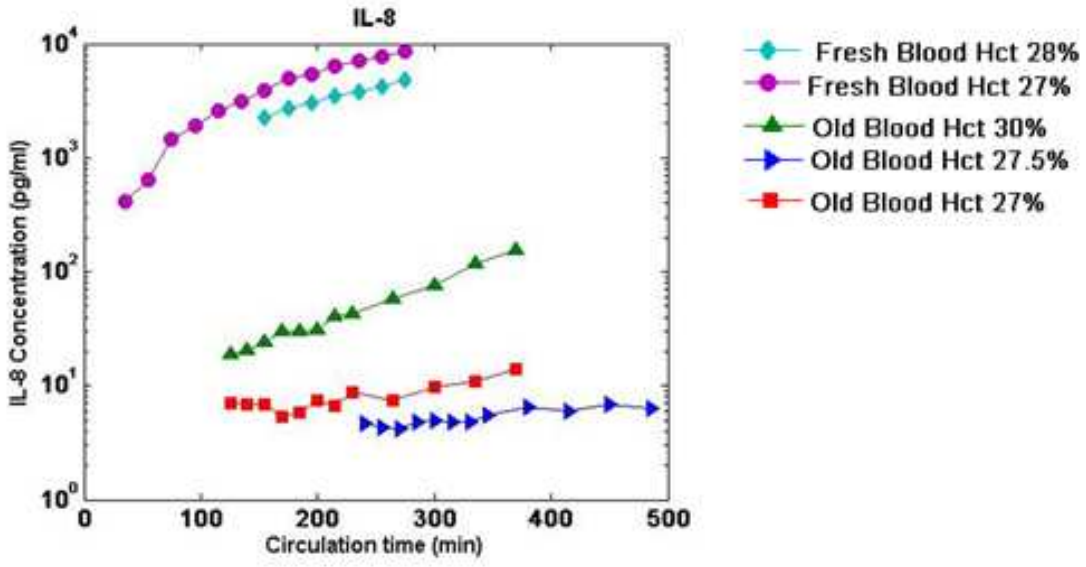

Figure 4-4: Comparison of cytokine concentration (IL-8) when using fresh blood and reconstituted blood.

The use of a simulated CPB circuit allowed comparisons to be made between circuits primed with freshly drawn blood and one week old blood. The results indicate that the use of fresh blood during simulated CPB increases the production of inflammatory mediators and should be used in studies of immune activation during CPB. However, these results cannot be used to predict the actual intensity of the inflammatory response during surgery. The results collected suggest that the role of blood storage age on outcomes in patient populations who require blood transfusion is very important in order to minimize the adverse effect induced by immune activation. These studies can also help researchers to better understand the advantage and disadvantage of fresh or reconstituted blood when evaluating the circuit components using simulated CPB.

4.4 Evaluating the Microfiltration Device Performance During Simulated CPB and Using Freshly Drawn Human

The results from section 4.3 indicates the importance of using fresh blood to evaluate the circuit components for studies of inflammatory mediators activation using simulated CPB circuit. Therefore, the performance of the microdevice was evaluated during an experiment using heparinized fresh human blood, with an in-vitro model CPB circulation loop which is identical to conditions used during cardiac surgeries (minus the patient).

4.4.1 Experimental Methods

The simulated extracorporeal circuit was used as described in section 4.2. The CPB circulation loop was primed (section 0 above4.2 above) with 500 ml of heparinized fresh human blood, drawn from healthy adult volunteers and brought into the lab within 30 min of collection. Fresh blood was chosen because it shows a significantly larger amount of immune activation than older blood products (as described in section 4.3 above).[82] The blood was hemodiluted to ~27%-30% hematocrit in Lactated Ringer's solution and heparinized up to ~5000 IU/blood bag (each blood bag contains between 300-500 ml of blood) consistent with surgical anticoagulation protocols. Hemodilution using crystalloid solution during CPB is a common procedure due to the required extracorporeal circuit priming volume and the limitation in donor blood availability from blood banks. It also reduces blood viscosity and improves microcirculatory flow. The blood was then circulated at a rate of 500 ml/min at an arterial circuit pressure of 100 mmHg. Nonpulsatile perfusion was performed and the temperature was set at normothermia (35 °C) for the duration of the experiments. After complete mixing of the blood and prime

fluid was accomplished, the inlet of the microfiltration device was connected to a manifold at the arterial port of the membrane oxygenator and a small portion of the blood was redirected to the microfiltration device without any further modification. Figure 4-5 shows a schematic of the microdevice integration with CPB circuit and Figure 4-6 shows a picture of the device being infused with human blood. The reservoir flow rate of the microdevice was approximately 80 μl/min, driven by pressure from the circulation circuit.

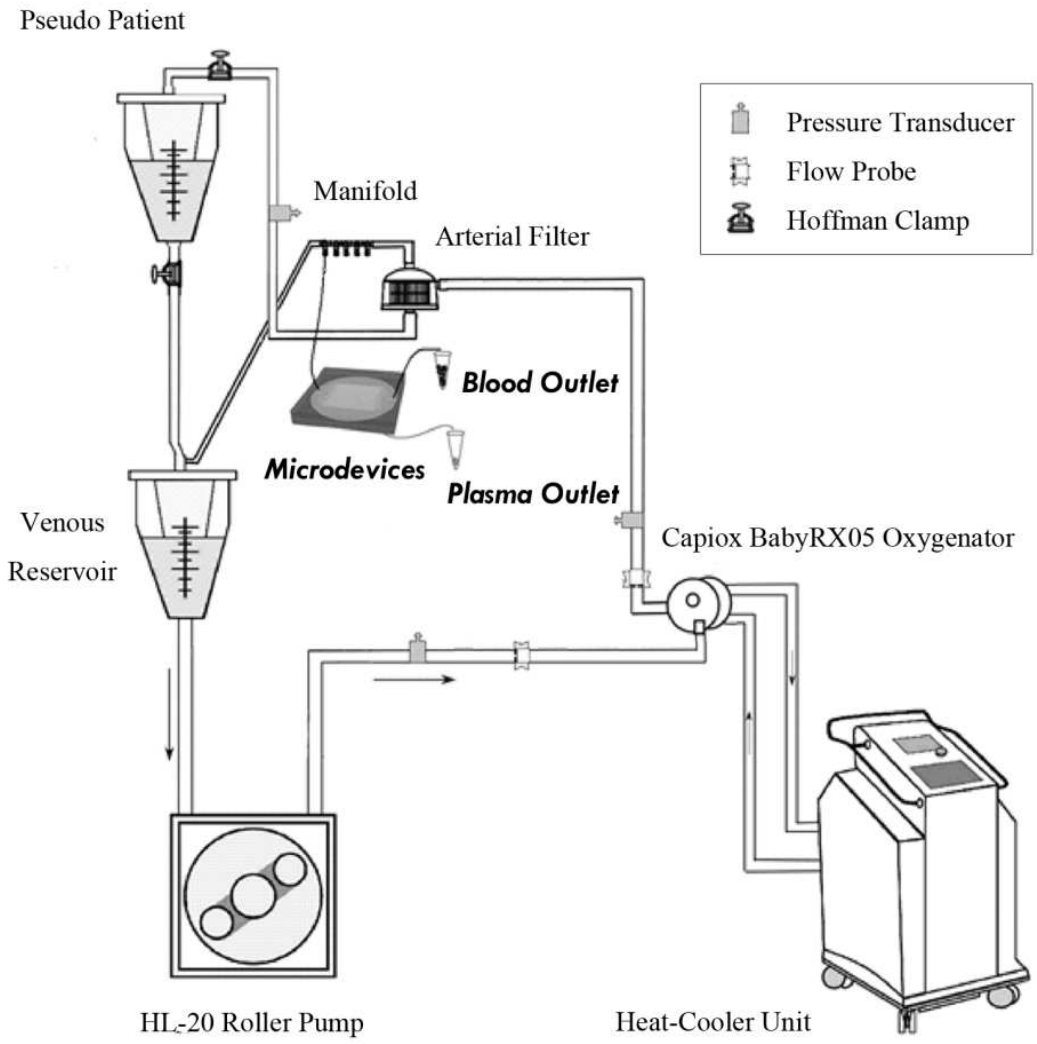

Figure 4-5: Schematics of the microfiltration device, integrated with simulated CPB circuit. (Note: this schematics was provided by Dr. Akif Ündar)

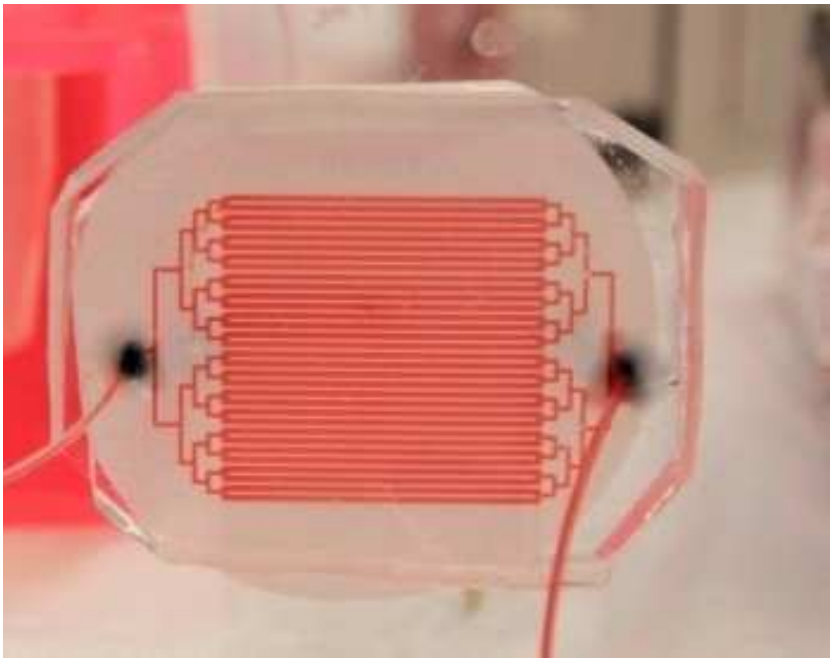

Figure 4-6: picture of the device while being perfused with blood.

The fluid fractions from both microdevice outlets of the reservoir and filtration channels were collected in 20 minute intervals for a total circulation time of 4 hours. Discrete blood samples of 1 ml volume were also collected from the arterial port of the membrane oxygenator as a control sample. Following collection, the direct draw and reservoir blood samples were centrifuged; the plasma was removed and snap frozen at -80 °C on dry ice until analyzed. Finally the device was cut and a small piece of membrane was removed, fixed in 2% glutaraldehyde, dehydrated, and inspected using scanning electron microscopy (AMRAY-1830I, AMRAY, Bedford, MA) to evaluate the membrane surface after being exposed to human blood. The concentration of inflammatory cytokines (TNF-α, IL-1β, IL-6, and IL-8) were measured using a human inflammatory cytokine cytometric bead assay (CBA) kit (BD Biosciences, San Jose, CA, USA) as described

previously.

4.4.2 Experimental Results

The ability of the microfiltration device to perform continuous separation of blood proteins from whole blood was characterized using the Penn State pediatric CPB simulated model. When using a 200 nm pore size, about 15% of the total blood volume was collected in the filtrate channels without any contaminating blood cells or indications of RBC hemolysis. Although no quantitative hemoglobin concentration quantification of the collected filtered plasma was conducted, each sample collected was clear with a slightly yellow tinge as is commonly seen in the plasma fractions of blood following centrifugation indicating only minimal hemolysis of red blood cells. Blood samples were also collected from the device reservoir, as well as a direct draw control sample, centrifuged to remove the cellular components, and stored at -80 °C for subsequent assaying to investigate the effect of the CPB circuit on immune activation. Figure 4-7, Figure 4-8, Figure 4-9 and Figure 4-10 show the temporal change in cytokine concentrations over a 4 hour circulation time for samples collected from both the reservoir and filtrate outlets using the microfiltration device and were comparable to those measured from the direct blood draw. In each graph, the error bars represent the standard deviation of the flow cytometry bead fluorescence.

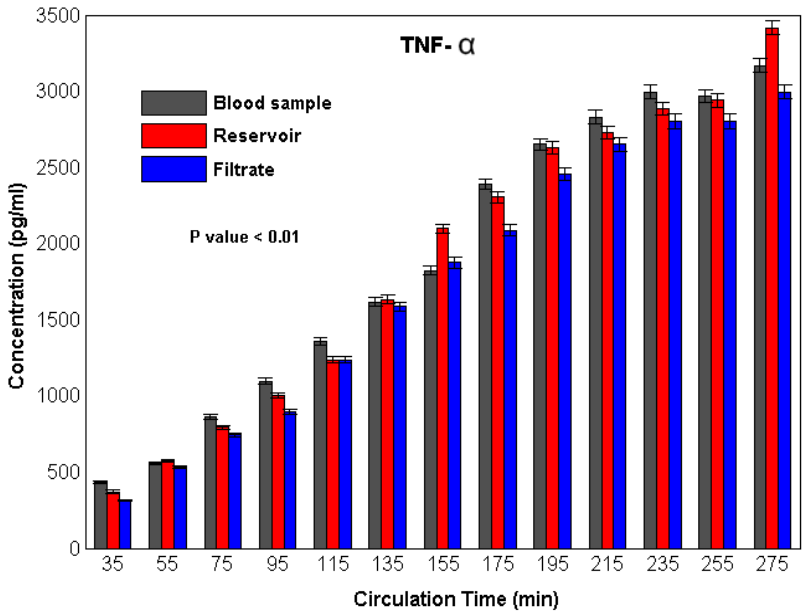

Figure 4-7: Comparison of outlet cytokine TNF-α concentrations from 13 discrete samples collected every 20 minutes

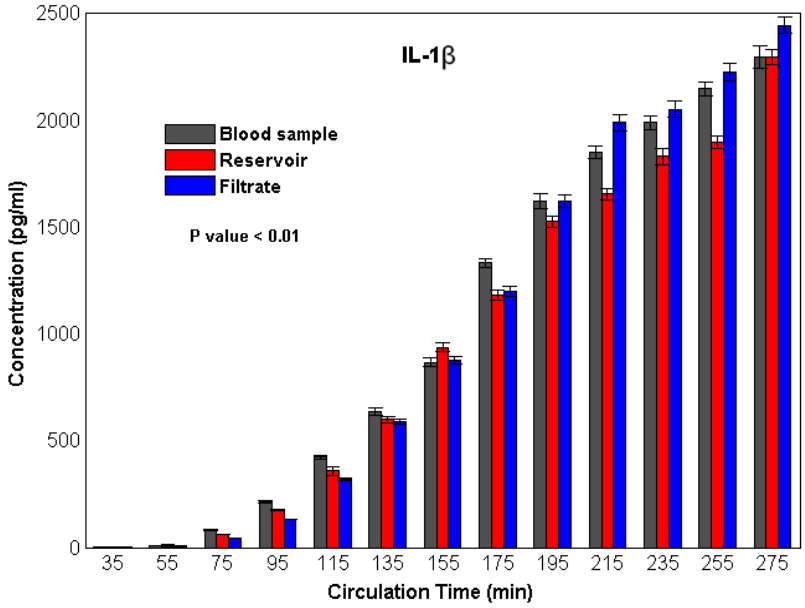

Figure 4-8: Comparison of outlet cytokine IL-1β concentrations from 13 discrete samples collected every 20 minutes.

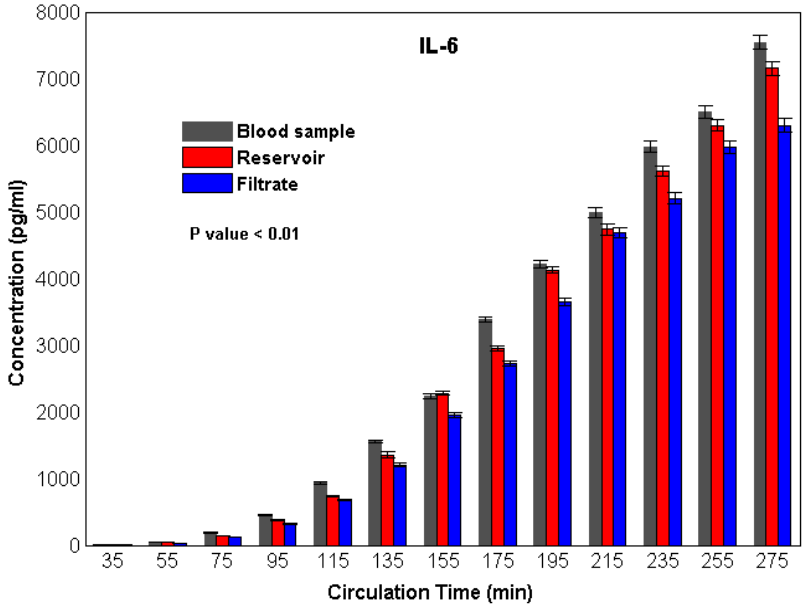

Figure 4-9: Comparison of outlet cytokine IL-6 concentrations from 13 discrete samples collected every 20 minutes.

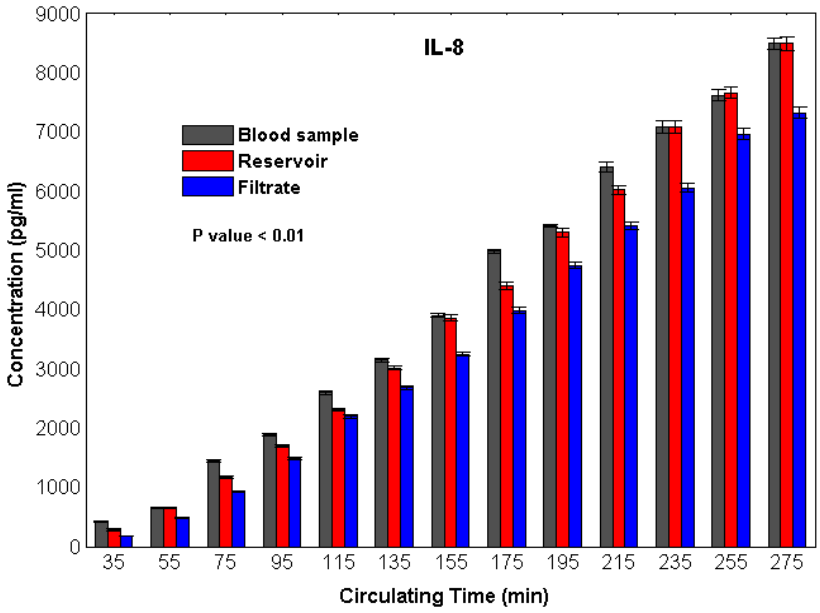

Figure 4-10: Comparison of outlet cytokine IL-8 concentrations from 13 discrete samples collected every 20 minutes.

Results from conducting a pair wise t-test at each sampling time compared to baseline cytokine concentration indicated that the cytokine concentrations for all groups tested increased significantly over the circulation time ($p < 0.01$). Table 4-3 shows the Pearson's correlation coefficient (r) calculated between both the reservoir and direct draw sample and the filtrate and direct draw sample, indicating a high level of recovery of cytokines ($r>0.99$ for all samples) using the microfiltration device.

Table 4-3: Pearson correlation coefficient, r, between microdevice samples and direct draw blood sample

Antigen	Comparison between concentrations of Reservoir and Direct Draw Sample	Comparison between concentrations of Filtrate and Direct Draw Sample
TNF-α	0.992	0.996
IL-1β	0.996	0.997
IL- 6	0.999	0.997
IL- 8	0.997	0.998

Finally, a comparison was done to quantify the cytokine recovery compared to the direct blood draw. At each time point, the measured cytokine concentration from the reservoir and filtrate outlets were normalized to the direct draw concentration and compared to each other. For all samples tested the recovery was greater than 80% (Figure 4-11).

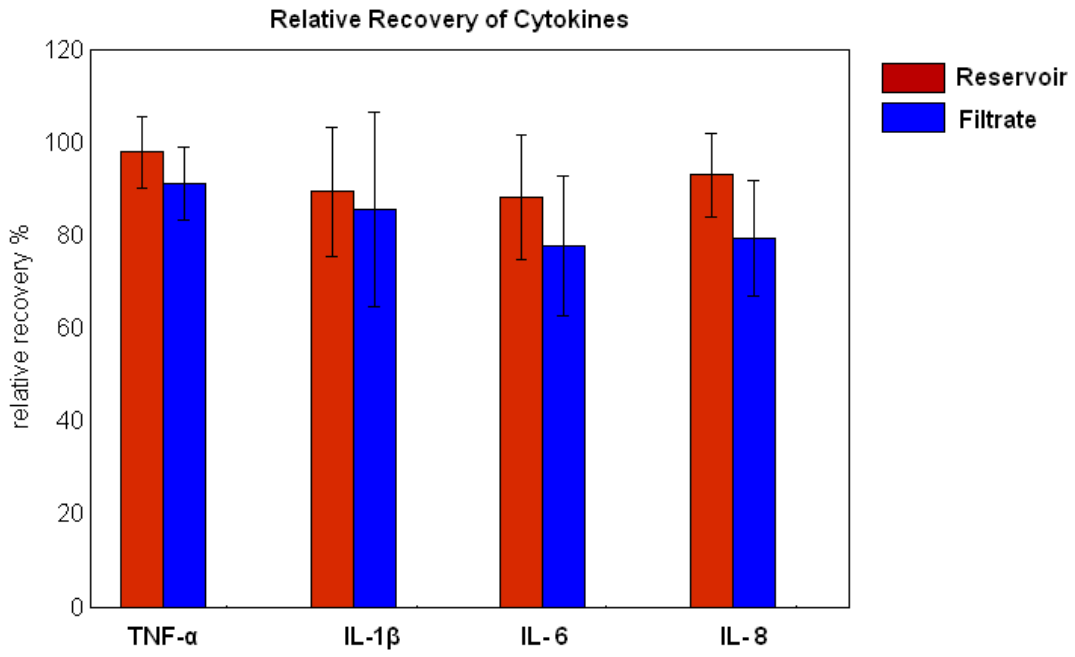

Figure 4-11: Average normalized recovery from the reservoir and filtration sample collected which was over 80% for all the analyzed samples.

Figure 4-12 shows SEM images after exposure to heavily heparinized (~5000 IU/blood bag) human blood (Hct=27-30%) for over than 4 hours. The SEM image of a 200 nm membrane after exposure to human blood during CPB procedure, showed little protein absorption and did not indicate any platelet adhesion. Contrarily, the SEM image of the membrane following exposure to sheep's blood (Chapter 3) revealed that at similar hematocrit levels (Hct~ 30%), protein and platelet adhesion was significant, most likely due to the lower amounts of anticoagulant used in the sheep's blood.

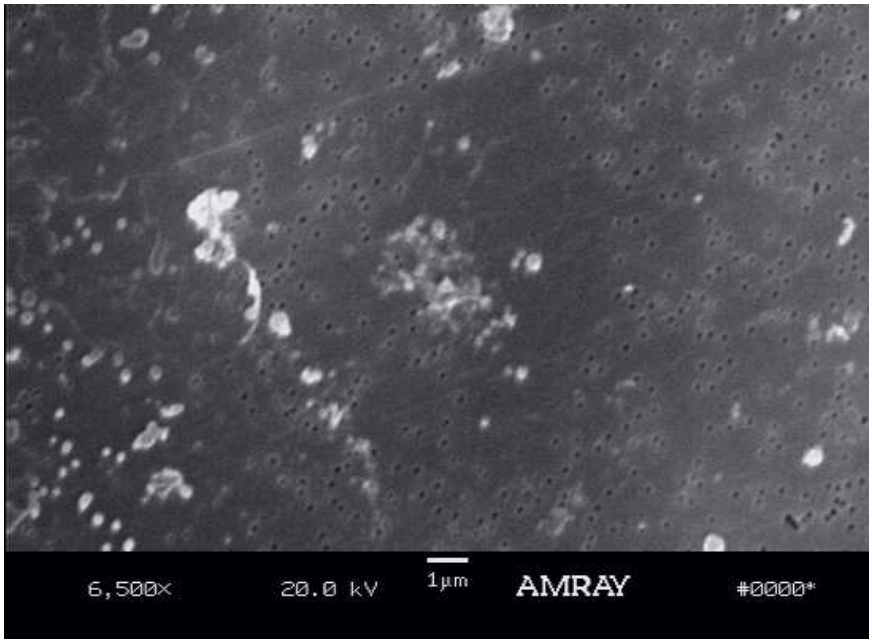

Figure 4-12: Representative SEM images of porous PCTE membrane after being exposed to human blood (Hct~30%).

Chapter 5 : Plasma Separation during In-Vivo Animal Model of ECLS

5.1 ECLS Circuit for Animal Model

The piglets (n=3) with size ranging from 9 to 12 kg were anesthetized with ketamine and midazolam. The technique of ECLS included veno-arterial vascular access where blood was drained through right jugular vein using a 12 french BioMedicus ECLS arterial cannula (Medtronic, Inc. Minneapolis, MN, USA) and reinfused into aorta through right carotid artery using a 10 french BioMedicus ECLS venous cannula (edtronic, Inc. Minneapolis, MN, USA). The ECLS circuit consisted of a Rotaflow Maquet Centrifugal Pump (Maquet, Inc. Wayne, NJ, USA) and a Quadrox-iD Pediatric PMP hollow fiber membrane oxygenator (Maquet, Inc. Wayne, NJ, USA), connected with heparin-coated tubes. Figure 5-1 shows schematics of ECLS circuit using the Quadrox-iD oxygenator and the Rotaflow centrifugal pump and the gas blender on a portable cart. Arterial blood pressure and blood gases were measured throughout the procedure and animals were euthanized after each experiment by administration of potassium chloride.

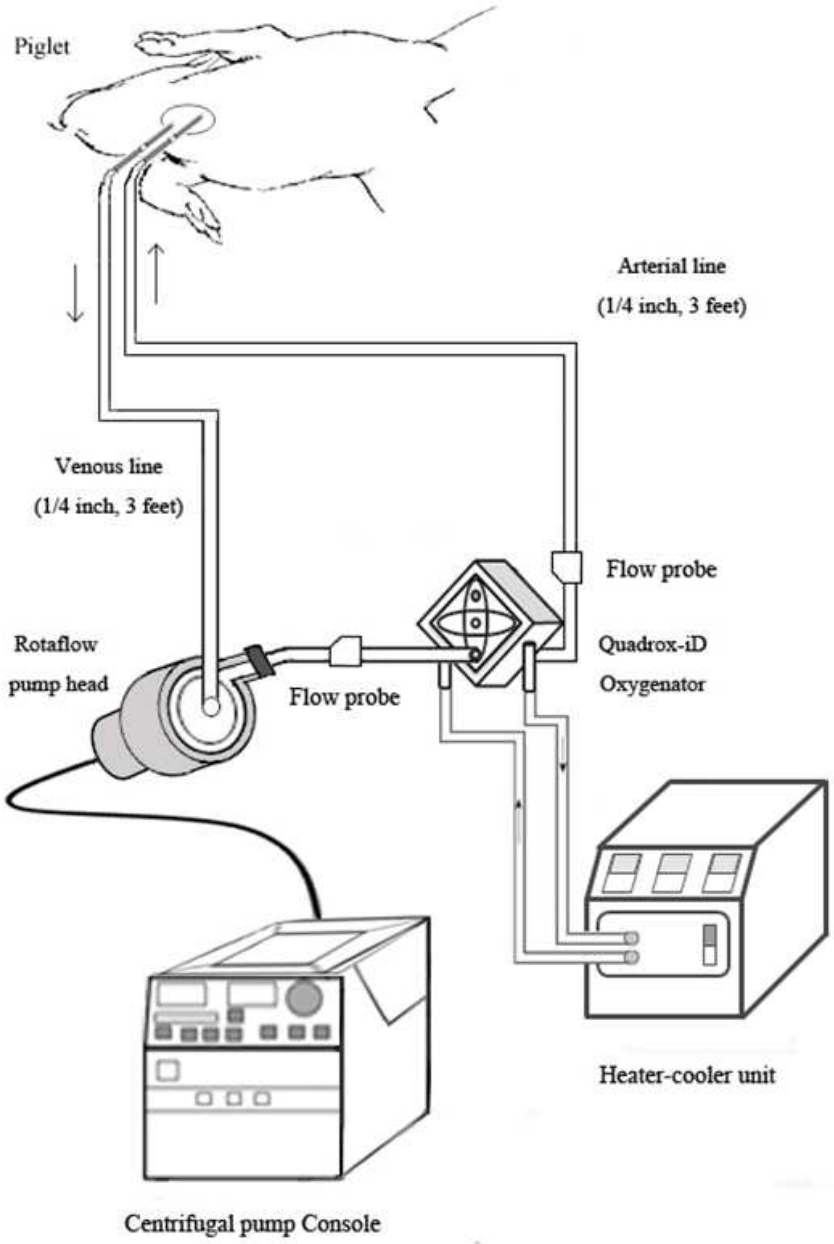

Figure 5-1: Schematics of animal model of ECLS, using the Quadrox-iD oxygenator and the Rotaflow centrifugal pump and the gas blender on a portable cart.

5.2 Circuit Priming

The ECLS circuit was primed using freshly drawn donor blood (porcine whole blood collected from a similarly-anesthetized pig) and Plasmalyte A solution. The blood was then circulated at a rate of 500 ml/min at an arterial circuit pressure of 100 mmHg. Also additional volume requirements to maintain circuit flow or desired hematocrit level were met by the addition of a porcine whole blood or saline solution throughout the procedure. Nonpulsatile perfusion was performed and the temperature was set at normothermia (35 °C) for the duration of the experiments. After all manipulations by the perfusionist were completed, the ECLS circuit was connected to the piglet.

5.3 Pre-coating the Microfiltration with Heparin Anticoagulant

Heparin is widely used in clinical environments as an anticoagulation to prevent blood clots from forming. The amount of heparin administered varies depending upon clinical guidelines. For example during short-term cardiac surgeries requiring CPB, high doses of heparin is used to prevent blood clot formation and maintain blood fluidity within CPB circuit components. However, during prolonged circulatory support such as ECLS, small amount of systemic anticoagulation is used because of the bleeding complications. The quantity of heparin administered is adjusted according to coagulation test results such as activated clotting time (ACT) to make sure the level of anticoagulation is in the required therapeutic range.

In an effort to limit or eliminate blood clot formation inside the microfiltration channels and maintain the filtration efficiency, it was critical to coat the surface of the microdevice with anticoagulant prior to blood infusion.

Prior to each experiment (n=3), the devices were perfused with water and de-bubbled overnight. Once the devices were completely de-bubbled, the microfiltration device was infused with a solution containing anticoagulant (1000 IU/ml of heparin in lactated ringer solution) for at least 30 min prior to blood infusion.

5.4 Integrating the Microfiltration Device with ECLS circuit

Once complete mixing of the blood and prime fluid (piglet, donor blood and plasmayte A solution) in ECLS circuit was accomplished, the microfiltration device was attached to a purge line connecting the arterial sampling port of the oxygenator and the venous line, which was composed of two 24 inch long 1/8 tubings and a five way manifold (SORIN GROUP, Inc, Arvada CO, USA). A small portion of blood was redirected from the manifold in to the reservoir channels of the microdevice using a peristaltic pump (Instech Laboratories, Inc, PA USA) at a flowrate of 80 ul/min. Figure 5-2 shows a picture of the device being infused with porcine blood during ECLS procedure.

Figure 5-2: A picture of a microfiltration device connected to ECLS circuit during an in vivo piglet model of ECLS.

5.5 Blood Analysis during ECLS Animal Model Experiments

To ensure blood chemistry, especially blood gases, were within acceptable physiological limits, they were continuously monitored throughout the experiments. Additionally blood anticoagulation was achieved by continuous heparin infusion maintaining an activated clotting time of 180-220 s. [83]

Table 5-1, Table 5-2 and Table 5-3 summarize the blood chemistry analysis and the ACT coagulation test results during ECLS model of animal experiment and heparin administration based on these results.

Table 5-1: (a) Blood gas analysis for ECLS animal model experiment (n1) and (b) ACT coagulation tests results and heparin administration

(a)

Time	9:50	10:50	11:29	12:41	13:30	14:30	15:30
Glu(mg/dl)	71	125	118	116	116	112	97
Na(mmol/L)	136	136	137	137	135	135	133
K+(mmol/L)	3.3	3.9	3.9	3.5	3.8	3.6	3.8
TCO2(mmol/L)	33	33	32	29	31	29	30
iCa(mmol/L)	1.24	1.17	1.32	1.35	1.38	1.26	1.21
Hct	18	21	24	23	25	22	21
Hb(g/dl)	6.1	7.1	8.2	7.8	8.5	7.5	7.1
At 37 c							
pH	7.45	7.486	7.504	7.456	7.466	7.469	7.483
pCO2(mmHg)	45.9	41.7	39.1	39.6	41.1	38.6	38.9
pO2(mmHg)	389	390	366	311	275	237	315
HCO3(mmol/L)	31.9	31.5	30.7	27.9	29.6	28.1	29.1
BE ecf (mmol/L)	8	8	8	4	6	4	6
SO2%	100	100	100	100	100	100	100
Calculated at patient Temp							
pH	7.461	7.474	7.488	Error	7.455	7.465	7.475
pCO2(mmHg)	44.5	43.2	40.8	Error	42.4	39.1	39.7
pO2(mmHg)	385	394	371	Error	278	238	3.7
Patient Temp	97.3	97.4	100.4	Error	99.9	99.1	99.5
FiO2(%)	100	100	100	Error	100	100	100
Spin Hct	23	26	31	30	27		

(b)

Time	ACT(sec)	Heparin administration	Time	ACT(sec)	Heparin administration
10:31	524		12:40	457	
11:00	217	300	1:00	359	
11:40	156	1000	1:20	284	
12:00	411		1:40	259	
12:20	252	1000	2:00	236	

Table 5-2: (a) Blood gas analysis for ECLS animal model experiment (n2) and (b) ACT coagulation tests results and heparin administration

(a)

Time	9:45	10:34	10:56	11:35	12:34	13:30	14:37
Glu(mg/dl)	83	107	109	94	94	93	87
Na(mmol/L)	139	139	137	136	136	133	134
K+(mmol/L)	3.2	3.7	3.7	3.6	3.9	3.9	3.8
TCO2(mmol/L)	36	35	35	32	33	34	31
iCa(mmol/L)	1.24	1.06	1.2	1.24	1.33	1.32	1.25
Hct	20	21	21	19	21	20	17
Hb(g/dl)	6.8	7.1	7.1	6.5	7.1	6.8	5.8
At 37 c							
pH	7.223	7.291	7.525	7.467	7.4767	7.472	7.449
pCO2(mmHg)	81.9	68.2	40.4	42.2	43.5	44.3	42.5
pO2(mmHg)	280	317	380	331	379	351	325
HCO3(mmol/L)	33.7	32.9	33.4	30.5	31.4	32.4	29.5
BE ecf (mmol/L)	6	6	11	7	8	9	5
SO2%	100	100	100	100	100	100	100
Calculated at patient Temp							
pH	7.226	7.287	7.522	7.448	7.446	7.45	7.428
pCO2(mmHg)	81.1	69.1`	40.8	44.6	46.2	47.1	45.1
pO2(mmHg)	279	318	381	337	387	358	332
Patient Temp	98.2	99.1	99	100.9	101.1	101.1	101.1
FiO2(%)	100	100	100	70	100	70	100
Spin Hct							

(b)

Time	ACT (sec)	Heparin administration
10:00		2000
10:45	216	
11:10		1000
12:30	122	2000
12:35	145	
13:05	200	
13:30	156	2000
13:50	209	
14:25	218	1500

Table 5-3: Blood gas analysis for ECLS animal model experiment (n3) and (b) ACT coagulation tests results and heparin administration

(a)

Time	9:22	10:38	12:51	13:44
Glu(mg/dl)	58	88	102	55
Na(mmol/L)	132	133	128	129
K+(mmol/L)	6.9	7.5	8.2	8.4
TCO2(mmol/L)	13	14	OOR	19
iCa(mmol/L)	0.89	0.89	0.93	0.94
Hct	31	30	29	30
Hb(g/dl)	10.5	10.2	9.9	10.2
At 37 c				
pH	7.06	7.225	OOR	7.26
pCO2(mmHg)	40.2	32	OOR	39
pO2(mmHg)	614	500	551	589
HCO3(mmol/L)	11.4	13.2	OOR	17.5
BE ecf (mmol/L)	-19	-14	OOR	-10
SO2	100%	100%	OOR	100%
Calculated at patient Temp				
pH	7.06	7.225	OOR	7.26
pCO2(mmHg)	39.4	32	OOR	39
pO2(mmHg)	609	500	551	589
Patient Temp	97.7	98.6	98.6	98.6
FiO2(%)	100			
Spin Hct				

(b)

Time	ACT (sec)	Heparin administration	Time	ACT (sec)	Heparin administration
10:00		2000	12:45	242	
10:25	303		13:15	148	500
10:45	216		13:30	563	
11:00	351	2000	13:45	298	
11:15	260		14:00	484	
11:30	382		14:15	330	
11:45	157		14:30	226	
12:00	348	2000	14:45	216	
12:15	272		15:00	159	
12:30	277		15:15	150	
13:00	183		15:30	150	

5.6 Sample Collection and Analysis

The fluid fractions from both microdevice outlets of the reservoir and filtration channels were collected in 20 minute intervals for a total circulation time of 4 hours. Discrete blood samples of 1 ml volume were also collected directly from circuit as a control sample. Following collection, the direct draw and reservoir blood samples were centrifuged; the plasma was removed and snap frozen at -80 °C on dry ice until analyzed. Finally the device was cut and a small piece of membrane was removed, fixed in 2% glutaraldehyde, dehydrated, and inspected using scanning electron microscopy (AMRAY-1830I, AMRAY, Bedford, MA) to evaluate the membrane surface after being exposed to porcine blood.

In this study the concentration of inflammatory cytokines (IL-1β, IL-4, IL-6, IL-8, IL-10, IFN-γ, TGF-β and TNF-α) was measured using Procarta® Cytokine Assay Kit (Affymetrix™, Santa Clara, US). Briefly, standard curves for each cytokine were generated using the kit-supplied reference cytokine samples (20000 pg/ml) diluted with Standard Buffer, to achieve final concentrations of 20000, 5000, 1250, 313, 78, 19.5, 4.9 and 1.22 pg/ml. This assay is designed to measure the concentration of multiple cytokines in a single well using very small amount of sample (25μL).

After pre-wetting the 96-well filter plate with washing buffer, the solution in each well was aspirated using a vacuum manifold. Next, the samples were incubated with antibody-conjugated beads first for 30min at room temperature on a shaker and then overnight at 4°C without shaking. After the overnight incubation and before proceeding to the detection, the assay plate was again incubated for 30 min at room temperature. Following

incubation detection antibodies were added and incubated for 30min. Subsequently, Streptavidin–PE was added to each well for 30 min. Then, after washing with buffer to remove the unbound Streptavidin–PE, the beads bound to each cytokine were analyzed in the Luminex instrument. Raw data (fluorescence intensity) were analyzed using the Bio-plex 5.0 software (Bio-Rad).

5.6.1 Experimental Results

The microfiltration device was successfully integrated with ECLS circuit for a total of 3 in-vivo ECLS procedure with no evidence of device clogging over long period of time (over 5 hours). These results showed no significant decrease in reservoir or filtrate output flow rates due to biofilm formation or membrane clogging throughout the experiment. When using a 200 nm pore size, about 10% to 15% of the total blood volume was collected in the filtrate channels without any contaminating blood cells or indications of RBC hemolysis. The filtration flowrate varied sometimes (not significantly) due to surgical protocol which affected the device performance. For example during the surgery in order to keep the Hct in range (30%-35%) lactated ringers solution was given to the piglet which ultimately resulted in lower blood viscosity, decreasing the reservoir channel hydraulic flow resistance, and higher reservoir and lower filtrate flow rates. However, the filtration flowrate volume over the sampling period was still sufficient for analysis (over 50 µl in 20 min). The SEM photographs of membrane after exposure to piglet blood for over 5 hours indicated no gross changes in pore morphology of the membranes. Although some protein aggregation was seen on the membrane surface, the underlying pores in the membrane were clearly seen and were not clogged (Figure 5-3). Figure 5-4 shows a SEM photograph of a **non-heparin** coated microfiltration device during one unsuccessful in-

vivo experiment which indicates the importance of the effect of heparin coating during procedures where systemic anticoagulation is not desired.

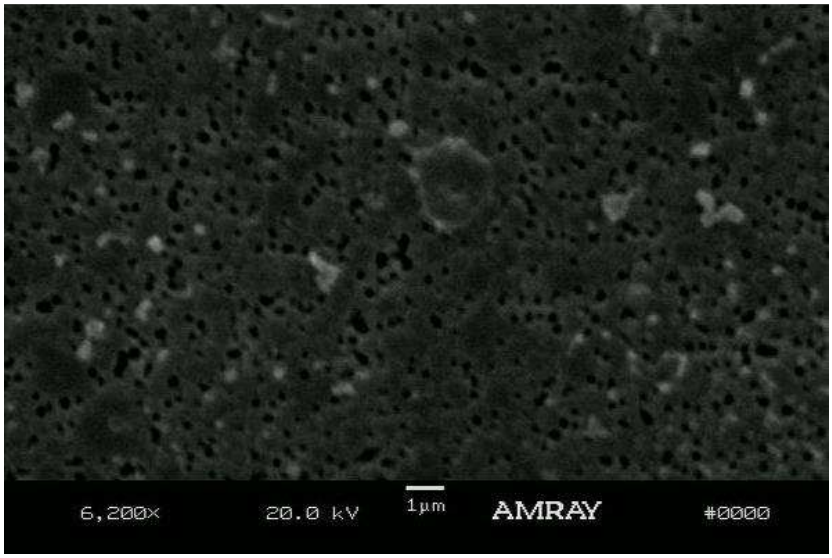

Figure 5-3: Representative SEM images of anticoagulant-coated PCTE membranes after exposure to porcine blood for over 5 hours during animal model of ECLS.

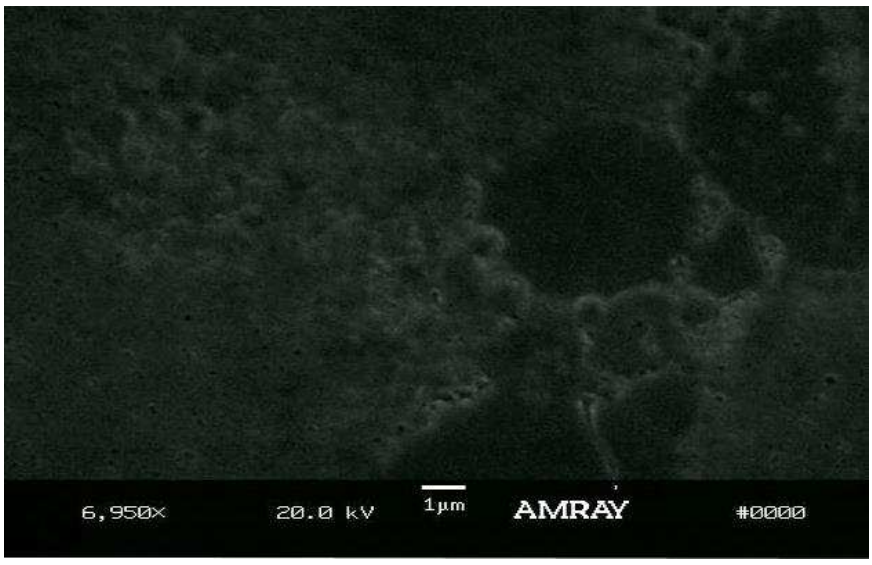

Figure 5-4: Representative SEM images of non-heparin coated porous PCTE membranes after exposure to porcine blood.

In this study serum samples were collected continuously from a total 3 in-vivo piglets model of ECLS and the cytokine concentrations were measured using fluorescent bead-based (Luminex) immunoassay kit to simultaneously measure interleukins IL-1β, IL-4, IL-6, IL-8, IL-10, IFN-γ and tumor necrosis factor-α (TNF-α) and transforming growth factor beta TGF-β Available Luminex assays theoretically have the capacity to measure multiple cytokines simultaneously in volumes of 25 to 50 µL of serum. In contrast, conventional individual measurement by ELISA requires 50 to 200 µL of serum per analyte. In addition, Luminex assays may have a greater dynamic range (~1-20,000 pg/mL) than ELISAs. [84, 85]

Despite successful integration of microfiltration device with the ECLS circuit and continuous sampling over 5 hours surgical period, the concentration of the major number of samples were below detectable range and final conclusion on the microfiltration biomarkers recovery could not be made. Among the analyzed proinflammatory cytokines, results: of IFN-γ ,TNF-α, IL-10, IL-4,IL-8 and IL-6 were undetectable in more than half of the serum samples and no conclusion could be made regarding the cytokine behavior during ECLS. Figure 5-6 show the temporal change in proinflammatory cytokines TGF-β and IL-1β during 2 experiments (animal experiment case 1 and 3) over the circulation time for samples collected from both the reservoir and filtrate outlets using the microfiltration device and those measured from the direct blood draw. Moreover, the results from analyzing proinflammatory cytokines TGF-β and IL-1β indicated no significant trend in the level of these cytokines.

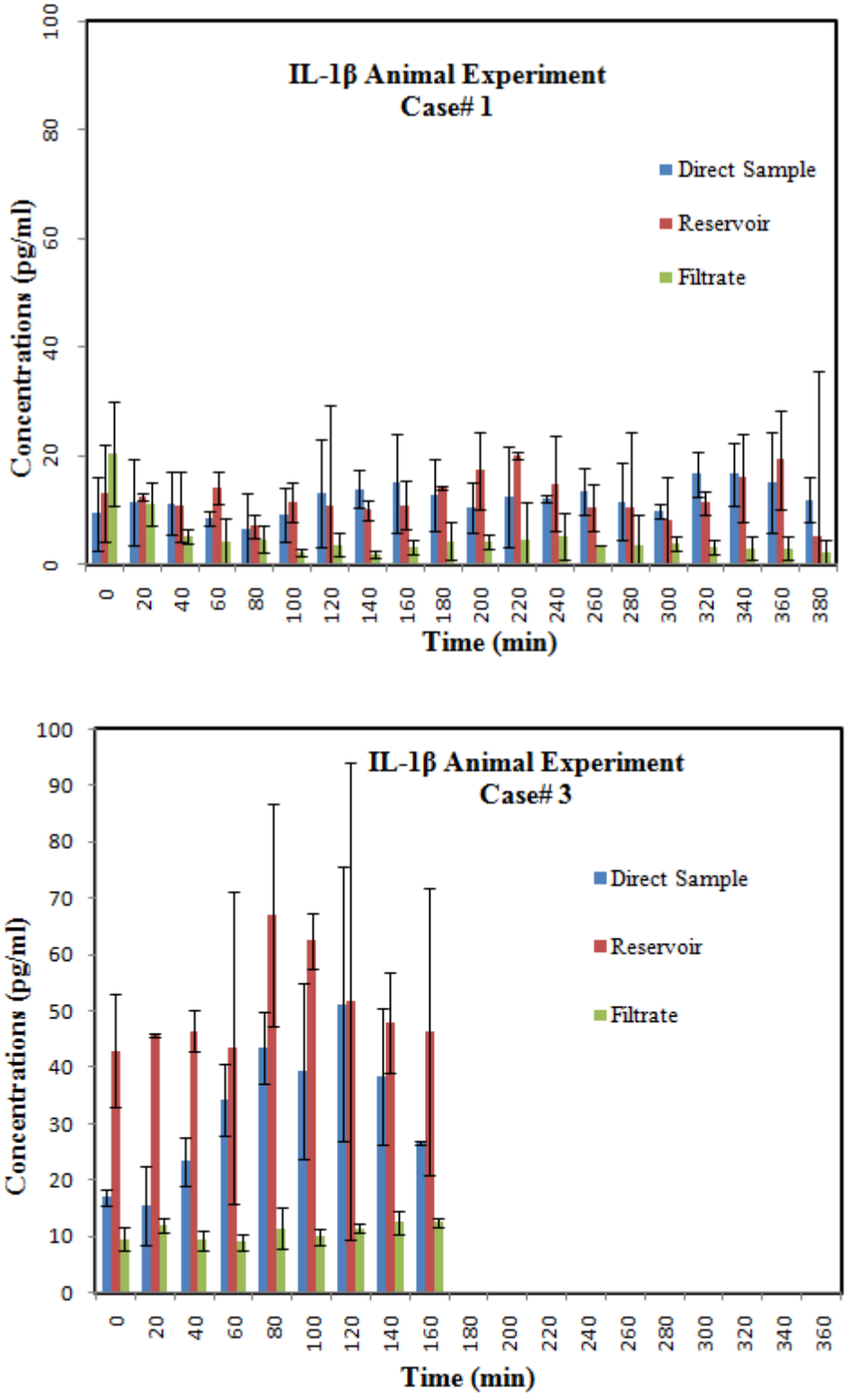

Figure 5-5: The concentration of cytokine (IL-1β) during 2 animal model of ECLS.

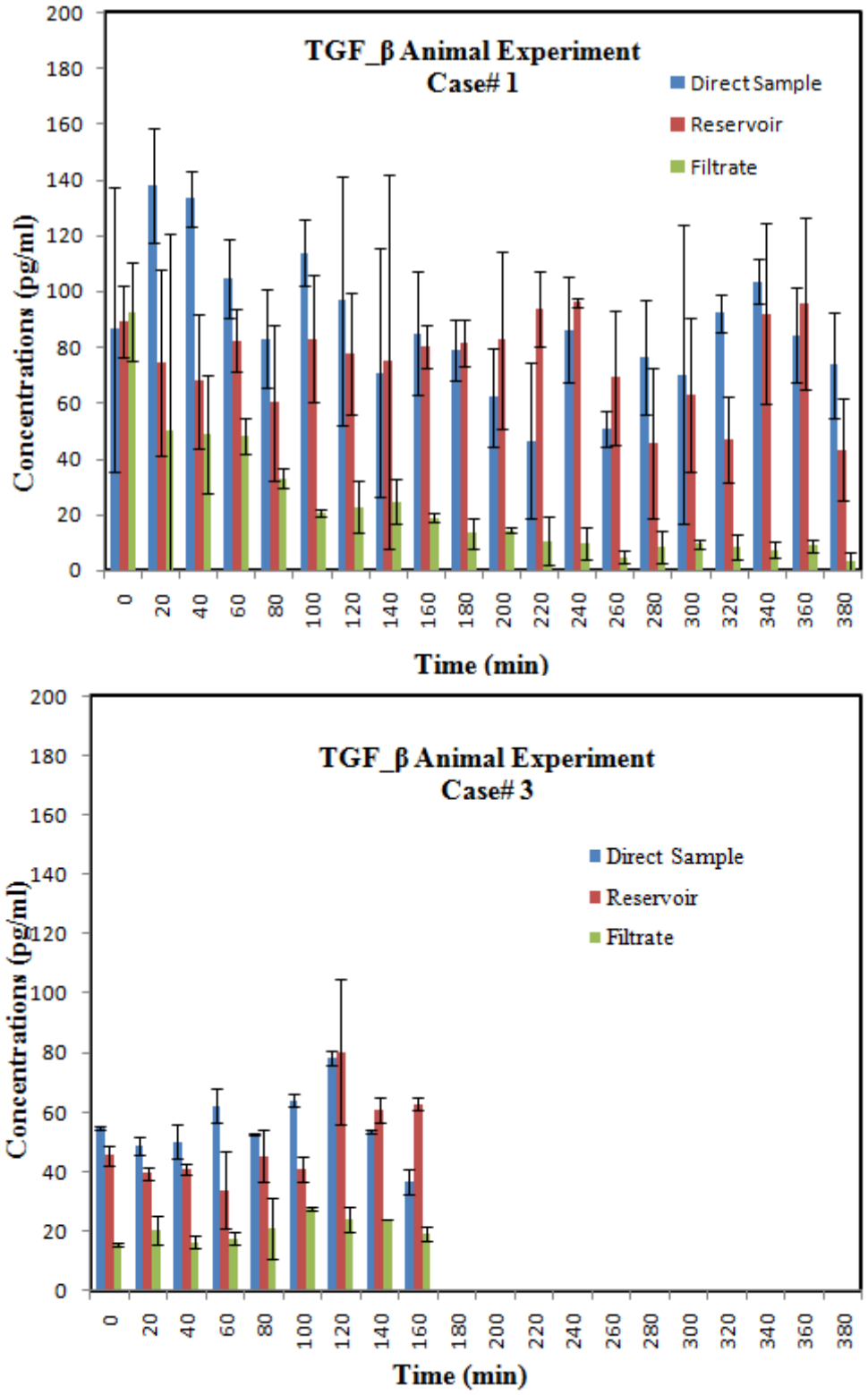

Figure 5-6: The concentration of cytokine (TGF-β) during 2 animal models of ECLS.

Finally, a comparison was done to quantify the cytokine recovery compared to the direct blood draw. At each time point, the measured cytokine concentration from the filtrate outlets were normalized to the direct draw concentration and compared to each other in 2 different experiments were the concentrations of the all samples were detectable (animal experiments 2 and 4).

Table 5-4: Average percentage recovery of TGF-β and IL-1β in filtrate samples

Experiment	**TGF-β**	**IL-1β**
Piglet model # 1	25.21%	44.64%
Piglet model # 3	38.07	39.26%

The results also indicated that the cytokine IL-1β recovery (~ 40%) of in-vivo ECLS experiment is much less than the recovery of IL-β (more than 80%) inside the microfiltration device during simulated CPB. This could have been a result of multiple factors. First, the piglet blood exhibits a different rheology than human blood. For example blood cells with smaller diameter than that of the human potentially can increase the chance of these cells being pushed into some of the membrane pores and increasing the membrane flow resistance. Achieving optimal recovery in this case is possible by varying the membrane pore size. Additionally, achieving a constant recovery is very challenging as blood hematocrit and viscosity is different between different clinical models and constantly changing and being adjusted even during one single experiment which can alter filtration efficiency. However, successful developing and integration of the microfiltration device within in-vivo animal model of ECLS, which was able to continuously extract blood plasma for extended period of time and providing sufficient

filtrate volume within short amount of time for analysis without further blood modification is very promising for diagnostic applications..

Chapter 6 : Microfiltration Device for Sepsis Treatment

6.1 Introduction to Sepsis

Sepsis is one of the primary causes of morbidity and mortality in hospitals, with ~750,000 cases per year in the United States. [86] Sepsis is caused by a severe infection originating from a variety of sources including: pneumonia, urinary track infection, wound infection, infection following burn, or as a complication of chemotherapy or immune compromised state such as those infected with HIV/AIDS. The infection can localize within the kidneys, the lungs, the gall bladder, or the liver. Once pathogenic organisms enter the bloodstream a patient may suffer from septicemia or bacteremia; the presence of bacteria in the blood. A patient with severe sepsis presents with symptoms of systemic inflammatory response syndrome (SIRS) characterized by acute inflammation throughout the body, fever and elevated white blood cell (WBC) count (leukocytosis). In patients with sepsis, regardless of the initial infecting pathogen, a cascade of inflammation with activation of the coagulation system leads to alterations in microvascular circulation, multiorgan dysfunction and death. [87] Despite therapeutic advances, powerful antibiotics, blood transfusion and improved intensive care support, the mortality rate still ranges from 30 to 50% and up to 90% for severe cases with multiple organ dysfunction. [88] A key difficulty for antibiotic administration for rapid intervention in septic patients is identifying the infectious pathogen which delays the treatment. Rapid elimination of microbial pathogens, even before they are identified, can be critical to patient survival. Therefore, there is a need for a high throughput blood cleansing device to remove pathogens from whole blood.

6.2 Microfluidic Devices for Bacteria Sparation

Recently, microfluidic and miniaturized lab-on-a-chip separation devices have been introduced to separate pathogenic bacteria from blood. Active actuation has been used to remove bacteria from contaminated blood by generating physical fields based on magnetic activated cell sorting, where specific bacterial pathogens were labeled with magnetic bead coated with pathogen specific antibodies and 80% of pathogens were removed from a contaminated blood sample at a rate of 20 ml/h. [89] This device requires identification of the pathogenic invader and a bead/sample incubation time between 30-60 min to obtain binding of 85 to 90% of the bacteria. Label-free hydrodynamic separations are another attractive separation method because they are cost effective and do not require external fields and labels. The ability to achieve high-throughput separation at high flowrates is important in some clinical applications where large volume of blood needs to be processed in a reasonable amount of time. In one method, a soft inertial force on varying sized particles was used to separate 99.87% bacteria from diluted blood (20x dilutions of RBCs and bacterial cell sample) at a maximum flowrate of 18µl/min. [90] In another report *E-coli* bacterium was separated from diluted blood (~0.5% (v/v)) at a high flowrate of 200 µl/min within a single channel. [91] The goal of this study is to design a microfluidic device for cell separation based on size differences between bacteria and other blood components for the continuous separation of bacteria and microorganism from undiluted whole blood for effective intervention in clinical settings for sepsis treatment.

6.2 Continuous Label-Free Bacteria Separation from Whole Blood

The use of microfiltration device technology was extended to continuously extract pathogens fromundiluted blood (Hct>38%) for treating sepsis. When a blood sample flows through the channels on one side of the membrane (Reservoir channels), the larger blood cells are sterically excluded from passing through the membrane while the smaller bacteria are removed by traversing the membrane into the filtration channels.

6.2.1 Experimental Methods

The microfiltration channels were fabricated using standard soft lithography as described previously in chapter 2. The microfiltration device for bacteria separation consists of two PDMS layers of microchannels, separated by a **2 μm** pore-size porous polycarbonate membrane (PCTE) (Nucleopore Polycarbonate Track-Etch Membrane, Whatman, Florham Park, NJ) as described in (chapter 2)

After fabrication, the microfiltration device was prepared for use by first degassing under water and priming by Lactated Ringer's solution. Then the microfiltration device was pre-infused with 1000 IU/ml of heparin (2 mg of sodium heparin in 1 ml of Lactated Ringer's solution) for at least 30 min prior to infusing blood. Heparin-coating was used as an approach to reduce the amount of platelet adhesion to the surface of the microdevice and prevent the microfiltration device from clotting as discuused in previous chapters.

Fresh human blood in an anticoagulant-treat collection bag was stored at 4°C and was used within one week of collection. For these experiments white blood cells which have

nucleus were separated from whole blood because they could interfere with detection process as nuclear staining was used as a bacteria quantification method. Whole blood was centrifuged at 5000 rpm for 15 min and all the supernatant was removed from the top. The volume of supernatant was then measured and the same volume of ringer's solution was added to resuspend the cell pellet and maintain the hematocrit level. The blood was hemodiluted to 38%, hematocrit by addition of Lactated Ringers solution (Baxter Healthcare Corp, Deerfield, Il) with the hematocrit verified using a Coulter cell and particle counter (Beckman Coulter Inc., Hialeah, FL, USA). The blood sample was then doped with 10 ^{8}CFU/ml of *E.coli* bacteria in 1 ml total volume of blood and was infused into reservoir inlet at a constant flowrate of 50 µl/min via a peristaltic pump and the reservoir outlet was recycled back to an external blood reservoir (Figure 6-1).

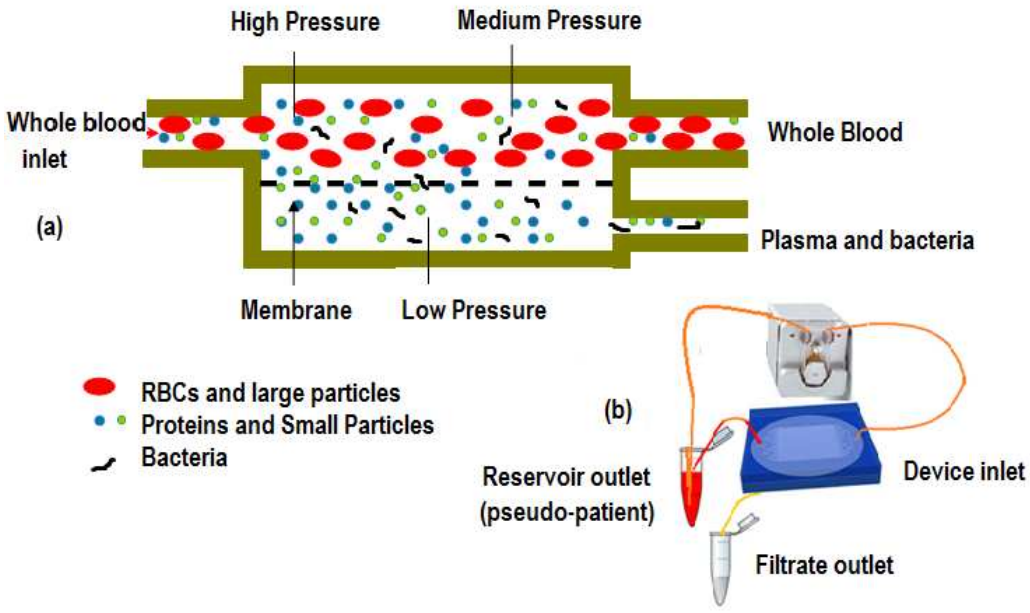

Figure 6-1: (a): Schematic of the microfiltration device for continuous separation of bacteria from whole blood.(b): Schematics of the set up

The blood inlet and filtrate samples were collected in fractions every 20 minutes and then analyzed via a Coulter cell and particle counter (Beckman Coulter Inc., Hialeah, FL,

USA) with counts verified via direct cell counts using a hemocytometer. Bacterial cells in 10 µl of undiluted sample taken from the blood reservoir and filtrate outlet were incubated in a staining solution containing Hoechst 33342 fluorescent dye and lactated Ringer's solution for 60 minutes at room temperature. Samples were then placed under the cover slip of the hemocytometer and counted via a fluorescence microscope at 10× magnification. Additionally, to determine the number of RBCs in the filtrate, samples from the blood reservoir and filtrate (at 80 minutes) were diluted (1:500) with lactated Ringer's solution and were placed under the cover slip of the hemocytometer and counted underbright-field microscopy at 10× magnification.

6.2.2 Experimental Results

Figure 6-2 shows the cell sizing and concentration data obtained via Coulter counting of the blood sample doped with *E.coli* bacteria in the blood reservoir and filtrate samples. These data indicate that after 80 minutes of blood circulation through the microfiltration channels, the reservoir bacteria peak was significantly smaller than at the beginning of the experiment. Additionally, the filtrate bacteria peak after 80 minutes showed the accumulation of bacteria with minimal RBC contamination which indicated that the hematocrit on the reservoir side was maintained.

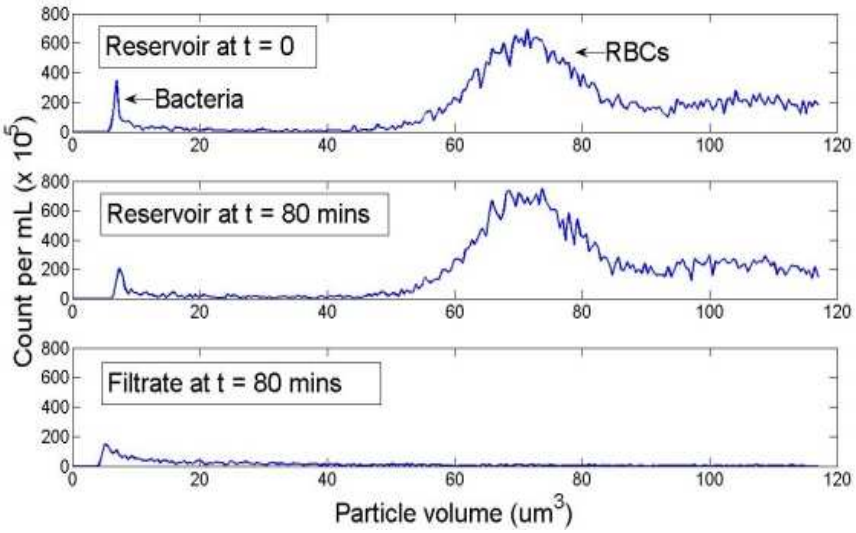

Figure 6-2: Coulter counts of a whole blood sample doped with *E.coli* bacteria at the device inlet (top), reservoir outlet (middle) and filtrate (bottom).

Figure 6-3 shows the cumulative amount of bacteria removed in each 20 minute fraction normalized to the blood reservoir. Using this device approximately 5-6% of the E.coli was removed from the blood in the reservoir sample in each collected fraction resulting in a cumulative removal of 22% over a period of 80 minutes.

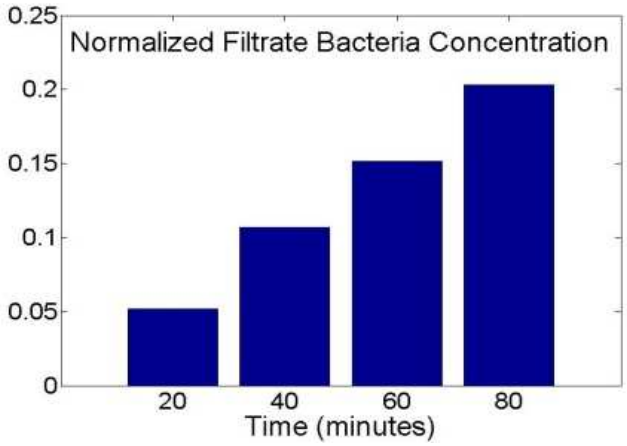

Figure 6-3: Cumulative *E.coli* removal from blood over a period of 80 minutes.

Figure 6-4 shows representative images taken during hemocytometer counting of cells observed under fluorescence microscopy in undiluted blood and Figure 6-5 RBCs observed under bright field microscopy in diluted blood. These images indicate the filtration capability of the microdevice, showing the accumulation of bacteria in the filtrate with minimal RBC contamination in filtrate. A few bacteria cells which can be observed under bright field illumination are indicated by white arrows.

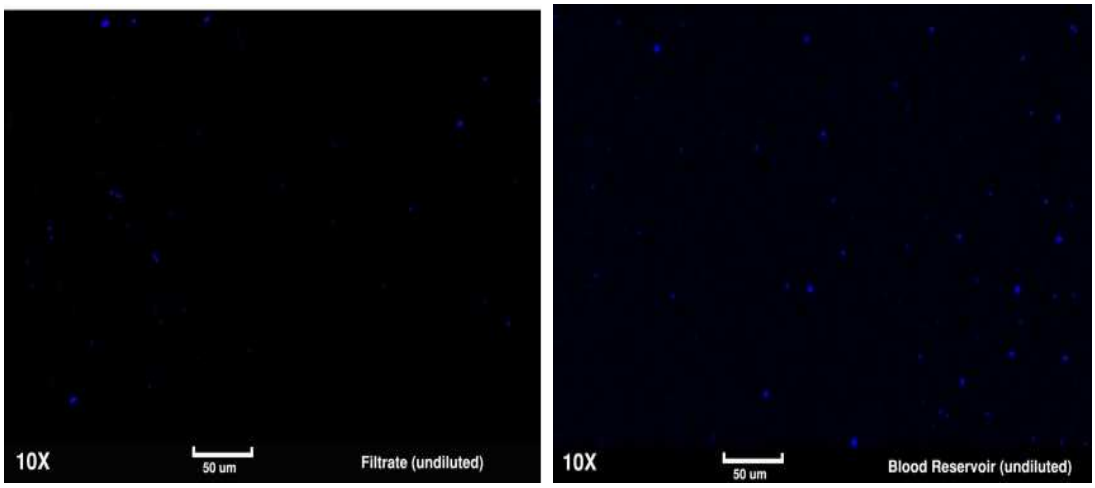

ɾr ultraviolet

les.

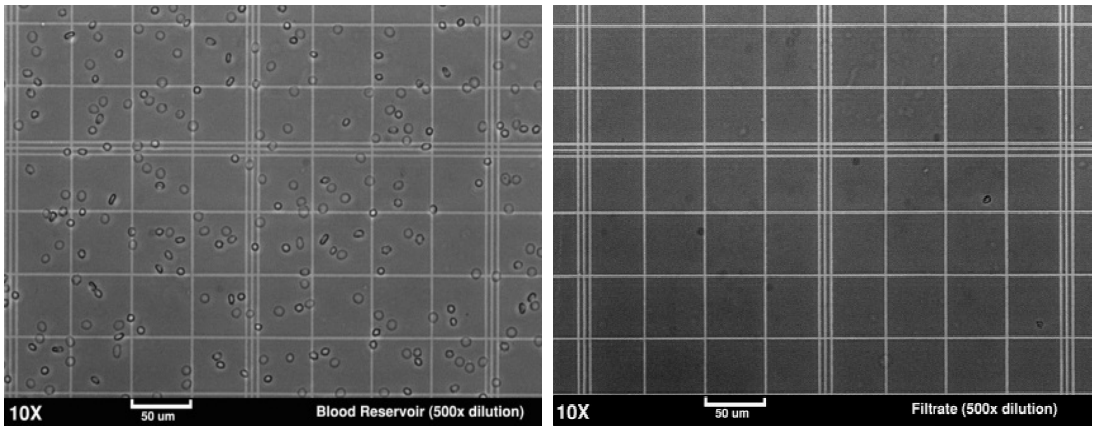

Figure 6-5: Representative images of red blood cells in diluted blood reservoir and filtrate samples under bright field microscopy.

These results demonstrate the ability of the microfiltration system described here to continuously remove bacteria from blood. The performance of the microdevice can be improved to increase the separation efficiency of bacteria from larger volume of blood in a reasonable period of time with the ultimate goal of creating a staged microfiltration device with increasing filter stringency which is capable of separating blood components from small pathogens as well as filtering blood plasma.

Chapter 7 : Summary and Future Work

The microfiltration device in this work target to achieve efficient plasma separation from unmodified whole blood for point-of-care clinical diagnostics. A passive membrane-based microfiltration device with a porous polymer filter to discriminate blood cells from blood sample have been designed, fabricated, and evaluated in this work. The polymer filter used in this study was a commercially available polycarbonate membrane which are available in a wide range pore size and density for medical/clinical applications. The developed technology with improved method of integration of porous polymer membranes with microfluidic devices can make these membranes immediately applicable for a number of lab-on-a-chip applications with a very robust and simple fabrication process.

The microfiltration device was fabricated by using two PDMS layers of microchannels and a polycarbonate (PCTE) porous membrane with low protein adsorption which enabled its utilization of complex fluids such as blood. Successful integration of polymer membranes with microfluidic devices, which relied on chemical modification of the membrane surface, resulted in an irreversible bond between the membrane and the PDMS device which was a great accomplishment in fabrication of membrane based devices.

The effects of various factors such as blood hematocrit, blood anticoagulant level and membrane morphology have been investigated using sheep's whole blood.

The microfiltration device was designed to continuously extract diagnostic plasma proteins such as complements and cytokines using a significantly smaller blood volume

as compared to traditional blood collection techniques. The microfiltration device was successfully tested using a simulated CPB circulation loop primed with donor human blood, in a manner identical to a clinical surgical setup, to collect plasma fractions in order to study the effects of CPB system components and circulation on immune activation. The microdevice, with 200 nm membrane pore size, was connected to a simulated CPB circuit, and was able to continuously extract ~15% pure plasma volume (100% cell-free) with high sampling frequencies which could be analyzed directly following collection with no need to further centrifuge or modify the fraction. Less than 2.5 ml total plasma volume was collected over a 4 hour sampling period (less than one Vacutainer blood collection tube volume). The results tracked cytokine concentrations collected from both the reservoir and filtrate samples which were comparable to those from direct blood draws, indicating very high protein recovery of the microdevice.

The anticoagulant pre-coated microdevice allow operation over a wide range of experimental flow conditions, blood hematocrit and blood systemic anticoagulant level and have the potential to be used during various clinical application. In this study, the heparin-coated microfiltration device was successfully integrated with in-vivo model of animal ECLS to evaluate its performance in another clinically relevant environment. The microfiltration device was able to extract pure plasma from whole with no sign of clogging over the entire surgical period.(over 5 hours).

The simple and robust design and operation of these devices allow operation over a wide range of experimental flow conditions and blood hematocrit levels to allow surgeons and clinicians autonomous usage in a clinical environment to better understand the

mechanisms of injury resulting from cardiac surgery, and allow early interventions in patients with excessive postoperative complications to improve surgical outcomes.

For all the experiments during in-vitro (simulated CPB) and in-vivo (animal model of ECLS) the plasma was 100% cell free. However, a study on the extent of hemolysis and plasma purity at different Hct levels and inlet flow rate is not included in this work, and further studies need to be undertaken to quantify the hemoglobin concentration in the filtrate to better evaluate the extent of hemolysis.

Ultimately, future work will focus on monolithic integration of the developed microfiltration device with a continuous microimmunoassay in order to construct a true micro total analysis system (μTAS) for continuous, real time monitoring of clinically relevant biomarkers during cardiac surgery and especially when extracorporeal circulation (ECC) is used. In order to integrate the two devices, the hydrodynamic fluidic resistances at each layer of the microfiltration device and microimmunoassay device have to be considered. Successful integration of the microfiltration device with microimmunoassay will have a great impact in clinical application for point-of-care diagnostics with reduce blood analysis times, costs and volume of blood samples required for repeated assays and allows surgeons and clinicians to better understand the mechanisms of injury resulting from cardiac surgery, and allow early interventions to improve surgical outcomes. (Figure 7-1)

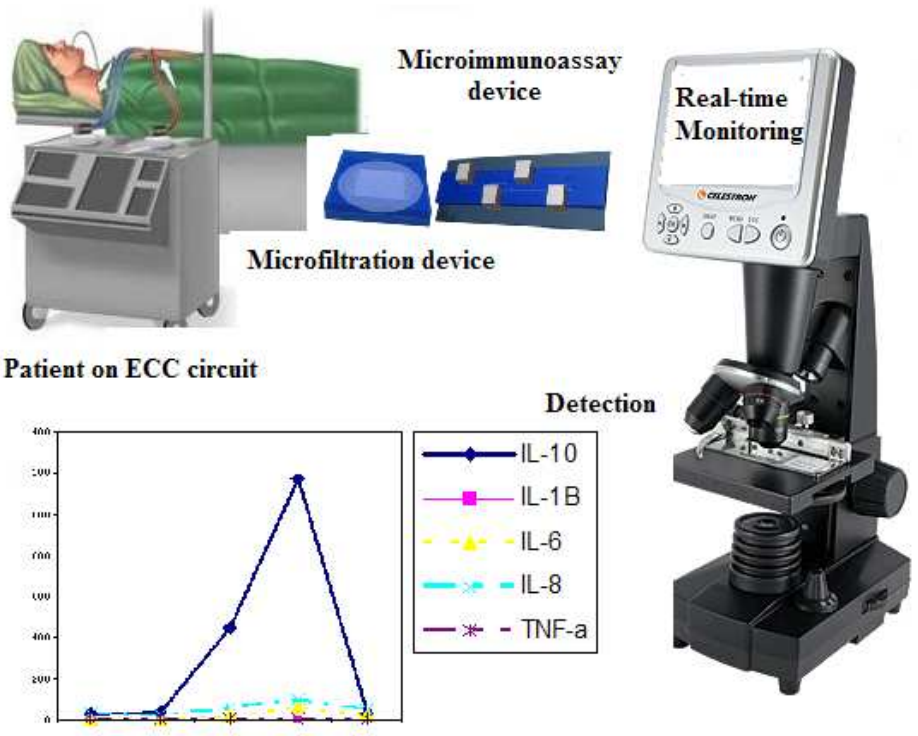

Figure 7-1: Schematics of the micro total analysis system (μTAS) for continuous, real time monitoring of clinically relevant biomarkers during ECC procedures. (Note: part of this image was created by lab member, Lawrence. Sasso)

Finally the microfiltration technology proposed in this study can also be used in applications such as continuous blood cleansing device. In this study, the use of microfiltration device technology was extended to continuously extract pathogens from undiluted blood (Hct>38%) for treating sepsis. A microfiltration device with a 2 μm pore-size PCTE membrane was fabricated and was used to separate *E.coli* from blood (packed RBCs diluted with lactated Ringer's solution to 38%Hct). These result demonstrated the ability of the microfiltration system to continuously remove bacteria from blood. Future work includes designing a microfiltration device using multiple filtration compartments

with decreasing filter pore size between them for separating blood components (6-8 µm diameter red blood cells and 5-10 µm white blood cells) from small pathogens such as *K. pneumonia, P. aeruginosa and S. aureus* of 1-3 mm diameter as well as filtering blood plasma to remove inflammatory proteins. (Figure 7-2)

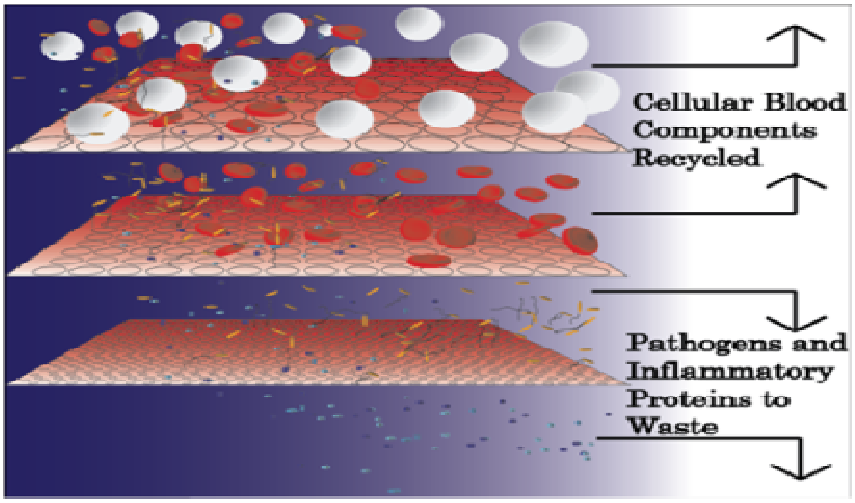

Figure 7-2: Schematics of the multistage device to separate blood components from small pathogens bacteria (note: image was created by lab member, Ian Johnson)

Bibliography

1 Cohn L.H. (2003) Fifty Years of Open-Heart Surgery. *Circulation*. **107**, 2168-2170

2 de Mendonca-Filho, H. T., Pereira, K. C., Fontes, M., Vieira, D. A., de Mendonça, M. L., Campos, L. A. and Castro-Faria-Neto, H. C. (2006) Circulating inflammatory mediators and organ dysfunction after cardiovascular surgery with cardiopulmonary bypass: a prospective observational study. Crit Care. **10**, p. R46

3 Khabar, K. S., Elbarbary , M. A., Khouqeer, F., Devol, E., Al-Gain , S. and Al-Halees, Z. (1997) Circulating endotoxin and cytokines after cardiopulmonary bypass: differential correlation with duration of bypass and systemic inflammatory response/multiple organ dysfunction syndromes. Clin Immunol Immunopathol,. **85**, p. 97-103

4 Moat , N., Shore, D. and Evans, T. (1993) Organ dysfunction and cardiopulmonary bypass: the role of complement and complement regulatory proteins. Eur J Cardiothorac Surg, . **7**, 563-573

5 Westaby, S. (1983) Complement and the damaging effects of cardiopulmonary bypass. Thorax. **38**, 321-325

6 Peris, A., Cianchi, G., Biondi, S., Bonizzoli, M., Pasquini, A., Bonacchi, M., Ciapetti, M., Zagli, G., Bacci, S., Lazzeri, C., Bernardo, P., Mascitelli, E., Sani, G. and Franco Gensini, G. (2010) Extracorporeal life support for management of refractory cardiac or respiratory failure: initial experience in a tertiary centre. Biomedical Central, 18-28

7 Morris, M., Ittenbach, R., Godinez, R., Portnoy , D., Tabbutt, S., Hanna, B., Hoffman, T., Gaynor, J., Connelly, J., Helfaer, M., Spray, T. and Wernovsky, G. (2004) Risk factors for mortality in 137 pediatric cardiac intensive care unit patients managed with extracorporeal membrane oxygenation. . Crit Care Med **32**, 1061-1069

8 Chang , A. and McKenzie, E. (2005) Mechanical cardiopulmonary support in children and young adults: extracorporeal membrane oxygenation, ventricular assist devices, and long-termsupport devices. Pediatr Cardiol . **26**, 2-28

9 Alsoufi, B., Shen, I., Karamlou, T., Giacomuzzi, C., Burch , G., Silberbach, M. and Ungerleider, R. (2005) Extracorporeal life support in neonates, infants, and children after repair of congenital heart disease: modern era results in a single institution. . Ann Thorac Surg **80**, 15-21

10 RM, U., Shen , I., Yeh, T., Schultz, J., Butler, R., Silberbach, M., Giacomuzzi, C., Heller, E., Studenberg, L., Mejak, B., You, J., Farrel , D., McClure, S. and Austin, E. (2004)

Routine mechanical ventricular assist following the Norwood procedure. Improved neurological outcome and excellent hospital survival. Ann Thorac Surg. **77**, 18-22.

11 Seghaye. MC, Duchateau. J and Grabitz . RG. (1993) Complement activation during cardiopulmonary bypass in infants and children: relation to post operative multiple system organ failure. *J Thorac Cardiovasc Surg*. **106**, 978-987.

12 Hall .RI, Smith. MS and Rocker. G. (1997) The systemic inflammatory response to cardiopulmonary bypass: Pathophysiological, therapeutic, and pharmacological considerations. Anesth Analg. **85**, 766-782

13 Westaby. S. (1987) Organ dysfunction after cardiopulmonary bypass: a systemic inflammatory reaction initiated by the extracorporeal circuit. Intensive Care Med. **13**, 89-95

14 Schlag. G, Redl. H and Hallstrom. S. (1991) The cell in shock: The origin of multiple organ failure. Resuscitation. **21**

15 Vasavada, R., Qiu, F. and Undar, A. (2011) Current status of pediatric/neonatal extracorporeal life support: clinical outcomes, circuit evolution, and translational research. Perfusion. **26**, 294-301

16 ELSO, I. S. o. (2010) Registry Report. Extracorporeal Life Support Organization (ELSO).

17 Alsoufi B, A.-R. O., Nazer RI, Gruenwald C, Foreman C, Williams WG, Coles JG, Caldarone CA, Bohn DG, Van Arsdell GS. . (2007) Survival outcomes after rescue extracorporeal cardiopulmonary resuscitation in pediatric patients with refractory cardiac arrest. . J Thorac Cardiovasc Surg. **134**, 952-959

18 Gessler, P., Schmitt , B., Prètre, R. and Latal, B. (2009) Inflammatory response and neurodevelopmental outcome after open-heart surgery in children. Pediatr Cardiol. **30**, 301-305

19 Madhok, A., Ojamaa, K., Haridas, V., Parnell, V. A., Pahwa, S. and Chowdhury, D. (2006) Cytokine Response in Children Undergoing Surgery for Congenital Heart Disease. Pediatric Cardiology. **27**, 408-413

20 Paparella, D., Yau, T. M. and Young, E. (2002) Cardiopulmonary bypass induced inflammation: pathophysiology and treatment. An update. Eur J Cardiothorac Surg. **21**, 232-244

21 Rizzo, G., Silvestri, E., Capponi , A., Servadei, F., Pietrolucci, M., Capece, A., Pisa, R. and Arduini, D. (2011) Histomorphometric characteristics of first trimester chorionic villi in pregnancies with low serum pregnancy-associated plasma protein-A levels: relationship with placental three-dimensional power doppler ultrasonographic vascularization. J Matern Fetal Neonatal Med. **24**, 253-257

22 Carr. JA and Silverman. N. (1999) The heparin-protamine interaction. *J. Cardiovasc Surg*. **40**, 659-666

23 Edmunds, L. J. (1998) Inflammatory response to cardiopulmonary bypass. Ann Thorac Surg. **66**, S12-16

24 Fosse. E, Mollnes. TE and Ingvalden. B. (1987) Complement activation during major operations with or without cardiopulmonary bypass. J Thorac Cardiovasc surg. **93**, 860-866

25 Kubes . P, Ibbotson. G and Russell. J. (1990) Role of platelet-activating factor in ischemia/reperfusion-induced leukocyte adherence. Am J Physiol. **259**, G300-305

26 Mollnes, T. (1998) Complement and biocompatibility. Vox Sang. **74**, 303-307

27 Aĝirbaşli, M., Nguyen, M.-L., Win, K., Kunselman, A. R., Clark, J. B., Myers, J. L. and Ündar, A. (2010) Inflammatory and Hemostatic Response to Cardiopulmonary Bypass in Pediatric Population: Feasibility of Seriological Testing of Multiple Biomarkers. Artificial Organs. **34**, 987-995

28 Haines, N., Rycus, P., Zwischenburger, K., Bartlett, R. and Undar, A. (2009) Extracorporeal life support registry report 2008: neonatal and pediatric cardiac cases. ASAIO J. **55**, 111-116

29 Lau, C., Posther, K., Stephenson, G., Lodge, A., Lawson, J., Darling , E., Davis, R. J., Ungerleider, R. and Jaggers, J. (1999) Mini-circuit cardiopulmonary bypass with vacuum assisted venous drainage: feasibility of an asanguineous prime in the neonate. Perfusion. **14**, 389-396.

30 Su, X. and Undar, A. (2010) Brain protection during pediatric cardiopulmonary bypass. Artif Organs. **34**, 91-102

31 Undar, A. (2005) Pulsatile versus nonpulsatile cardiopulmonary bypass procedures in neonates and infants: from bench to clinical practice. ASAIO J. **51**, vi-x

32 Wernovsky, G. (2006) Current insights regarding neurological and developmental abnormalities in children and young adults with complex congenital cardiac disease. Cardiology in the Young. **16**, 92-104

33 Newman, M. F., Kirchner, J. L., Phillips-Bute, B., Gaver, V., Grocott, H., Jones, R. H., Mark, D. B., Reves, J. G. and Blumenthal, J. A. (2001) Longitudinal Assessment of Neurocognitive Function after Coronary-Artery Bypass Surgery. New England Journal of Medicine. **344**, 395-402

34 Alsoufi, B., Al-Radi, O. O., Gruenwald, C., Lean, L., Williams, W. G., McCrindle, B. W., Caldarone, C. A. and Van Arsdell, G. S. (2009) Extra-corporeal life support following cardiac surgery in children: analysis of risk factors and survival in a single institution. Eur J Cardiothorac Surg. **35**, 1004-1011

35 Toner, M. and Irimia, D. (2005) Blood-on-a-chip. Annual Review of biomedical Engineering. **7**, 77-103

36 Crowely, T. A. and Pizziconi, V. (2005) Isolation of plasma from whole blood using planar microfilters for lab-on-a-chip applications. Lab Chip. **5**, 922-929

37 Mainwaring, R. D., Lamberti, J. J. and Hugli, T. E. (1998) Complement Activation and Cytokine Generation after Modified Fontan Procedure. Annals of Thoracic Surgery. **65**, 1715-1720

38 Williams. GD, Ramamoorthy. C, Chu. L and (2006) Modified and conventional ultrafiltration during pediatric cardiac surgery: clinical outcomes compared. J Thorac Cardiovasc surg. **132**, 1291-1298

39 VanDelinder, V. and Groisman, A. (2006) Separation of Plasma from Whole Human Blood in a Continuous Cross-Flow in a Molded Microfluidic Device. Analytical Chemistry. **78**, 3765-3771

40 Mukherjee, S., Kang, T., Chen , Y. and Kim, S. (2009) Plasma separation from blood: the 'lab-on-a-chip' approach (REVIEW). Crit Rev Biomed Eng. **37**, 517-529

41 Choi, S. and Park, J.-K. (2007) Hydrophoresis: A New -Phoretic Method for High-Resolution Particle Separation. In Solid-State Sensors, Actuators and Microsystems Conference, 2007. TRANSDUCERS 2007. International ed.)^eds.). pp. 1769-1772

42 Gu, Y. and Miki, N. (2007) A microfilter utilizing a polyethersulfone porous membrane with nanopores. Journal of Micromechanics and Microengineering. **17**, 2308-2315

43 Gu, Y. and Miki, N. (2009) Multilayered microfilter using a nanoporous PES membrane and applicable as the dialyzer of a wearable artificial kidney. Journal of Micromechanics and Microengineering. **19**, 065031

44 Huang, L. R., Cox, E. C., Austin, R. H. and Sturm, J. C. (2004) Continuous Particle Separation Through Deterministic Lateral Displacement. Science. **304**, 987-990

45 Moorthy, J. and Beebe, D. J. (2003) In situ fabricated porous filters for microsystems. Lab on a Chip. **3**, 62-66

46 Sollier, E., Rostaing, H., Pouteau, P., Fouillet , Y. and Luc Achard, J. (2009) Passive microfluidic devices for plasma extraction from whole human blood. Sensors and Actuators. **B 141**, 617-624

47 Thorslund, S., Klett, O., Nikolajeff, F., Markides, K. and Bergquist, J. (2006) A hybrid poly(dimethylsiloxane) microsystem for on-chip whole blood filtration optimized for steroid screening. Biomedical Microdevices. **8**, 73-79

48 Yang, S., Ündar, A. and Zahn, J. D. (2006) A microfluidic device for continuous, real time blood plasma separation. Lab on a Chip. **6**, 871-880.

49 Sollier, E., Rostaing, H., Pouteau, P., Fouillet , Y. and Luc Achard, J. (2009) Passive microfluidic devices for plasma extraction from whole human blood

Sensors and Actuators. **B 141**, 617-624

50 Yang, S., Undar, A. and Zahn, J. D. (2006) A microfluidic device for continuous, real time blood plasma separation. Lab on a Chip. **6**, 871-880

51 Sollier, E., Rostaing, H., Pouteau, P., Fouillet , Y. and Luc Achard, J. (2009) Passive microfluidic devices for plasma extraction from whole human blood

Sensors and Actuators **B 141**, 617-624

52 Di Carlo, D., Edd, J. F., Irimia, D., Tompkins, R. G. and Toner, M. (2008) Equilibrium Separation and Filtration of Particles Using Differential Inertial Focusing. Analytical Chemistry. **80**, 2204-2211

53 Kersaudy-Kerhoas, M., Dhariwal, R., Desmulliez, M. P. Y. and Jouvet, L. (2010) Hydrodynamic blood plasma separation in microfluidic channels. Microfluid Nanofluid **8**, 105-114

54 Rodriguez-Villarreal, A. I., Arundell, M., Carmona, M. and Samitierabc, J. (2010) High flow rate microfluidic device for blood plasma separation

using a range of temperatures. Lab Chip. **10**, 211-219

55 Fung, Y. C. (1993) Biomechanics: Mechanical Properties of Living Tissues. Springer New York

56 Fung, Y. B., Mechanical Properties of Living Tissues. . (1984) Biomechanics, Mechanical Properties of Living Tissues. Springer Verlag,

57 Nguyen, N.-T. and S. Wereley. (2009) Fundamentals and Applications of Microfluidics. Artech House Publishers., Norwood

58 Lawal , O. W., Adeosun, T. A., Olayiwola, M. A. and Falade, A. O. (2010) Application Of Navier-Stokes Equations Via A Model For Water Flow In Green Plant. Journal of American Science. **6**, 795-798

59 Xia, Y. N. and Whitesides, G. M. (1998) Soft lithography. Annual Review of Materials Science. **28**, 153-184

60 Duffy, D. C., McDonald, J. C., Schueller, O. J. A. and Whitesides, G. M. (1998) Rapid Prototyping of Microfluidic Systems in Poly(dimethylsiloxane). Analytical Chemistry. **70**, 4974-4984

61 Chanard, J. (2003) Biocompatible membranes must be hemocompatible: the role of heparin adsorption onto dialysis membranes. Nephrologie. **24**, 359-365

62 Ouseph, R. and Ward, Richard A. (2000) Anticoagulation for Intermittent Hemodialysis. Seminars in Dialysis. **13**, 181-187

63 de Jong, J., Lammertink, R. G. H. and Wessling, M. (2006) Membranes and microfluidics: a review. Lab on a Chip. **6**, 1125-1139

64 Chueh. Bor-han, Huh. Dongeun , Kyrtsos. Christina R., Houssin. Timothée , Futai. Nobuyuki and Shuichi, T. (2007) Leakage-Free Bonding of Porous Membranes into Layered Microfluidic Array Systems. Anal Chem. . **79** 3504-3508

65 Wu, D. and Steckl, A. J. (2009) High speed nanofluidic protein accumulator. Lab on a Chip. **9**, 1890-1896

66 Wu, H., Huang, B. and Zare, R. N. (2005) Construction of microfluidic chips using polydimethylsiloxane for adhesive bonding. Lab on a Chip. **5**, 1393-1398

67 Kimura, H., Yamamoto, T., Sakai, H., Sakai, Y. and Fujii, T. (2008) An integrated microfluidic system for long-term perfusion culture and on-line monitoring of intestinal tissue models. Lab on a Chip. **8**, 741-746

68 Kuo, T.-C., Cannon, D. M., Chen, Y., Tulock, J. J., Shannon, M. A., Sweedler, J. V. and Bohn, P. W. (2003) Gateable Nanofluidic Interconnects for Multilayered Microfluidic Separation Systems. Analytical Chemistry. **75**, 1861-1867

69 Vlachopoulou.M-E, Tserepi.A, Pavli.P, Argitis.P, Sanopoulou.M and Misiakos.K. (2009) A low temperature surface modification assisted method for bonding plastic substrates. J. Micromech. Microeng. **19**, 015007

70 Bart, J., Tiggelaar, R., Yang, M., Schlautmann, S., Zuilhof, H. and Gardeniers, H. (2009) Room-temperature intermediate layer bonding for microfluidic devices. Lab on a Chip. **9**, 3481-3488

71 Höök, F., Rodahl, M., Brzezinski, P. and Kasemo, B. (1998) Energy Dissipation Kinetics for Protein and Antibodyâˆ’Antigen Adsorption under Shear Oscillation on a Quartz Crystal Microbalance. Langmuir. **14**, 729-734

72 Johnson, P. A., Luk, A., Demtchouk, A., Patel, H., Sung, H.-J., Treiser, M. D., Gordonov, S., Sheihet, L., Bolikal, D., Kohn, J. and Moghe, P. V. (2010) Interplay of anionic charge, poly(ethylene glycol), and iodinated tyrosine incorporation within tyrosine-derived polycarbonates: Effects on vascular smooth muscle cell adhesion, proliferation, and motility. Journal of Biomedical Materials Research Part A. **93A**, 505-514

73 Voinova, M. V., Rodahl, M., Jonson, M. and Kaseme, B. (1999) Viscoelastic acoustic response of layered polymer films at fluid-solid interfaces: Continuum mechanics approach. Phys. Scr. **59**, 391-396

74 Höök, F., Vörös, J., Rodahl, M., Kurrat, R., Böni, P., Ramsden, J. J., Textor, M., Spencer, N. D., Tengvall, P., Gold, J. and Kasemo, B. (2002) A comparative study of protein adsorption on titanium oxide surfaces using in situ ellipsometry, optical waveguide lightmode spectroscopy, and quartz crystal microbalance/dissipation. Colloids and Surfaces B: Biointerfaces. **24**, 155-170

75 Windberger, U., Bartholovitsch, A., Plasenzotti, R., Korak, K. J. and Heinze, G. (2003) Whole blood viscosity, plasma viscosity and erythrocyte aggregation in nine mammalian species: reference values and comparison of data. Experimental Physiology. **88**, 431-440

76 Hellums, J. (1994) 1993Whitaker lecture: biorheology in thrombosis research. Ann Biomed Eng. **22**, 445-455

77 Guan, Y., Palanzo , D., Kunselman, A. R. and Ündar, A. (2009) Evaluation of membrane oxygenators and reservoirs in terms of capturing gaseous microemboli and pressure drops. Artificial Organs. **33**, 1037-1043

78 Haines , N. M., Wang , S., Myers , J. L. and Ündar, A. (2009) Comparison of pumps and oxygenators with pulsatile and non-pulsatile modes in an infant cardiopulmonary bypass model. Artificial Organs, 993-1001

79 Miller, A., Lu , K., Wang, S., Umstead, T., Freeman, W., Vrana, K., Yang, S., Myers, J. L., Phelps, D. S., Zahn, J. D. and Ündar, A. (2009) Pediatric cardiopulmonary bypass circuits: a review of studies conducted at the Penn State Pediatric Cardiac Research Laboratories. Journal of Extracorporeal Technology **41**, 50-58

80 Talor, J., Yee, S., Rider, A., Kunselman, A. R., Guan , Y. and Ündar, A. (2010) Comparison of perfusion quality in hollow-fiber membrane oxygenators for neonatal extracorporeal life support. Artificial Organs, 330-341

81 Fung, M., Loubser , P. G., Ündar, A., Mueller, M., Sun , C., Sun, W. N., Vaughn, W. K. and Fraser, C. D. (2001) Inhiibition of complement, neutrophil, and platelet activation by an anti-factor D monoclonal antibody in simulated cardiopulmonary bypass circuits. Journal of Thoracic and Cardiovascular Surgery. **122**, 113-122

82 Aran, K., Fok, A., Guan, Y., Sun, Q., Zahn, J. D. and Ündar, A. (2010) Differential Immune Activation During Simulated Cardiopulmonary Bypass Procedure Using Freshly Drawn and Week-Old Blood—A Pilot Study. Artificial Organs. **34**, 1048-1053

83 Levine. MN. (1986) Nonhemorrhagic complications of anticoagulnat therapy. Semin Thromb Hemost. **12**, 63-66

84 Elshal , M. and McCoy, P. (2006) Multiplex bead array assays: Performance evaluation and comparison of sensitivity to ELISA. Methods. **38**, 317-323.

85 Dupont, N., Wang, K., Wadhwa, P., Culhane, J. and Nelson, E. (2005) Validation and comparison of luminex multiplex cytokine analysis kits with ELISA: determinations of a panel of nine cytokines in clinical sample culture supernatants. . J Reprod Immunol. **66**, 175 - 191

86 Schlichting, D. and McCollam, J. S. (2007) Recognizing and Managing Severe Sepsis: A Common and Deadly Threat. Southern Medical Journal. **100**, 594-600

87 Balk, R. A. (2000) PATHOGENESIS AND MANAGEMENT OF MULTIPLE ORGAN DYSFUNCTION OR FAILURE IN SEVERE SEPSIS AND SEPTIC SHOCK. Critical Care Clinics. **16**, 337-352

88 Bernard, G. R., Vincent, J.-L., Laterre, P.-F., LaRosa, S. P., Dhainaut, J.-F., Lopez-Rodriguez, A., Steingrub, J. S., Garber, G. E., Helterbrand, J. D., Ely, E. W. and Fisher, C. J. (2001) Efficacy and Safety of Recombinant Human Activated Protein C for Severe Sepsis. New England Journal of Medicine. **344**, 699-709

89 Yung, C. W., Fiering, J., Mueller, A. J. and Ingber, D. E. (2009) Micromagnetic-microfluidic blood cleansing device. Lab on a chip. **9**, 1171-1177

90 Wu, Z., Willing, B., Bjerketorp, J., Jansson, J. K. and Hjort, K. (2009) Soft inertial microfluidics for high throughput separation

of bacteria from human blood cells. Lab on a chip. **9**, 1193-1199

91 Mach, A. J. and Di Carlo, D. (2010) Continuous scalable blood filtration device using inertial microfluidics. Biotechnology and Bioengineering. **107**, 302-311